EFFECTS OF NON-UNIFORM STIFFNESS ON PROPULSIVE PERFORMANCE OF CANONICAL AND BIO-INSPIRED FOILS

by

Ruijie Zhu

A Dissertation

Presented to the

Faculty of the School of Engineering and Applied Science

University of Virginia

In Partial Fulfillment

of the Requirements for the Degree of

Doctor of Philosophy

Mechanical and Aerospace Engineering

Charlottesville, VA

Dec 2020

APPROVAL SHEET

The dissertation is submitted in partial fulfillment of the

requirements for the degree of

Doctor of Philosophy

Ruijie Zhu, Author

Hilary Bart-Smith, Advisor
Mechanical and Aerospace Engineering

Daniel B. Quinn, Committee Chair
Mechanical and Aerospace Engineering

Haibo Dong, Committee Member
Mechanical and Aerospace Engineering

Matthew A. Reidenbach, Committee Member
Environmental Sciences

Natasha L. Smith, Committee Member
Mechanical and Aerospace Engineering

Trevor H. Kemp, Committee Member
School of Architecture

Accepted for the School of Engineering and Applied Science:

Craig H. Benson, Dean
School of Engineering and Applied Science

Dec 2020

Dedication

I dedicate my work to my family and many friends. A special feeling of gratitude to my loving parents, whose words of encouragement and push for tenacity ring in my ears.

ACKNOWLEDGMENTS

Firstly, I would like to express my sincere gratitude to my advisor Prof. Hilary Bart-Smith for the continuous support of my Ph.D. study and related research, for her patience, motivation, and immense knowledge. Her guidance helped me in all the time of research and writing of this thesis. I could not have imagined having a better advisor and mentor for my Ph.D. study.

Besides my advisor, I would like to thank the rest of my thesis committee: Prof. Daniel Quinn, Prof. Haibo Dong, Prof. Matthew Reidenbach, Prof. Natasha Smith and Dr. Trevor Kemp, for their insightful comments and encouragement, and questions which incented me to widen my research from various perspectives.

My sincere thanks also go to Prof. Frank Fish, Prof. George Lauder and his team (David Matthews, Dr. Dylan Wainwright and Dr. Valentina Di Santo), who provided many biological and experimental data. Without their precious support it would not be possible to conduct this research.

I thank my fellow researchers (Carl White, Gregory Lewis, Dr. Joseph Zhu) for the stimulating discussions, for the sleepless nights we were working together before deadlines, and for all the fun we have had in the last five years. I also thank Dr. Kelly Cunningham and fellow students at Peer Review Group for proofreading my work and providing valuable feedback.

Last but not the least, I would like to thank my family and friends for supporting me spiritually throughout writing this thesis and my life in general.

TABLE OF CONTENTS

LIST OF TABLES

LIST OF FIGURES

ABSTRACT

Traditional underwater vehicle design is usually composed of a rigid hull and rotating propeller. The vehicle is driven by steady thrust produced from the rotation of the propeller. In the last 20 years, researchers have been inspired by biology to develop vehicle test platforms that use unsteady lift-based propulsion mechanisms for swimming. One common type of lift-based propulsion is body-caudal-fin (BCF) propulsion, where the fish contracts its body muscle to produce a side-way motion of its peduncle and caudal fin. To design a high-performance bio-inspired propulsor, fluid-structure interaction behind BCF swimming needs to be better understood before exploring the design space of a propulsor with high performance. The body and fins of fish are structures with non-uniform flexibility that undergo complex motion underwater. However, most previous studies have used simplified models regarding flexibility distribution or shape to study bio-inspired propulsion. The purpose of this dissertation is to study and develop new mechanical models with additional complexity compared to those, such as non-uniform flexibility distribution inspired by tuna peduncle and caudal fin rays.

In this dissertation, a combination of experimental and computational methods was employed to study the role of non-uniform stiffness in underwater propulsion, and its effects on propulsive performance and wake structure. Mechanical testing was employed to quantify the range of stiffness observed in biology, serving as guidance for design of experiments and simulation. A variety of propulsors with canonical and bio-inspired shapes were designed and tested under pure heave or pitch motion inside a water tunnel setup with uniform incoming flow. Propulsive performance including thrust, power, and efficiency were measured for each trial, and Particle Image Velocimetry (PIV) was used to visualize 2D/3D flow structure for certain cases of outlying performance. The data collected from water tunnel experiments were both used for validating the

Computational Fluid Dynamics (CFD) solver and serving as baseline cases for the larger design space. Then CFD was employed to simulate additional kinematics and material design to help exploring propulsor design beyond biology or rapid prototyping capability.

With a simplified tuna tail model, the effects of phase offset and peduncle joint stiffness are studied. The results of computational study of phase offset show that a passively flexing foil is as efficient or more efficient than any foil model where the caudal peduncle is actively controlled. The experimental results show that although there is no one optimal peduncle stiffness across all parameter spaces, there are clear differences in performance due to peduncle stiffness. Design should be focused on the ability to actively modulate stiffness such that we can achieve optimal performance at any set of swimming parameters.

With simplified square and rectangular foil models, the effects of anisotropic stiffness and shape are studied. Results show that the square foils with pure chordwise stiffness distribution have overall higher thrust and efficiency than foils with pure spanwise stiffness distribution. When comparing all the square foils, the trend of efficiency versus frequency always has a local maximum within the range of frequencies tested. A highly flexible square foil (with similar properties as most flexible fish propulsor) has the highest efficiency at lower frequency. However additional stiffness is needed to maintain efficiency when frequency increases.

1. INTRODUCTION

1.1 Motivation and Goals

Traditional underwater vehicle design is usually composed of a rigid hull and propeller. The vehicle is driven steadily by thrust produced from the rotation of the propeller. In the last 25 years, researchers have been inspired by biology to develop vehicle test platforms that use unsteady lift-based propulsion mechanisms for swimming (F. E. Fish, 1996; Kato, 2000; Michael S Triantafyllou & Triantafyllou, 1995) (Figure 1.1a). One common type of lift-based propulsion is body-caudal-fin (BCF) propulsion (Figure 1.1b), where the fish contracts its body muscle to produce a side-way motion of its peduncle and caudal fin. This lift-based propulsion produced by the caudal fin enables the fish to swim with high efficiency and speed (I. Borazjani & Sotiropoulos, 2010).

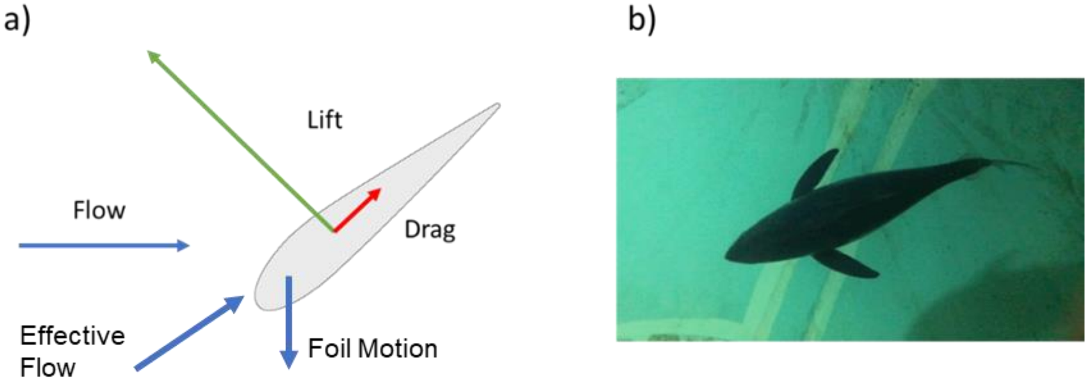

Figure 1.1 (a) Lift-based propulsion, where incoming flow coupled with ; (b) Body-caudal-fin propulsion

The focus for this study is the tuna, which is part of the family *Scombridae*. Tuna, as representative species of BCF swimmers, are fast, efficient, and with high aspect ratio lunate caudal fins. Previous studies (Feilich & Lauder, 2015; M. L. N. Rosic, Thornycroft, Feilich, Lucas, & Lauder, 2017) on tuna and similar species using passive models suggest that the shape or uniform flexibility of the caudal fin cannot determine swimming performance alone. Given the complex morphology of tuna (Figure 1.2) and tuna-like species, it is important to build more complex models to further explore these characteristics. This dissertation will be mostly focusing on non-uniform stiffness observed in nature and bio-inspired stiffness distribution designed in simulation and experiments. Fin-fin interaction between dorsal fins and caudal fin has been studied to demonstrate its contribution to propulsive performance enhancement (Han, Lauder, & Dong, 2020). Finlets (Wang, Wainwright, Lindengren, Lauder, & Dong, 2020), caudal peduncle keels and pelvic fins (Wainwright & Lauder, 2020) also demonstrate propulsive performance enhancing characteristics.

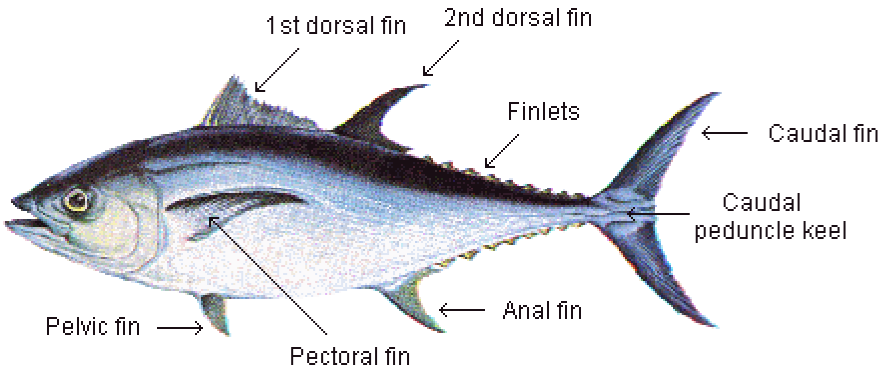

Figure 1.2 Morphology of Tuna (Adapted from http://www.fao.org/fishery/topic/16082/en)

This dissertation will focus on the peduncle joint and non-uniform stiffness distribution of caudal fin. Among the previous studies mentioned, few have looked at models that have non-uniform stiffness distribution, even though non-uniform flexibility is considered an important feature of tuna tails. The most recent study on fin flexibility models the tuna tail as a foil with uniform stiffness. Such a simplified model ignores a critical region of the tuna tail – the peduncle area which connects the caudal fin to the main body. From videos of tuna swimming kinematics (Figure 1.1b), it is observed that the flexible peduncle provides an extra degree of bending, which allows the caudal fin to form a phase offset from body during swimming. This dissertation aims at exploring how non-uniform stiffness of peduncle and caudal fin contributes to the high propulsive performance of tuna tail, and if there exists a bio-inspired propulsor with optimized characteristics inspired by tuna tail.

To design a high-performance bio-inspired propulsor, detailed observation and analysis are needed on the fluid-structure interaction behind BCF swimming, to help explore the design space of a propulsor with optimal performance. The body and fins of fish are structures with non-uniform flexibility that undergo complex motion underwater. However, most previous studies have used an simplified model, especially regarding flexibility distribution to study bio-inspired propulsion (Dewey, Boschitsch, Moored, Stone, & Smits, 2013; M. N. Rosic, Thornycroft, Feilich, Lucas, & Lauder, 2017). The bio-inspired models used in my research have additional complexity compared to those, such as non-uniform flexibility distribution inspired by tuna fin ray structure (Potthoff, 1975; Westneat & Wainwright, 2001).

Research covered in this dissertation has three main objectives (figure 1.2). Biology lays the foundation for this work and will be used as a reference as the work progresses. Working with biologists, detailed observations will be made on the morphology and kinematics of tuna (using both μCT scans or high-resolution video recording. By fully understanding the biology, key parameters will be identified for study to understand their influence in propulsive performance. Hypotheses are generated and explored using innovative engineering analysis tools, such as a coupled computational fluid-structure interaction solver. Experiments are performed using the results from the numerical analysis. Ultimately, these results will be used to generate design guidelines for bio-inspired propulsors.

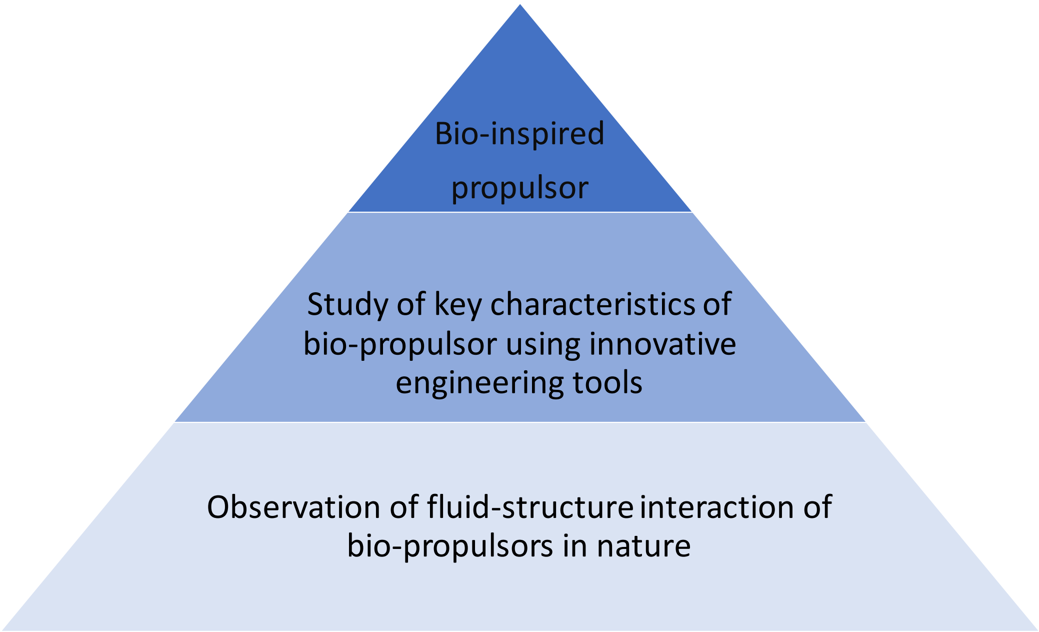

Figure 1.3 Research objectives

The goal of the dissertation research is to better understand non-uniform stiffness as a key characteristic that contributes to a high-performance bio-inspired propulsor. Performance in this study will be focusing on propulsive efficiency during rectilinear swimming. Non-uniform stiffness in the study is manifested as peduncle stiffness, anisotropy and 2D stiffness distributions. To achieve the goal, the following questions will be addressed:

1. What is the range of structural and material flexibility observed in biology (tuna)?
2. How does peduncle joint (stiffness) affect propulsive performance of a bio-inspired foil?
3. How does shape and directional stiffness affect performance of rectangular foils?
4. Using a square foil as baseline, how should engineers design a bio-inspired propulsor, from the perspective of stiffness distribution?

1.2 Approach

In this study, a combination of experimental and computational methods will be used to study the non-uniform flexibility in underwater propulsion, and its effects on propulsive performance and wake structure. A variety of propulsors with canonical and bio-inspired shapes will be designed and tested under sinusoidal motion inside a water tunnel setup with uniform flow. Propulsive performance including thrust, power and efficiency will be measured for each trial, and high-speed photography and Particle Image Velocimetry (PIV) will be used to visualize kinematics and flow of selected cases, highlighting the difference between high performance and low performance propulsion. The data collected from water tunnel experiments will be used for both validating the CFD solver and serving as baseline cases for the larger design space. Additionally, CFD will be used to visualize the 3D flow structure and to explore the design space beyond current manufacturing and experimental capabilities. Conversely, the preliminary results from CFD will be used to trim down the parameter space for physical experiments to areas of interest.

1.3 Overview

- **Chapter 2** gives an introduction to the field of bio-inspired propulsion and flexibility. The underlying mechanisms of fish-like swimming are considered and a literature review is given to highlight the theoretical, computational and experimental study by past research projects. In particular it highlights the areas of the field where significant further effort is needed.

- In **Chapter 3** mechanical testing is employed to determine the range of biological stiffness observed in biology, especially the fin rays and tendons of tuna. Video tracking is employed to quantify direction and extent of bending in tuna swimming, or thunniform swimming (Chapter 2.2). Results in this section together with other previous study provide guidance for my simulation and experiment design in the following chapters.

- **Chapter 4** explores the role of peduncle in thunniform swimming. A simplified fish-shaped foil model is used to study the effects of phase offset (computationally) and flexural stiffness (experimentally) on swimming.

- **Chapter 5** demonstrates the preliminary study of the effects of shape and stiffness on flexible rectangular propulsors. Most results here serve as inspiration for work described in Chapter 6.

- **Chapter 6** studies effects of non-uniform stiffness on propulsive performance of heaving square foils. The results are used to study if the chordwise and spanwise stiffness can be modeled as linear additive properties to predict efficiency gain. Design guidelines for bio-inspired propulsors are also derived from the results.

- **Chapter 7** gives a brief discussion of the results, gives concluding remarks, and considers some projects for future work.

PUBLICATIONS

Works adapted from Chapter 3

Zhu, R., Wang, J., Lewis, G., Zhu, J., Dong, H., Bart-Smith, H., ... & Lauder, G. V. (2017). Propulsive performance of pitching panels with bio-inspired passive directional flexibility. In *47th AIAA Fluid Dynamics Conference* (p. 3980).

Works adapted from Chapter 4

Zhu, R., Wang, J., Dong, H., Quinn, D., Bart-Smith, H., Di Santo, V., ... & Lauder, G. (2019). Computational study of fish-shaped panel with simultaneously heaving and bending motion. In *AIAA Scitech 2019 Forum* (p. 1655).

Effects of Passive Peduncle Joint Stiffness on Propulsive Performance of Tuna-Inspired Foils (Draft prepared for Bioinspiration and Biomimetics)

Works adapted from Chapter 5

Zhu, R., Wang, J., Lewis, G., Zhu, J., Dong, H., Bart-Smith, H., ... & Lauder, G. V. (2017). Propulsive performance of pitching panels with bio-inspired passive directional flexibility. In *47th AIAA Fluid Dynamics Conference* (p. 3980).

Works adapted from Chapter 6

Zhu, R., Wang, J., Dong, H., & Bart-Smith, H. (2020). Effects of Chordwise Non-uniform Stiffness on Propulsive Performance of Passively-flexing Square Foil. In *AIAA Scitech 2020 Forum* (p. 0804).

The effects of combining chordwise and spanwise stiffness on propulsive performance of heaving foils (Draft prepared and under review for Bioinspiration and Biomimetics)

2. BACKGROUND AND LITERATURE REVIEW

In this chapter, fundamental knowledge on fluid physics and biology are introduced to prepare the readers for latter chapters. Then a survey of previous research is conducted to clarify the current progress and works to be done in fields related to this dissertation.

Research has been carried out for more than a century on the effects of shape and stiffness of caudal fin on swimming performance in fishes (Affleck, 1950; Breder, 1926; Gibb, Dickson, & Lauder, 1999; Lauder, Flammang, & Alben, 2012). One major subfield of interest is high-speed economical swimming of Scombrid fishes (Dewar & Graham, 1994; Donley, Sepulveda, Konstantinidis, Gemballa, & Shadwick, 2004; S. L. Katz, Syme, & Shadwick, 2001), including tuna. Extensive research has been conducted on the lunate tail theoretically (Chopra & Kambe, 1977; Lighthill, 1970; Wu, 1971), computationally (Iman Borazjani & Daghooghi, 2013), and experimentally (Feilich & Lauder, 2015; M. N. Rosic et al., 2017).

2.1 Lift-Based Unsteady Propulsion

When engineers and biologists are studying fish swimming, models of different levels of complexity are often used. It is important to have uniform definition of key parameters for unsteady propulsion, whether observing a live fish swimming or a 2D canonical foil in computer simulation. In the simplest form (Figure 2.1), a fish or the tail part can be approximated as a foil of length L oscillating with frequency f and amplitude of motion A in a fluid environment. The exact definition of amplitude of motion differs. Most researchers either use the tip-to-tip amplitude of the leading edge or the trailing edge. From this simplistic perspective, two canonical non-dimensional parameters can be derived. They are the Reynolds number to describe the flow regime of a fish through a fluid and the Strouhal number to characterize the ratio of lateral foil motion (heave and pitch combined) to streamwise motion.

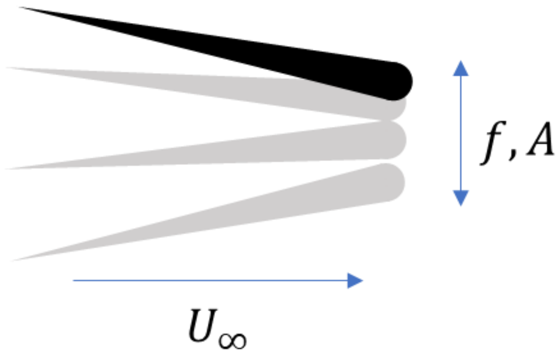

Figure 2.1 Oscillating foil with frequency f, amplitude A traveling at speed U_∞ in fluid, with mechanism of force generation explained in Figure 1.1

The Reynolds number is given by

$$Re = \frac{U_\infty L}{\nu}$$

Equation 2-1

where U_∞ is the swimming speed of the fish, L is the length of its propulsor (tail in the case of tuna), and ν is the kinematic viscosity of the fluid. It represents the ratio, and thus the relative importance, between inertial and viscous forces. In general, large fish like tuna typically swim in the inertial regime at $Re > 5000$ where the viscous effects are negligible. In this dissertation, all the Reynolds numbers are calculated using the chord length of propulsors, instead of the whole-body length.

The Strouhal number is given by

$$St = \frac{fA}{U_\infty}$$

Equation 2-2

where f is the oscillation frequency of hydrofoil in Hz and A is the width of the wake (approximated as the peak-to-peak oscillation amplitude of the hydrofoil in most previous research (Dewey et al., 2013), as in simulation and experiments covered in this dissertation). To estimate the range of Strouhal number during the experiment and simulation design phase, a preliminary Strouhal number is calculated using the prescribed leading-edge amplitude. When further analysis involving Strouhal number is needed in the results and discussion sections, value based on trailing edge amplitude is used if such measurement is feasible. An experimental study on oscillating foils was conducted by marine engineers to predict an optimal Strouhal number for swimming animals within the range of $St = 0.25 - 0.35$ (G. S. Triantafyllou, Triantafyllou, & Grosenbaugh, 1993), and previous study collecting swimming data showed that many animals do swim within this regime (Taylor, Nudds, & Thomas, 2003; G. S. Triantafyllou et al., 1993).

2.2 Tuna and Other Bio-Inspired Propulsion

The main function of the caudal fin of tuna and tuna-like species (Figure 2.2) is for propulsion (Lauder et al., 2012). The high aspect ratio (Figure 2.2), lunate-shaped flexible tails of *Scombridae* fishes (generally predators of the open ocean) such as mackerel and tuna contributed to high-speed, propulsively efficient swimming and high thrust generation. Aspect ratio in most cases and previous research is defined as the ratio of span to chord. The only exception is in section 5.2.1 where the aspect ratio is defined as ratio of chord to span to make comparison with other results in literature (Yeh & Alexeev, 2016) more straightforward.

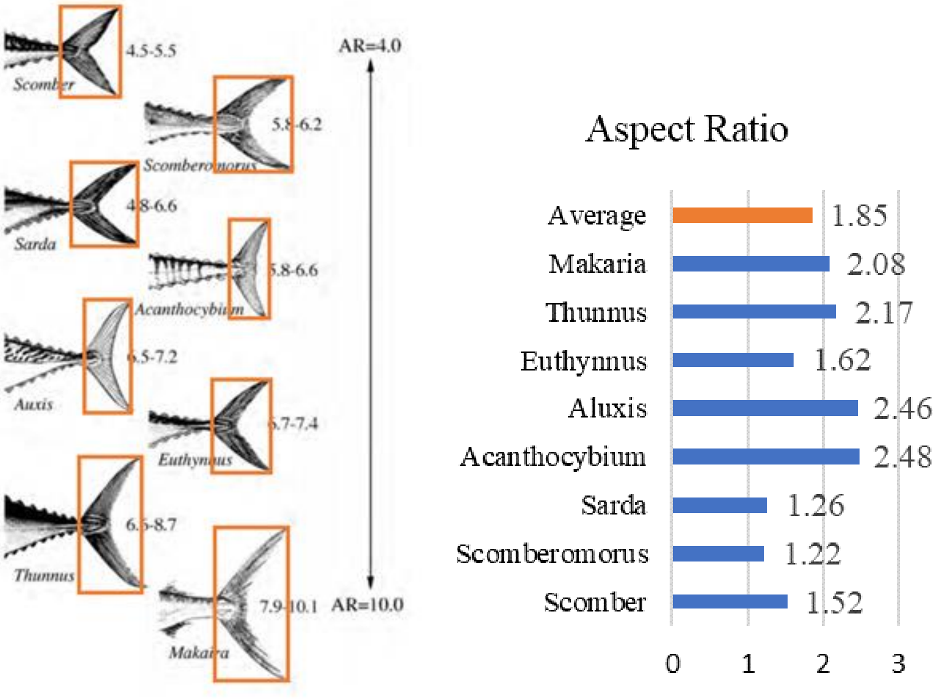

Figure 2.2 Scombrid caudal fins (Adapted from Westneat & Wainwright 2001)

Tuna, as representative species of BCF swimmers, are fast, efficient, and with high aspect ratio lunate caudal fins. In BCF locomotion the fish generates a backward moving traveling wave along the length of its body and extending to the caudal fin. BCF locomotion is further classified by the fraction of the body length that participates in generating the traveling wave motion as shown in Figure 2.3 (Lindsey, 1978). There has been ongoing unpublished research on reconsidering the classification of fish by waveforms of centerlines. Thus, thuuniform swimming is used in this dissertation only to refer to swimming of tuna and tuna-like species, rather than emphasizing the uniqueness of their centerline kinematics.

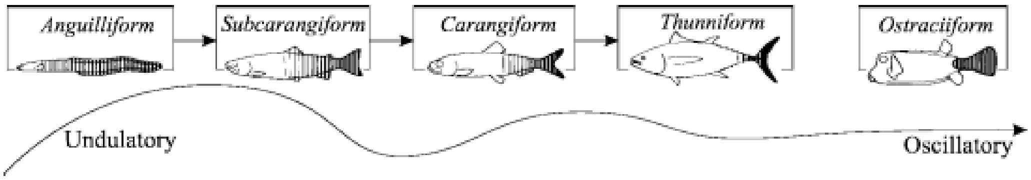

Figure 2.3 Swimming modes associated with BCF propulsion. Shaded area contributes to thrust generation. (Adapted from Lindsey 1978)

Simplified physical models and more bio-inspired models have been developed to study the effects of shape and flexibility on swimming performance(Affleck, 1950; Chopra, 1974; Feilich & Lauder, 2015; Karpouzian, Spedding, & Cheng, 1990; Lighthill, 1970; Wu, 1971). It is a challenge to uncouple these two parameters in order to quantify their respective roles in the propulsive performance. Attempts have been made to decompose underwater animal locomotion orthogonally (F. Fish et al., 2016; G. Liu, Ren, Zhu, Bart-Smith, & Dong, 2015).

For more simplified models, experimental flow tunnel tests of homogenous flexible foils (Dewey et al., 2013; Kancharala & Philen, 2014; Quinn, Lauder, & Smits, 2015, 2014; Shelton, Thornycroft, & Lauder, 2014) exhibit a combination of chordwise and spanwise deformations but the relative contributions cannot be determined. Additionally, the amount of flexion exhibited in either orientation is greatly influenced by the method of attachment at the leading edge. In almost all the flow tunnel tests, the homogeneous flexible foils exhibit dominantly chordwise flexibility, due to the common leading-edge fixture method, where the leading edge is fully mounted to the pitching/heaving rod.

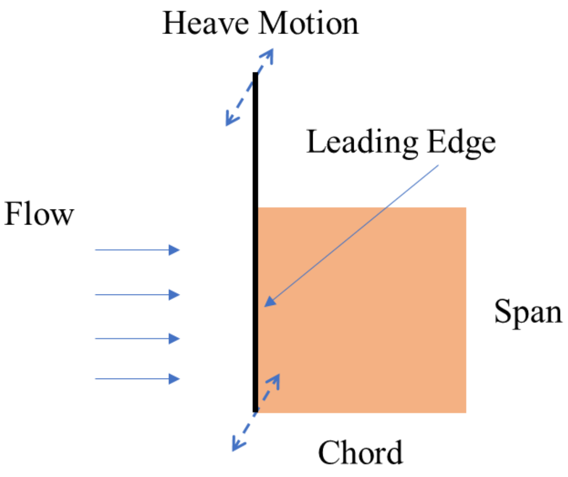

Figure 2.4 Definition of chordwise, spanwise, leading edge and other common terms referred in later chapters

A previous numerical study conditions (Q. Zhu, 2007) has explored the effects of spanwise versus chordwise flexibility of airfoil panels under low versus high Reynolds number. The simulation prescribed pitching motion with pure chordwise or spanwise flexibility by changing the fixed boundary from leading edge to mid-span, which is challenging for biological and bioinspired propulsors, since the propulsor is attached to the body at a constant location and cannot be changed during propulsion.

2.3 Peduncle Joint

Previous efforts to understand lift-based propulson in high-performance swimming has focused primarily on the effects of shape and stiffness of the caudal fin. However, the peduncle region of tuna tail (Figure 2.5) lacks a parametric study to determine its effects on propulsive performance. Previous morphology studies by biologists (Westneat, Hoese, Pell, & Wainwright, 1993; Westneat & Wainwright, 2001) show that the peduncle of mackerels (Figure 2.6) has similar structure as that of tuna.

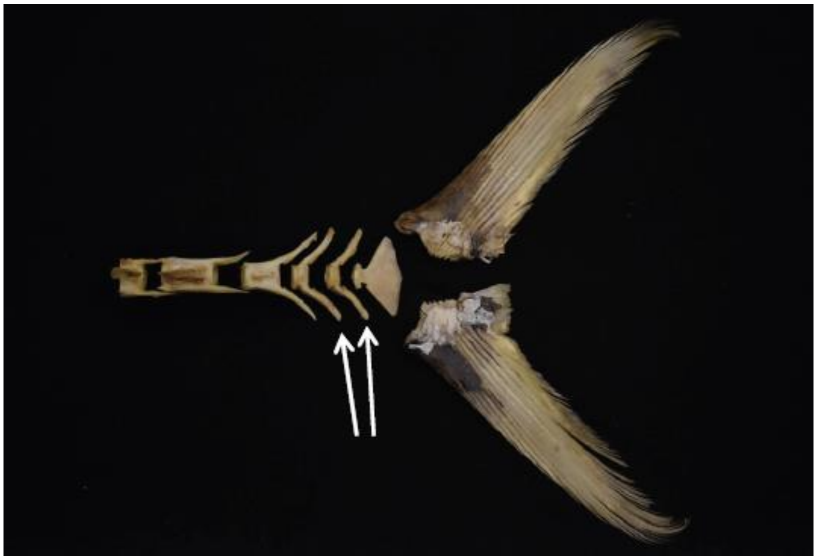

Figure 2.5 The skeletal structure of the tail of an albacore tuna. White arrows designate the two narrow bones which allow the peduncle to rotate. Adapted from master thesis by Lewis 2017, UVa.

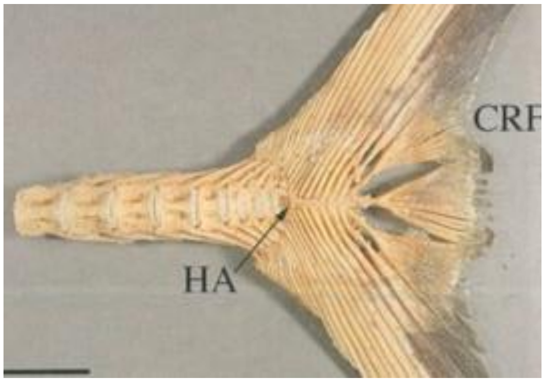

Figure 2.6 Morphology of the caudal fin skeleton in Atlantic Spanish mackerel (*Scomberomorus maculatus*) Adapted from Westneat & Wainwright, 2001.

The bending stiffness is provided mostly by tendons covering the joint (Figure 2.7). Previous research (J. Zhu et al., 2019) has shown that an artificial peduncle joint can improve the performance of a tuna-inspired robot testing platform, however only one single value of stiffness was tested.

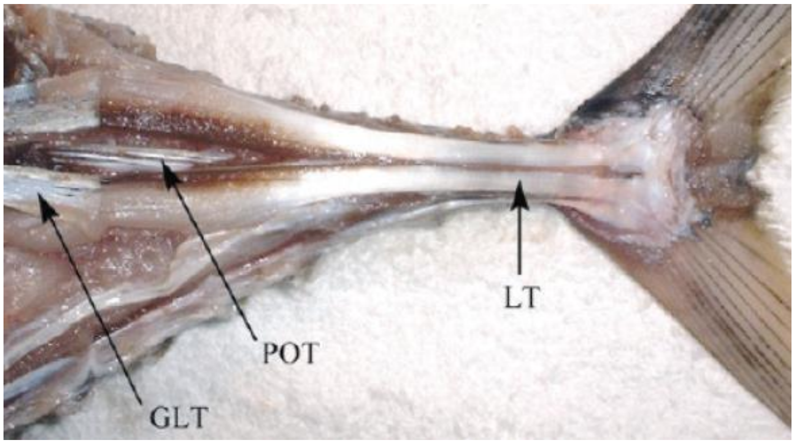

Figure 2.7 A dissection of a yellowfin tuna showing the great lateral tendon (GLT), lateral tendons (LT), and posterior oblique tendons (POT). The secondary pair of lateral tenons is not visible here. Adapted from Shadwick et al. 2002.

There exists a gap between the canonical model and the complex geometry of a tuna tail, which is composed of a peduncle joint and a caudal fin. Previous research has shown that adding a certain amount of uniform flexibility to a fish-inspired foil (Feilich & Lauder, 2015; M. N. Rosic et al., 2017) can improve its propulsive performance. However in these studies, the peduncle region has the same material properties as the rest of the system. There lacks a clear understanding of how changing the extent of stiffness at the peduncle region can affect propulsive performance of a fish-inspired foil system composed of lateral body, peduncle and caudal fin. The biological peduncle stiffness is non-uniform within its own region due to the complex tissue structure. However the peduncle model studied in Chapter 4 is simplified, where the non-uniform stiffness is referring to the different material propeties of peduncle region compared to those of the rest of the fish-shaped foil.

2.4 Fluid-structure Interaction of Bio-Propulsors and Bio-Inspired Foils

Fluid-structure interaction (FSI) (Dowell & Hall, 2001) in the case of underwater propulsion means that the deformable structure of fish body and fins interact with the surrounding fluid (water) to reduce the effects of certain fluid forces.

In engineering, the fish fins are often simplified as flexible foils. In general, uniform flexibility can improve the thrust and efficiency of foils with sinusoidal motion (Dewey et al., 2013; Quinn et al., 2015), and optimal performance is achieved when the uniform flexibility and kinematics are tuned for resonance. Biomimetic models mimicking caudal fins have been used to study individual forms of flexibility. For example, adding chordwise flexibility to a rigid foil can increase its efficiency with little compromise on thrust, regardless of the shape of the foil(J. Katz & Weihs, 1978; Lucas et al., 2015; Prempraneerach, Hover, & Triantafyllou, 2003). Adding spanwise flexibility to a foil is going to reduce its thrust and efficiency when the flexibility is dominantly passive, but efficiency enhancement can be achieved when the spanwise flex is actively controlled to be out of phase with the foil kinematics (P. Liu & Bose, 1997; Q. Zhu, 2007). Artificial fin ray rigidity has been demonstrated to be proportional to thrust and lift generated by the artificial pectoral fin (Flammang, Alben, Madden, & Lauder, 2013; Tangorra et al., 2010), but little research has been done on changing the stiffness distribution of caudal fin.

For tuna, almost all body parts demonstrate FSI during swimming (Wainwright & Lauder, 2020). Tuna caudal fin is chosen as the inspiration of FSI study in this dissertation because its deformation is mostly caused by passive material properties. The morphology and material properties of flexible bluegill sunfish caudal fin (Figure 2.8) composed of fin rays has been studied carefully (Esposito, Tangorra, Flammang, & Lauder, 2012; Lauder, Madden, Tangorra, Anderson, & Baker, 2011). These caudal fins, including those of tuna (Figure 2.9) tend to have 2D stiffness distribution due to the fin ray arrangement (Wainwright & Lauder, 2020). The mechanical properties of tuna caudal fin rays lack studying. Chapter 3 of this dissertation will take some initial steps at addressing the knowledge gap.

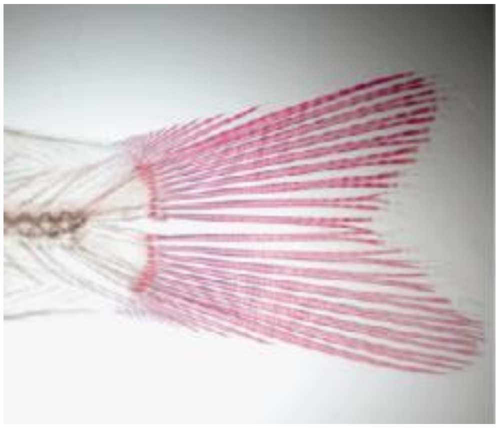

Figure 2.8 Flexible caudal fin of a bluegill sunfish (Adapted from Lauder 2011)

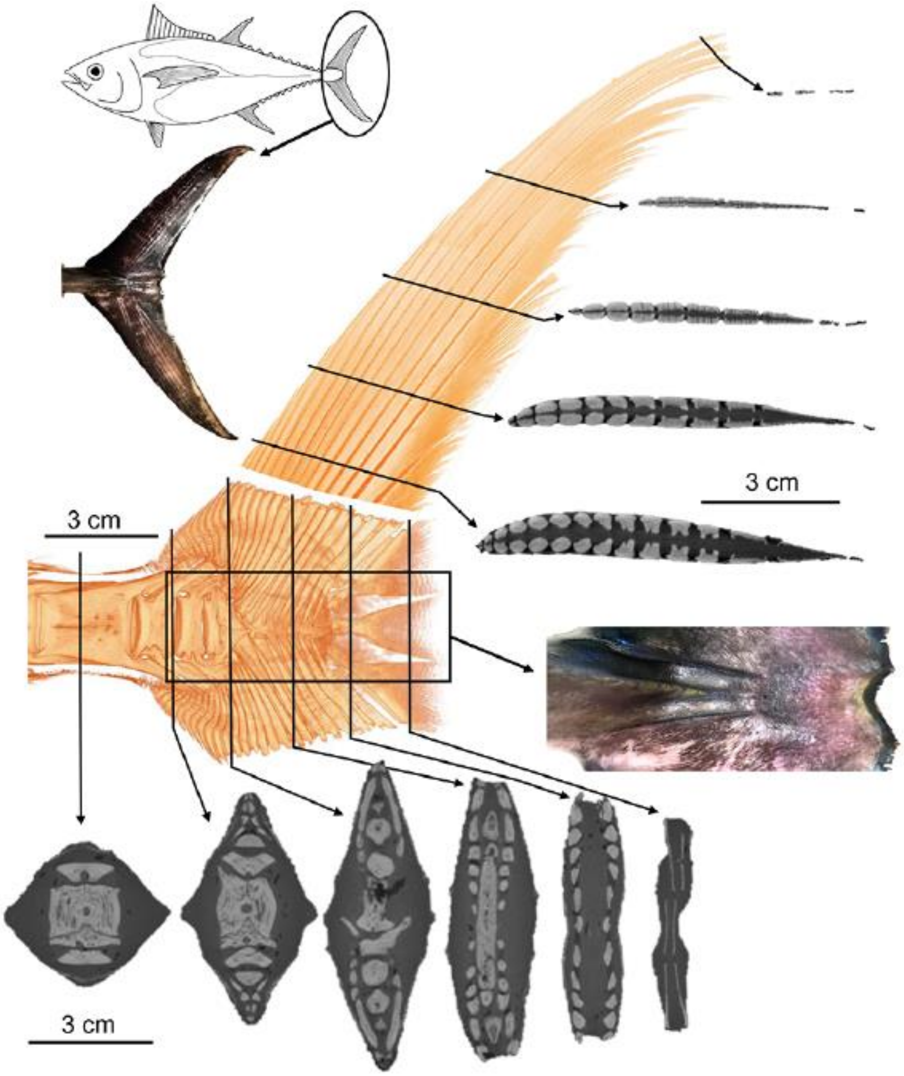

Figure 2.9 Caudal fin morphology of yellowfin tuna (Thunnus albacares) with a volume render of two µCT scans shown in orange color. Adapted from Wainwright 2020.

Animal propulsors such as fins bend during motion and these bending patterns as shown in Figure 2.10 are believed to contribute to the high efficiency of animal movements compared with those of man-made designs (Lucas et al., 2014). Observation of kinematics shows an average bending location around two-thirds of the body or propulsor length with an average angle of 30 degrees across different species. However, this research does not clarify the causes of bending for different species, whether it is due to active control or passive properties. There lacks clear understanding of the role played by passive propulsor flexibility or how bio-inspired flexible propulsors should be designed for optimal performance.

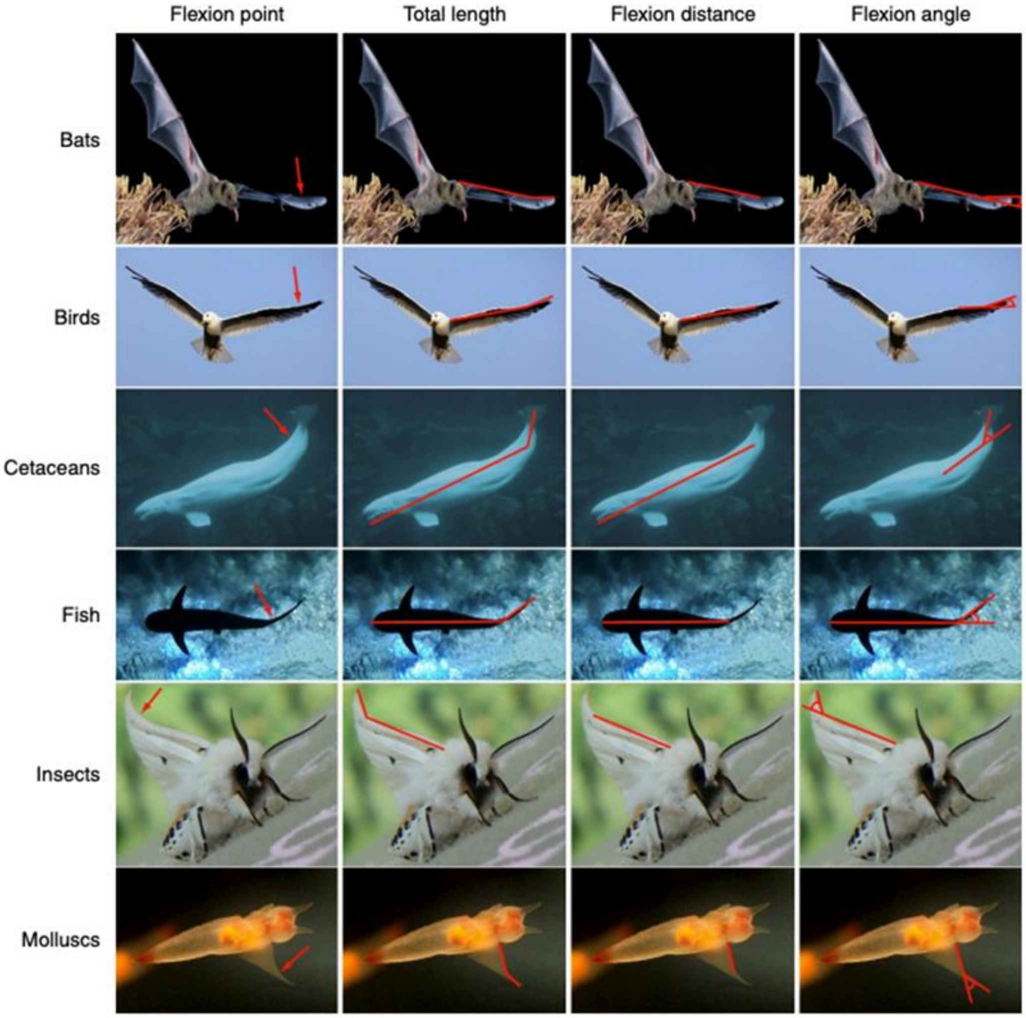

.

Figure 2.10 Bending patterns observed in biology, where bending usually happens around two-thirds of the length. Adapted from Lucas 2014.

On the engineering side, the stiffness distributions designed in the previous studies are either purely chordwise, purely spanwise, or a complex replica of a biological fin. On the biology side, the study of underwater propulsor flexibility is mostly focused on observation of overall kinematics, which engineers find hard to transfer the knowledge of biological flexibility to underwater vehicle design. There has not been a parametric study of how two-dimensional (2D) distributions of chordwise and spanwise stiffness collectively affect the propulsive performance of a canonical propulsor like a heaving foil. In the dissertation, a range of simplified 2D stiffness distribution is applied to canonical shapes to isolate the effects of 2D stiffness from bio-inspired shapes. The last project covered in this dissertation aims at addressing this question and provides a methodology framework for future study.

Another question that requires further attention is the role that resonance plays in enhancing underwater propulsive performance. It is now generally accepted that thrust enhancement can be achieved through operating near a structural resonant frequency in water or air (Dewey et al., 2013; Kang, Aono, Cesnik, & Wei, 2011), however the relation between resonance and efficiency enhancement is quite different regarding the surrounding fluid. Optimal frequency in terms of efficiency is closer to first resonant frequency for underwater propulsors (Dewey et al., 2013; Leftwich, Tytell, Cohen, & Smits, 2012), while much lower than first resonant frequency for air propulsors (Kang et al., 2011; Ramananarivo, Godoy-Diana, & Thiria, 2010; Vanella, Fitzgerald, Preidikman, Balaras, & Balachandran, 2009).

2.5 Summary

A survey of past literature highlights that most of the research conducted in bio-inspired propulsion has focused on foils with uniform or non-uniform chordwise stiffness. There is a clear void of in the literature when it comes to understanding the propulsive performance of three-dimensional foils with anisotropic non-uniform stiffness. To understand the hydrodynamics of tuna, which utilize a complexly flexible tail to generate thrust, these parameters need to be further explored. This thesis strives to achieve this by conducting a series of experiments and simulation that systematically isolate variables associated with bio-inspired propulsion.

3. MATERIAL AND MORPHOMETRIC PROPERTIES OF TUNA

3.1 Introduction

This chapter aims at getting quantitative data on the material and morphometric properties of tuna to better understand the fluid-structure interaction (FSI) and serves as the foundation for the dissertation.

Tuna belong to the family *Scombridae* with mackerel, spanning about 15 species and sharing several key internal and morphological features that make them high-performance swimmers. Features being studied in this chapter include peduncle joints covered with tendons, caudal fin with individual fin ray structure and the consequent caudal fin bending during swimming.

Tuna caudal tendons is the most studied feature among the three. A biomechanical study on tendons still attached to caudal fin (Robert E. Shadwick, Rapoport, & Fenger, 2002) has been conducted to determine the mechanical properties of tuna caudal tendons (mean modulus of elasticity of 1.3 GPa), comparable with those of leg tendons from adult mammals. However, the individual properties of the tuna tendons have not been tested. This chapter provides additional tensile test results of fully excised tendons to the current pool of tuna tendon test results.

Individual tuna caudal fin rays have not been studied biomechanically before. Biologists have tried using them as aging character for certain species (Cort, 1991).

A biomechanical study (Lauder et al., 2011) has been carried out on bluegill sunfish (*Lepomis macrochirus*) fin rays to show that the fin rays are very deformable given the swimming kinematics of sunfish. This chapter provides dimension measurements of individual tuna fin rays and flexural modulus calculated from three point bending tests.

Last, curvature method is used to measure the degree of flexibility observed in rectilinear swimming of a tuna. Similar methods have been applied to study trunk deformation of other fish species during swimming (Han et al., 2017). The curvature data of tuna swimming demonstrate flexibility of the caudal fin in both chordwise and spanwise directions and inspired the work in Chapter 5 and 6 on non-uniform stiffness.

3.2 Methodology

3.2.1 Tensile Test of Tendons

Protocol of tendon tests:

1. The tuna tail sample is excised.
2. Individual tendons are excised using a lancet, after removing the surface tissue (skin and flesh).
3. Each tendon is wrapped in paper soaked with 35,000 ppm saline water during the overnight transportation process.
4. The tendon is clamped between standard tensile test fixtures with sandpaper on the inner surface to increase grip.
5. Strain rate of 0.01 s^{-1} is applied during the tensile test, with slipping as the ending condition.
6. Each specimen can only undergo one trial, since plastic deformation is involved in the process.
7. Dimensions are measured after the tensile test (detailed in method section).

The structure of the tuna peduncle is mostly skeletal, with tendons spanning the joint, connecting the red muscle mass in the trunk to the base of caudal fin. There are several major tendons on each side as shown in Figure 3.1a (Robert E. Shadwick et al., 2002): the great lateral tendon (GLT), one pair of lateral tendons (LT), one pair of minor LTs and several posterior oblique tendons (POT). The joints at the peduncle region are constrained by the stiffness mostly provided by tendons, with some additional stiffness from skin and other tissue. There also exists a maximum bending angle due to the bone structure of the joints.

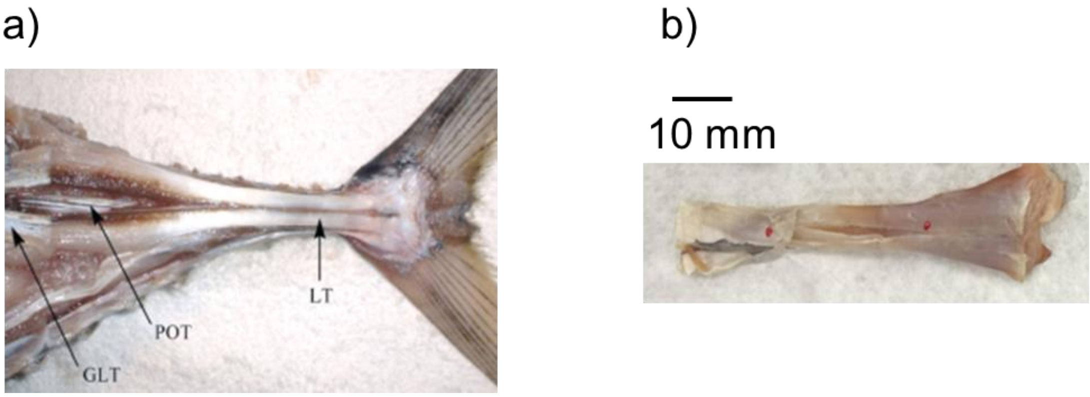

Figure 3.1 (a)Tuna tendons (adapted from Shadwick et al. 2002), (b) Example of a single excised tuna lateral tendon

Samples of the LTs from yellow fin tuna were subjected to tensile mechanical tests, using an Instron 5848 micro tester (Instron, Norwood, MA, USA). Specimens were dissected completely off the tail (Figure 3.1b), wrapped in paper soaked with 35,000 ppm saline water during the transportation, and clamped in standard Instron tensile test fixture with additional grip from sand paper, then mounted in the test machine as shown in Figure 3.2. Two 1-mm-wide reflective strips were glued perpendicular to the tendon axis and tracked by a laser extensometer. The distance separating these markers was used for calculating strain. The tendon samples were subjected to a linear stretch motion, at strain rates of 0.01 s^{-1}, until tensile failure or more often, slipping at the grips occurred. Force and strain data were recorded on a computer using Instron data acquisition software (Figure 3.3). At the end of the experiment, the section of tendon between the reflected markers was excised and its length and blotted weight were recorded. The average cross-section area was calculated by dividing the mass by its length and assumed density, 1120 kg m^{-3} (R. E. Shadwick, 1990). For all mechanical tests, the data were normalized by the sample dimensions to yield tensile stress in MPa and dimensionless strain. The Young's modulus, a measure of the elastic stiffness of the tendon was calculated as the slope of the near-linear portion of the stress-strain curve after linear fit and expressed in GPas.

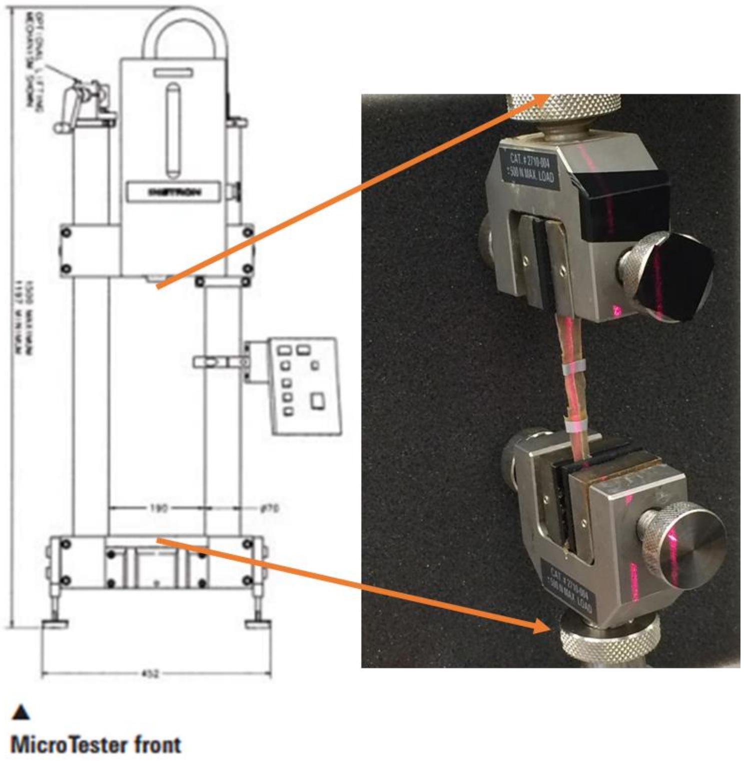

Figure 3.2 Mechanical testing apparatus, schematic of MicroTester provided by Instron. The orange arrows show where the tensile testing fixture (with a tendon specimen clamped) are attached to the rig.

3.2.2 Bending Test of Fin Rays

Protocol of fin ray tests:

1. The half tuna tail sample is excised and frozen during the overnight transportation process. The sample is thawed in room temperature.

2. Individual fin rays are excised using a lancet, where the cut location should align with the gap between individual fin rays (Figure 3.4a)
3. Fin ray specimen 1 to 7 (Figure 3.4a) is chosen based on length, as it needs to be longer than 30 mm to stay stable on the three-point bending fixture
4. The mid 30 mm section of each fin ray is chosen, and width and thickness values at tip and base are measured using a caliper.
5. Strain rate of 0.01 min^{-1} is applied during the three-point bending test following ASTM D790 protocol. The three-point bending test is repeated for 3 times.

Fin rays excised from half of a caudal fin (Figure 3.4a) were tested using a standard 3 point bending test protocol (ASTM D790) as shown in Figure 3.3. Tip and base are defined as 15 mm from the center of the fin ray on each side, with total support span L of 30 mm (Figure 3.4b). Dimensions (width b and thickness d) at tip and base of each fin ray is measured using a caliper, recorded in Table 3.1 and presented in Figure 3.5, from which we can see that the fin rays all have an almost linearly tapered shape, similar to observation from µCT scan of bluegill sun fish pectoral fin rays in previous study (Lauder et al., 2011; Tangorra et al., 2010). Flexural modulus is calculated and presented in Figure 3.6 using the 3-point bending test formula,

$$E_f = \frac{L^3 m}{4bd^3}$$

Equation 3-1

where m is the slope of the near-linear portion of the load deflection curve (N/mm), b and d are averages of tip and base, and error bar comes from 3 repeated trials per test.

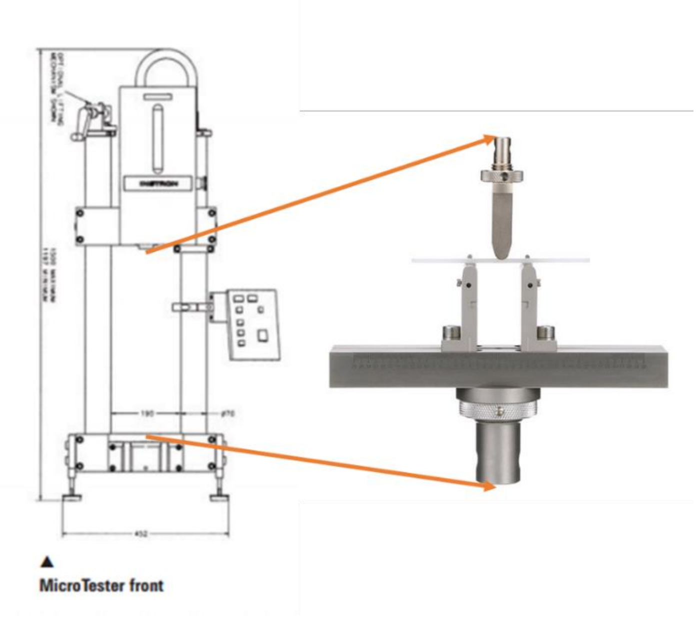

Figure 3.3 Mechanical testing apparatus, with schematic of MicroTester provided by Instron. The orange arrows show where three point bending test fixture is attached to the rig.

Table 3.1 Dimensions of fin ray specimens (mm), measurement error +/- 0.05mm

Specimen	Tip Width	Base Width	Tip Thickness	Base Thickness
1	2.2	2.4	3.7	3.9
2	2.6	2.8	3	3.2
3	4	4.2	2.9	3.1
4	3.1	3.4	2.9	3.1
5	3.3	3.5	2.4	2.7
6	2.2	2.5	3.2	3.5
7	2.7	3	2	2.4

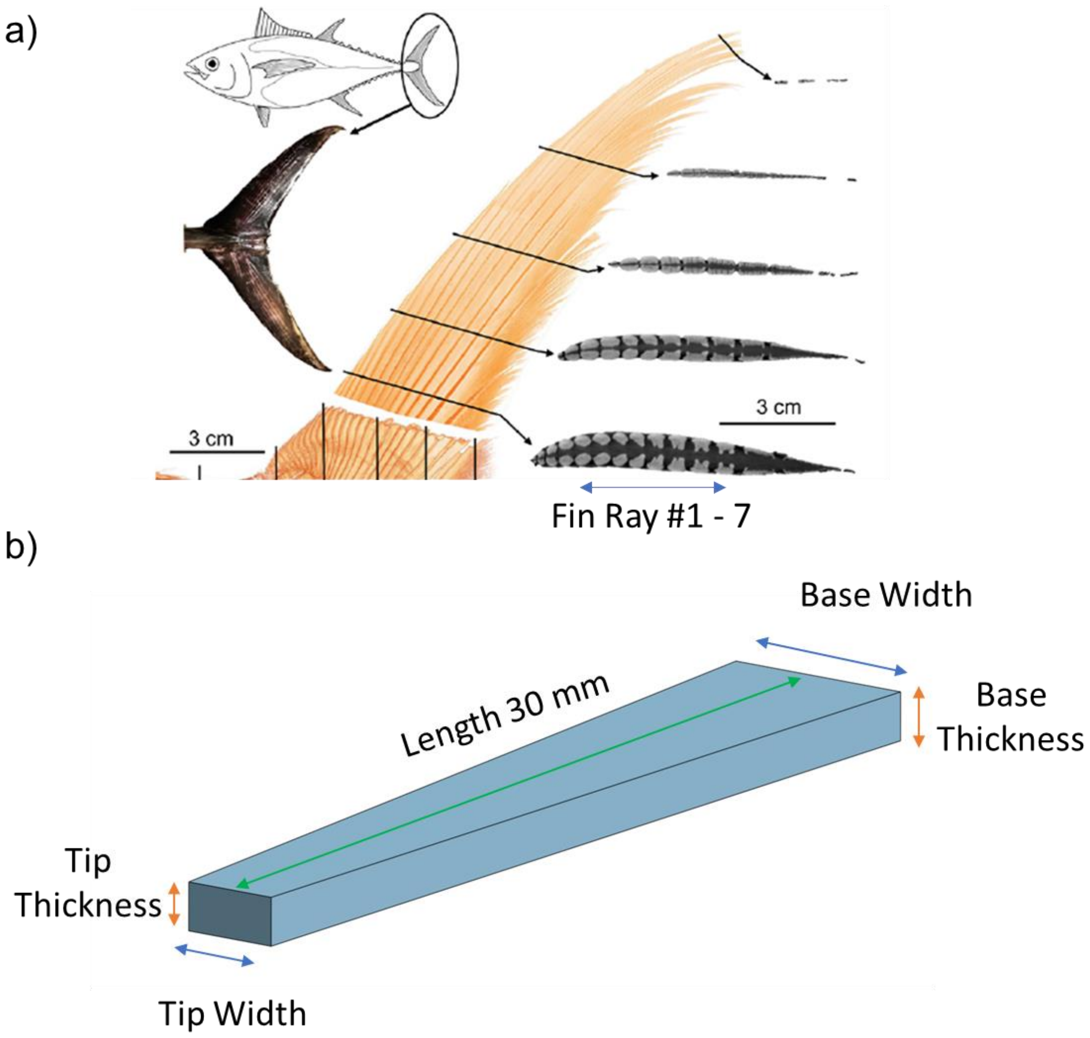

Figure 3.4 (a) Tuna caudal fin ray volume render and selected specimen labels. Adapted from Wainwright et al. 2020 (b) Fraction of the fin ray specimen between the two supporting points

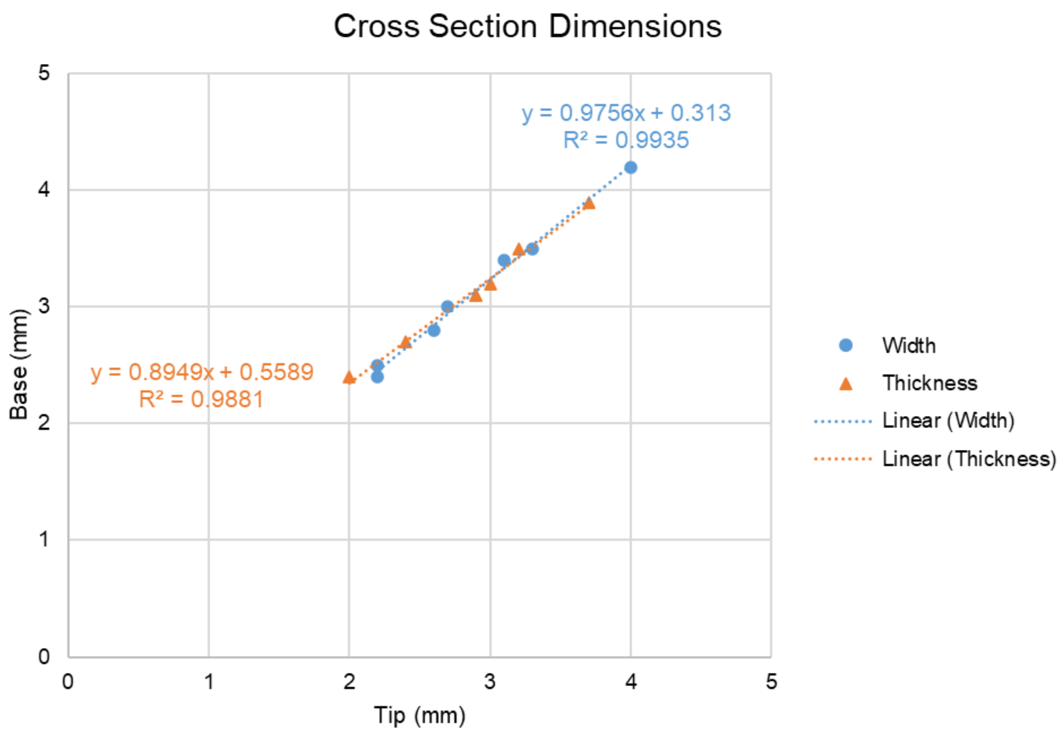

Figure 3.5 Dimensions of fin ray specimen. The measurement error of caliper is 0.05 mm, which is about the same size as the symbols in the plot.

3.2.3 Measurement of Tuna Caudal Fin Curvature during Rectilinear Swimming

Body and tail kinematics from freely-swimming yellowfin tuna (*Thunnus Albacares*) were obtained at the Greenfins tuna facility at the University of Rhode Island courtesy of Prof. Terry Bradley, which is the first step of our workflow as shown in Fig. 1. Tuna swam in a 151,000-liter tank. Two synchronized Photron high-speed cameras were used to obtain high resolution (1 megapixel) dorsal and side views of the tail at 500 frames per second. As tuna moved past the side view camera and turned, we were able to obtain posterior views showing tail curvature from behind.

There are many ways to define the amount of fin bending. Here the curvature method (Han et al., 2017) is used, which requires tracking of 3 points, as shown in Figure 3.7 and 3.8. We break the video into images sequences using Adobe Photoshop and import images into MATLAB for tracking purpose. For the top view, we choose the start, middle and end point of the caudal fin, while for back view, we choose the top, center and bottom point of the caudal fin. As long as the 3 points are not in one straight line, center location and radius of one and only circle can be determined. We also assign positive (negative) sign to the curvature value if the circle is on the left (right) side of the fish body.

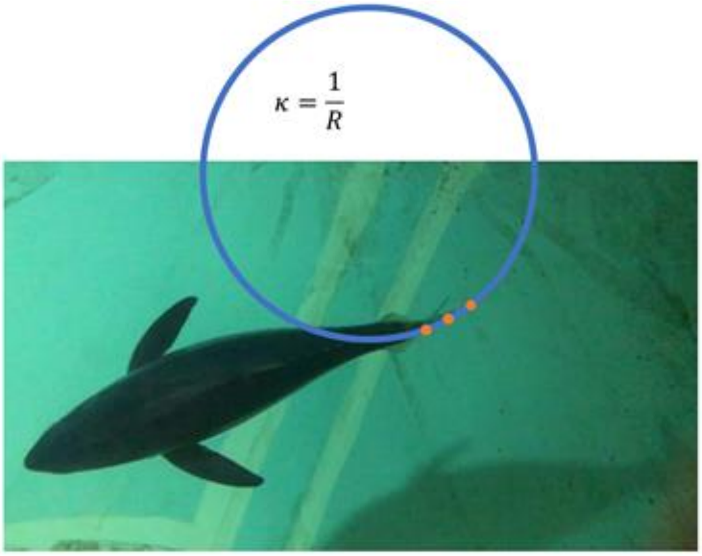

Figure 3.6 Chordwise curvature calculation

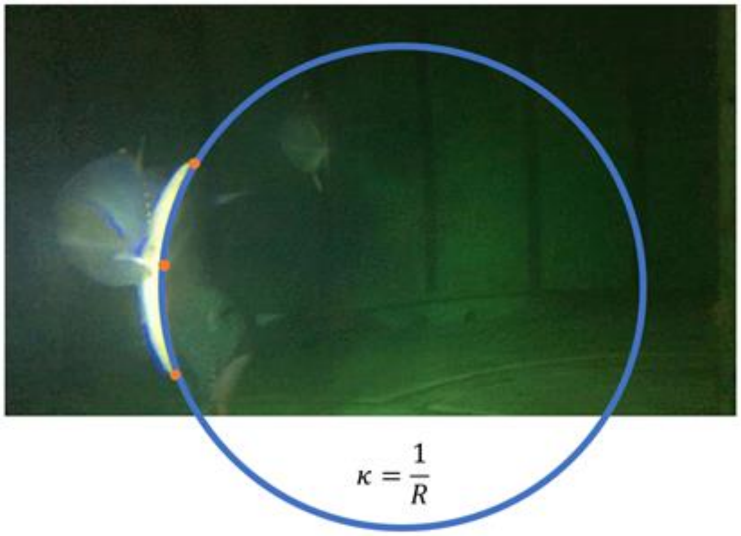

Figure 3.7 Spanwise curvature calculation

3.3 Results

3.3.1 Modulus of Tuna Caudal Tendons

The material properties and dimensions of the four specimens are provided in Table 3.2. The modulus values (Figure 3.8) are comparable with the range of 1.43±0.29 GPa for yellowfin tuna in previous literature (R. E. Shadwick, 1990). All 4 lateral tendons should produce similar force values under same elongation since they are located symmetrically inside the tuna tail. Thus, tendon specimen 4 has a higher modulus due to its smaller cross section.

Table 3.2 Material properties of tuna tendons

Specimen	Length (mm)	Mass (g)	Area (mm^2)	Modulus (GPa)
1	15.1 +/- 0.05	0.27 +/- 0.005	16.1 +/- 0.30	1.54 +/- 0.029
2	14.8 +/- 0.05	0.28 +/- 0.005	16.9 +/- 0.31	1.34 +/- 0.025
3	15.3 +/- 0.05	0.19 +/- 0.005	11.2 +/- 0.30	1.27 +/- 0.034
4	15.2 +/- 0.05	0.16 +/- 0.005	9.44 +/- 0.30	1.93 +/- 0.061

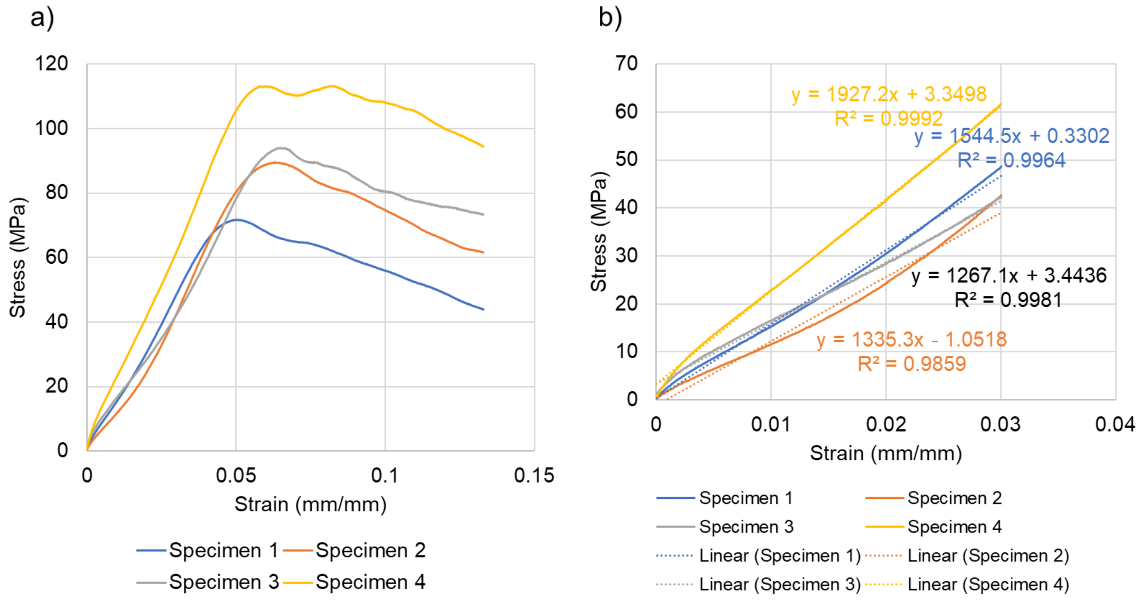

Figure 3.8 (a) Stress-strain curve from tensile tests and (b) Elastic modulus calculated using linear fit for the four lateral tendons from one tail sample

3.3.2 Tuna Caudal Fin Ray Stiffness Distribution

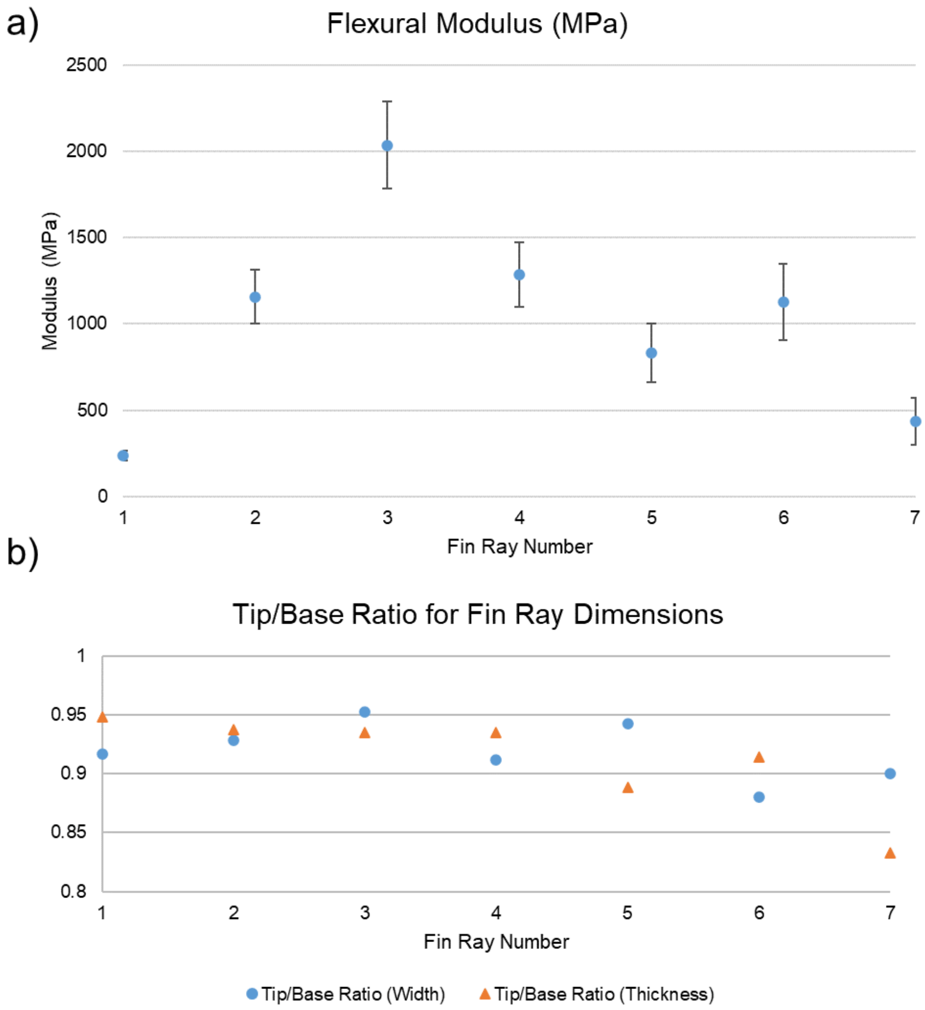

Figure 3.9 (a) Flexural modulus E_f of fin ray specimens, where error is based on three repeated trials per fin ray; (b) Tip/Base Ratio for Fin Ray Dimensions

Flexural modulus and dimensions data show that the caudal fin has higher stiffness near mid-chord due to higher modulus and moment of area. The values are comparable with results in previous study of bluegill sunfish (Lauder et al., 2011), where the average modulus is 1.34 GPa (range of 0.24 – 3.72 GPa). The fin ray modulus for the specimen towards the edges are similar to those for human tendons (0.5 GPa), as pointed by Lauder (2011) that it is because the adjacent fin ray segments are connected collagenous fibers which undergoes stretching during the bending test.

3.3.3 Chordwise and Spanwise Flexibility of Tuna Caudal Fin

If we plot tail motion and curvature data over the same time axis, we find out there is a time lag between flapping motion and curvature, close to half cycle in both chordwise and spanwise views as shown in Figure 3.10 and 3.11. This lag means when the tuna moves its caudal fin from left to right, the fin bends passively towards left, and vice versa. Now if we compare the extent of bending by combining the two curvature plots as shown in Figure 3.12, we find out that the caudal fin bends more in chordwise than spanwise direction.

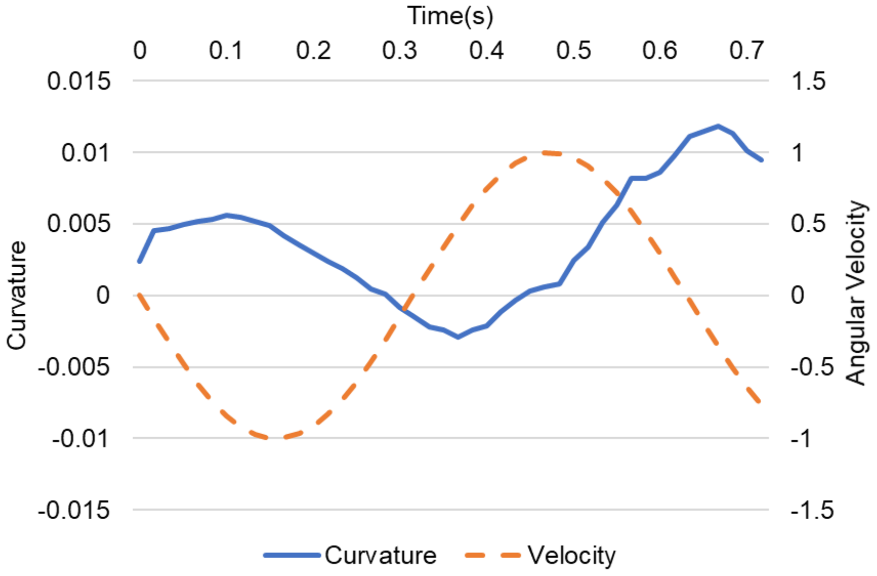

Figure 3.10 Chordwise curvature and angular velocity

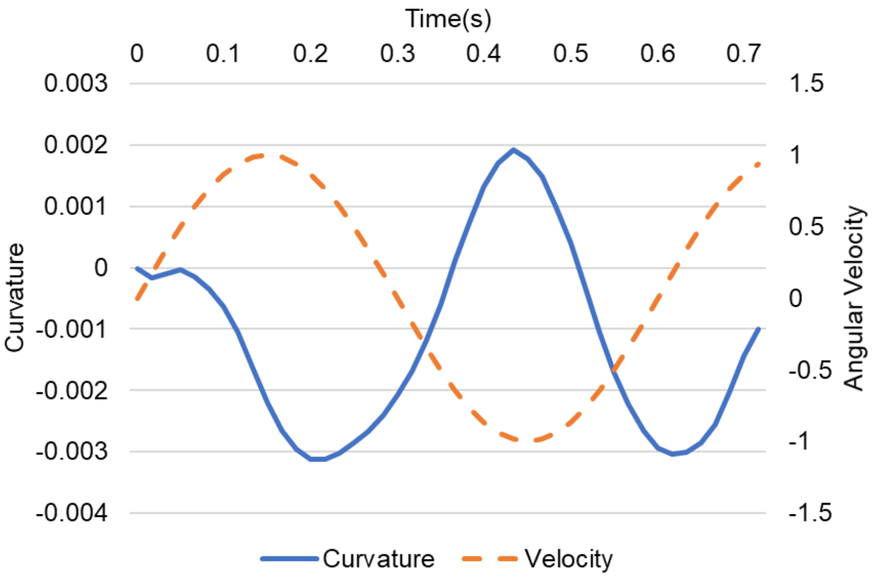

Figure 3.11 Spanwise curvature and angular velocity

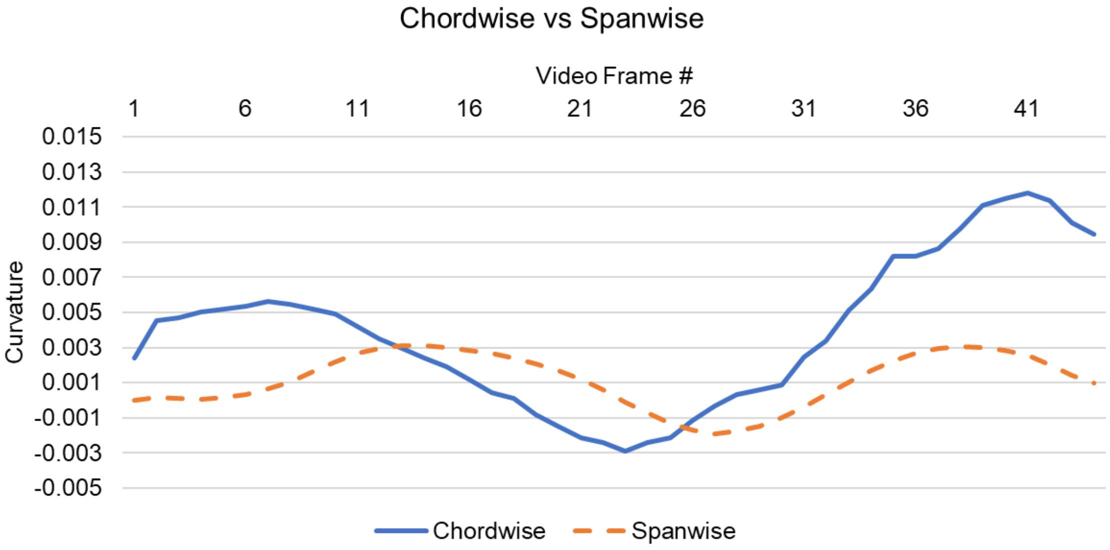

Figure 3.12 Chordwise versus spanwise curvature

3.4 Discussion and Summary of Chapter

Mechanical testing is employed to determine the range of biological stiffness observed in biology, especially the fin rays and tendons of tuna. From the dissection and tensile tests of tuna caudal tendons, elastic modulus is calculated. The values are comparable with those in previous study of tuna tendons (Shadwick et al., 2002). There is one outlying case in my results where the specimen has a higher modulus value to compensate for its smaller cross-section area, so that the overall load-displacement behavior is comparable with other 3 tendon specimens to achieve force balance. Same previous study shows that tuna caudal tendons operate within the elastic regime, which has inspired a simplified elastic beam model for peduncle, covered in Chapter 4. There are more complex and biomimetic models of peduncle in previous and ongoing research. A sandwich beam model is chosen to isolate the stiffness from other factors such as cross-section shape.

From the three-point bending test of fin rays, flexural modulus is calculated. The values are higher than those observed in the study of bluegill sunfish (Lauder et al., 2011). The distribution with higher stiffness towards midspan of the fin is observed in both species, which has inspired the experiment and simulation design in Chapter 5 and 6.

The modulus properties of these tissues are also comparable with ABS plastics (Suarez, Barlow, & Paul, 1984). Thus, it is feasible to use rapid prototyping techniques to design propulsors inspired by tuna. The material property values found in this study support material choice in study covered in Chapter 4 and 5.

Video tracking is employed to quantify direction and extent of bending in thunniform swimming. The bending in both chordwise and spanwise direction is dominantly passive. In addition, the caudal fin bends more in chordwise than spanwise direction. The observation is made based on one video of rectilinear swimming. The difference has inspired a parametric study of chordwise and spanwise flexibility in both isolated and combined arrangement, covered in Chapter 6.

4. THE ROLE OF PHASE OFFSET AND PEDUNCLE STIFFNESS ON PROPULSIVE PERFORMANCE

A simplified model of peduncle joint is studied after achieving better understanding of the material and morphological properties of tuna tail in chapter 3. The peduncle part of the tail connects the core muscle at the trunk to the caudal fin, so muscle contraction can be transduced to lateral motion of tail. This chapter will focus on using a bio-inspired foil model to study effects of peduncle on propulsive performance. First half of the chapter will be focusing on the effects of various phase offset between heave motion of body and pitch motion of caudal fin on propulsive performance. The study is inspired by a similar study on 2D hydrofoil (Van Buren, Floryan, & Smits, 2019) and extends the conclusion from rectangular planform shape to a more bio-inspired planform shape. Second half of the chapter will be focusing on the effects of various peduncle joint stiffness on propulsive performance. Previous studies on fish swimming using simplified canonical models suggest that the shape or flexibility of the propulsor cannot solely determine performance. We propose a tuna-tail-inspired non-uniform foil model that focuses on the effects of passive peduncle joint on propulsive performance. Figure 4.1a shows the rotational freedom from peduncle joints, which causes the phase offset between the body and caudal fin. Figure 4.1b shows the tendons covering the joints, adding bending stiffness to the free rotation. First, we used a computational method called Immersed Boundary Method to determine the optimal range of kinematic phase offset between body and caudal fin for a bio-inspired foil. Results demonstrated that passive bending generates the highest propulsive efficiency. Next, we experimentally studied the effects of passive joint stiffness using a non-uniform foil model of the same shape as the computational model, with a variety of joint stiffnesses. We found that there is no one single optimal joint stiffness for all kinematic configurations. However, choosing the right stiffness for each specific configuration can provide high propulsive performance by maintaining the foil at an optimal angle for lift-based propulsion relative to the swimming direction.

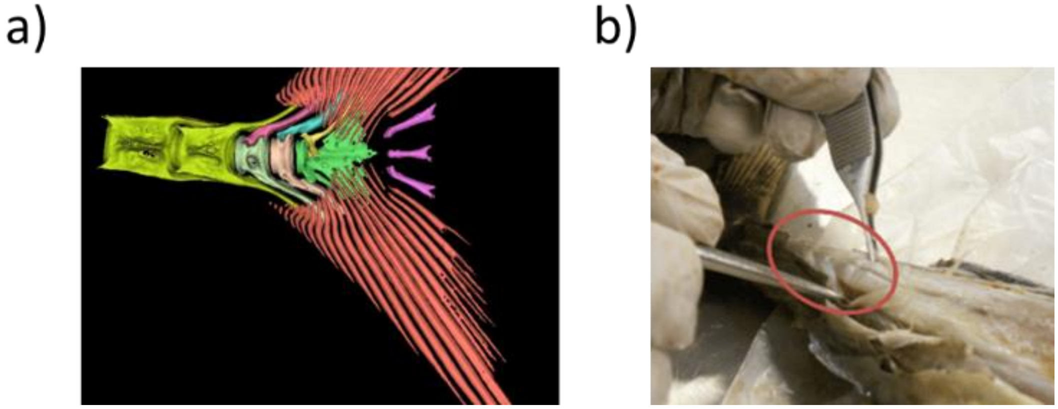

Figure 4.1 (a) µCT scan of yellowfin tuna (*Thunnus albacares*) peduncle and caudal fin. (b) Tendons covering peduncle joints, providing rotational stiffness. Images retrieved at Lauder Lab, Harvard University, 2015.

In this study, we focus on the role of stiffness of the peduncle joint on the propulsive performance of tuna swimming. The planform and cross-section shape of the model stays constant in both the experiments and simulation (Figure 4.2). Specifically, we explore the effect of flexibility at the peduncle region on thrust, power, and efficiency. We first hypothesize that a passive joint is within the optimal performance range. We then hypothesize that altering passive joint stiffness will change the performance of the foil due to its effect on passive bending and therefore on the angle between the body and caudal fin. Additionally, we expect that the direction and magnitude of any change in performance will depend on the extent of joint stiffness.

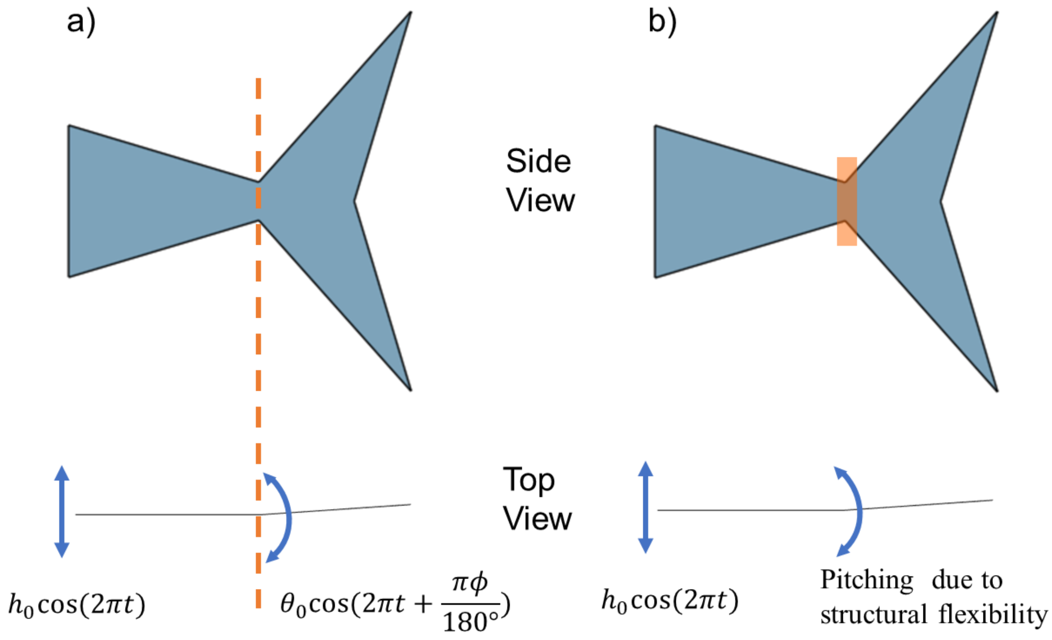

Figure 4.2 (a) Simulation study of phase offset, where all motions are prescribed and material properties are fully rigid (b) Experimental study of passive peduncle joint stiffness, where the pitch motion is caused by structural flexibility rather than active actuation. Dimensions and variables are described in details in the methodology section.

To test this hypothesis, various bio-inspired foils were built and tested, first in simulation, then in lab environment. For the simulation cases (Figure 2a), we prescribed the same sinusoidal heave motion onto both the body and fin part of the foil as well as a pitching motion at the leading edge of the fin of the same frequency. However, we varied the phase offset between the body and the caudal fin to understand which motion pattern led to the best performance. In the simulation, the phase offset at peduncle location is the only controlling factor in determining the performance difference. No material flexibility is prescribed to the foil. A similar study done on a 2D rigid airfoil found an optimal phase offset in terms of efficiency (Van Buren et al., 2019). When a 2D foil starts pitching quarter period after heaving motion of same frequency, maximal efficiency is achieved. Our simulation study extended the conclusion to 3D bio-inspired foil. Simulation results show that that phase offset mimicking passive bending leads to higher thrust and efficiency.

The simulation results (described in detail later) show that a passive joint is within the high-performance regime. To understand better how the extent of passive joint stiffness affects propulsive performance, we manufactured four foils with the same shape as those in the simulation but with variable joint stiffness at the peduncle region (Figure 4.2b). The peduncle joint region of the foil is a simplified physical model of tuna caudal peduncle We tested the foils with pure heave motion at the leading edge using a range of frequencies and amplitudes. Since the foil is only actuated at the leading edge, any pitching motion of the caudal fin is caused by passive bending of the composite structure rather than prescription in simulation. Trends observed from the experiments were compared with previous studies using a similar setup.

4.1 Methodology

This study uses both computational and experimental approaches to explore the role of phase offset and bending angle. First, a numerical solver using Fluid-Structure Interaction (FSI) and Immersed Boundary Method (IBM) was employed to investigate the effects of the phase offset (Figure 4.2a) between the body and the caudal fin on the propulsive performance, including thrust, power and efficiency of a tuna-shaped foil. Phase offset between heave motion of body and pitch motion of caudal fin was altered to find the optimal value. Next, we tested four foils of different joint stiffness at the peduncle region using a flow channel setup with a force transducer and with Particle Image Velocimetry (PIV). The relation between joint stiffness and the change in propulsive performance were investigated.

4.1.1 FSI-IBM Solver

An in-house Picar3D flow solver (Flow Simulation Research Group, UVa) and an open-source structure solver (Vega FEM, University of Southern California, Los Angeles, CA) were strongly coupled to solve the FSI simulation. In this process, as shown in Figure 4.2, the convergence check guaranteed the convergence of the flow and structure results at each time iterations to achieve strong coupling between the fluid solver and the structure solver.

The fluid solver solves the incompressible Navier-Stokes (N-S) equations. The equations are nondimensionalized by chord length and incoming flow speed. The equations are then solved numerically by an in-house finite-difference based Cartesian-grid sharp-interface immersed-boundary-method direct numerical simulation solver. This approach has been successfully applied to the flapping propulsion of insects (Dong, Liang, & Harff, 2009), birds (Ren, Dong, Deng, & Tobalske, 2016), fish (Khalid, Akhtar, & Dong, 2016; R. Zhu et al., 2019), as well as various canonical problems (Wang et al., 2018; R. Zhu, Wang, Dong, & Bart-Smith, 2020; R. Zhu et al., 2017). A detailed description of the sharp-interface method and validation of this solver can be found in previous publications (Ghias, Mittal, Dong, & Lund, 2005; Mittal et al., 2008). The structure solver uses the open-source Vega Finite Element Modeling (FEM) Library, chosen for its ability to handle large deformations. The solver numerically solves an ordinary differential equation derived from finite element analysis. A more detailed description of the coupled numerical algorithms is listed in a previous publication (Wang, Deng, Lauder, & Dong, 2019).

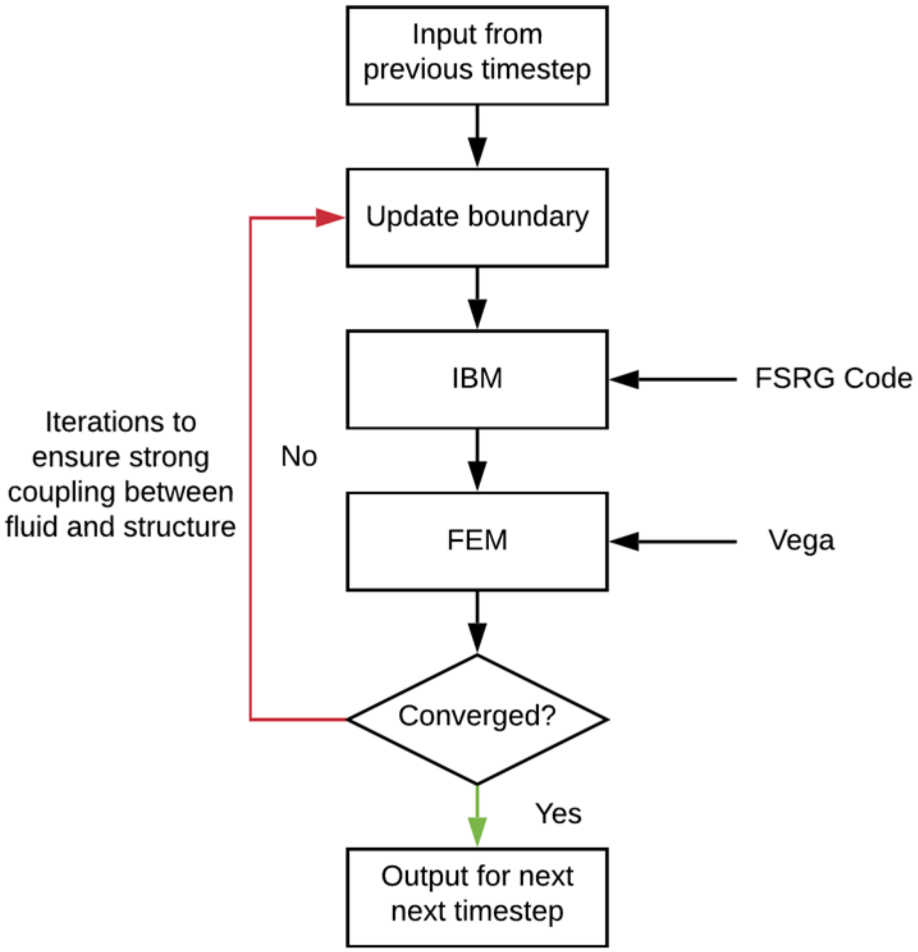

Figure 4.3 Solver workflow

The CFD configuration of this study is shown in Figure 4.4. We model a foil (same shape as shown in Figure 4.7, ½ dimension) inspired by a tuna tail (Figure 4.5), with span s, body chord c_1, fin chord c_2 and use a computational domain with non-uniform density. The section of the foil anterior to the peduncle is driven with prescribed sinusoidal heave motion of amplitude h_0 = 0.025 m. The section posterior to the peduncle has the same heave motion but is also driven with a pitching motion of amplitude θ_0=15°. For the posterior part, pitching and heaving both have the same frequency of f = 1 Hz, but are phase offset by ϕ = 0° to 270° in intervals of 90°, with a more refined spacing of 30° between 210° and 330° (Table 4.1). In total, the parameter space has 24 simulation cases. Representative kinematics of foils are shown in Figure 4.6.

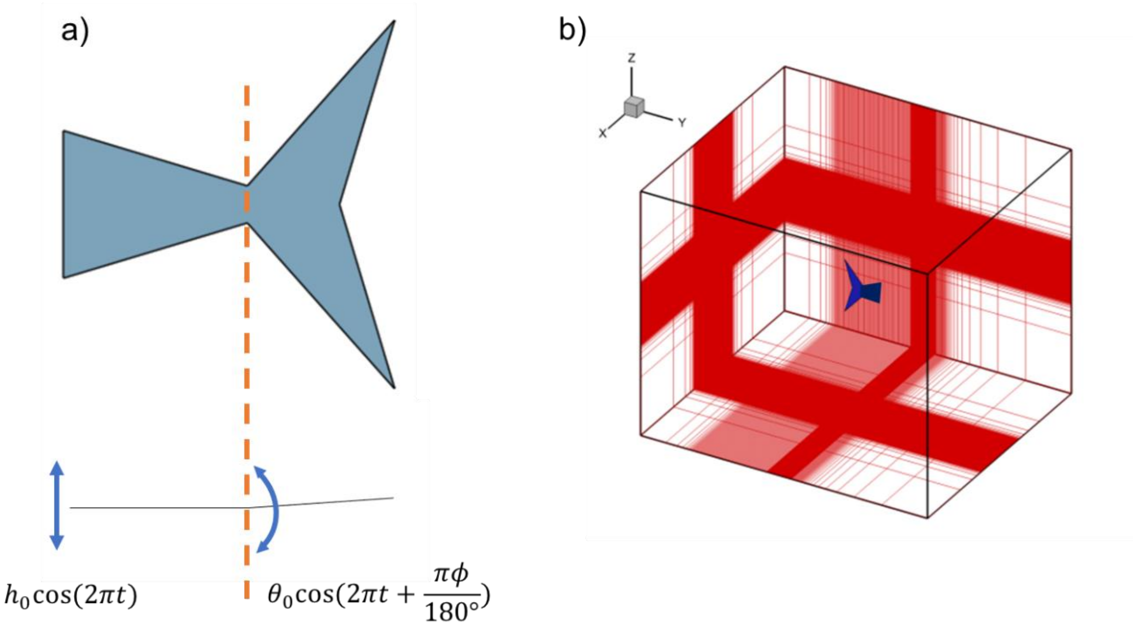

Figure 4.4 (a) Foil kinematics prescribed in simulation (b) CFD mesh setup

Figure 4.5 Biological sample with maximum bending angle in air about 29°. The simulation and experiment samples are modelled with similar shape and the pitch angle of caudal fin in simulation is prescribed with a smaller value due to extra resistance in water.

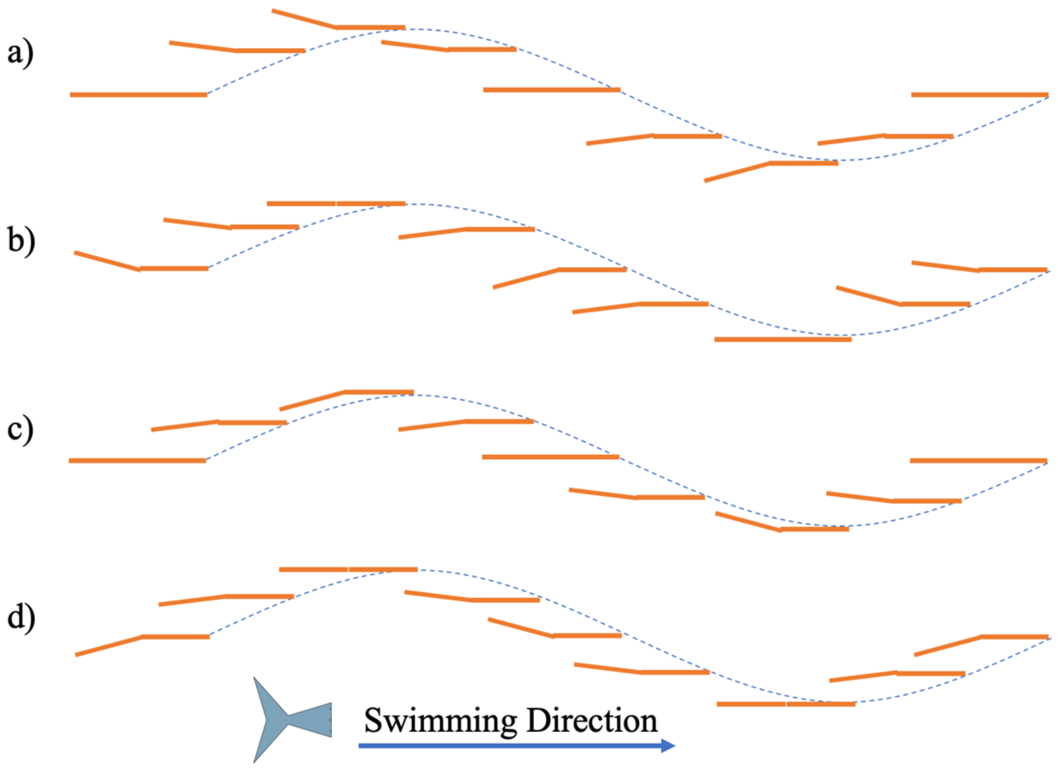

Figure 4.6 Motion of a foil swimming from left to right via heave pitch and pitch motions with a phase offset (defined in Figure 4.4a): (a) ϕ = 0°, (b) 90°, (c) 180°, and (d) 270°.

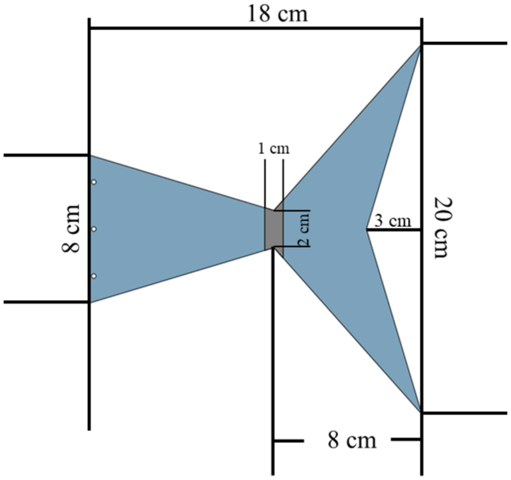

	Foil	Peduncle Thickness (cm)	Flexural Stiffness EI at center of Peduncle (N cm^2)
🟨	S1	0.03	6.75
🟥	S2	0.05	31.25
🟪	S3	0.07	85.75
🟦	S4	0.1	250

Figure 4.7 Bio-inspired panels with non-uniform stiffness. The maximum stiffness is same as the fully rigid portion of the foil, while the other stiffness values were chosen based on the resolution of the rapid prototyping 3D printer.

Table 4.1 Simulation setup for phase offset study

Parameter	Range
Free Stream Velocity	U_∞ = 0.08, 0.12, 0.16 m/s
Chord	c_1 = 0.05 m, c_2 = 0.04 m
Span	s = 0.1 m
Frequency	f = 1 Hz
Heave Amplitude	h_0 = 0.0125 m
Bend Angle	θ_0 = 15°
Phase Offset	ϕ = 0°, 90°, 180°, 210°, 240°, 270°, 300°, 330°

4.1.2 Manufacturing Physical Foils

Four foils of the same shape (Figure 4.7) as that in the computational simulations were manufactured and tested in the water tunnel setup using setup shown in Table 4.2. All the panels for experiments with non-uniform flexibility are manufactured using a Stratasys Object Printer with a layer resolution of 0.03 mm. The stiffness of the peduncle is controlled by the thickness of the central layer, created through solidifying photosensitive polymer liquid (VeroWhite by Stratasys) under UV light. We keep the thickness of the foil uniform by filling in the peduncle with a rubber-like material (TangoBlack by Stratasys) to minimize effects from surface roughness. Three-point bending tests are carried out to validate that overall stiffness (EI) is proportional to the cube of thickness of the central layer (Figure 4.8). Bending test specimens all have cross-section of 20mm x 2mm, with span of 60 mm. Five different material ratio is designed and 3 specimens for each trial are manufactured for repeated trials. The fraction of VeroWhite material for each specimen is measured after 3D printing. The three-point bending protocol is described in Chapter 3.2.2. Theoretical prediction is based on flexural modulus listed on spec sheet provided by Stratasys. The test results are consistently lower than theoretical prediction, due to the fact that the modulus values on spec sheet are estimates according to Stratasys and no sources of testing protocols are cited. Thus a correctional coefficient of 0.73 is applied to match the test results with prediction and also used in calculation of flexural stiffness shown in Figure 4.7. This systematic deviation demonstrates the importance of testing rapid prototyped parts for real material properties.

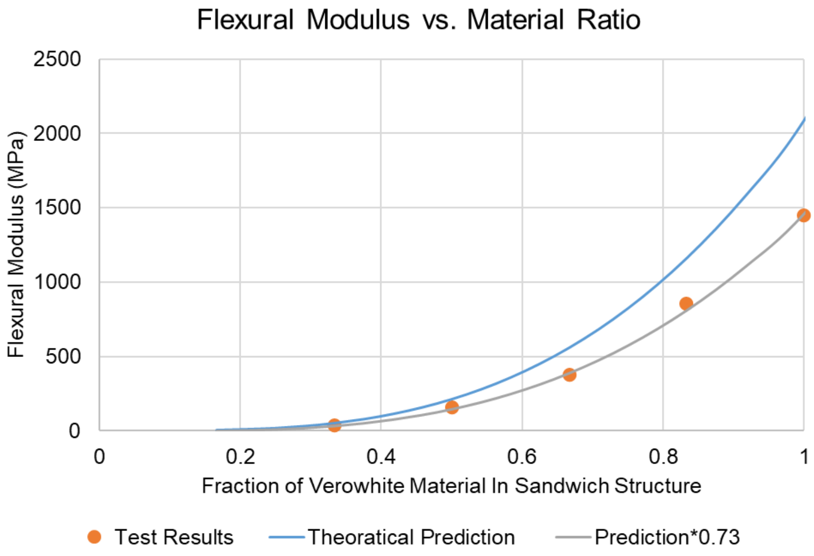

Figure 4.8 Flexural modulus from test and theoretical prediction. Standard deviation of test results is significantly smaller than the size of orange circle symbols.

Table 4.2 Experiment setup for joint stiffness study

Parameter	Range
Free Stream Velocity	U_∞ = 0.24 m/s
Chord	c_1 = 0.1 m, c_2 = 0.08 m
Span	s = 0.2 m
Frequency	f = 0.4, 0.6, 0.8.. 2 Hz
Heave Amplitude	h_0 = 0.025, 0.0375, 0.05 m

4.1.3 Water Channel Experiments and PIV

The water channel setup (Figure 4.9) follows that used in previous foil experiments (Lauder, Anderson, Tangorra, & Madden, 2007). Each foil is fixed onto a flat shaft at the leading edge, with an ATI-Nano 17 six-axis force-torque transducer (ATI Industrial Automation, Apex, NC, USA) at the top of the shaft. Raw data are taken for 10 cycles and averaged. Five repeated trials are conducted for each kinematic configuration for mean and standard deviation.

In all the trials, the shaft is fixed in streamwise direction to measure thrust, power consumption, and Froude efficiency (Equations 4.1, 4.2, and 4.3) using the ATI transducer. Raw parameters measured are streamwise force (F_x), lateral force (F_y) and torque in gravity direction (M_z). The shaft is attached to a carriage system sitting on top of the water channel and moved by an actuator. Custom LabVIEW programs written by Anderson (2007) (National Instruments Corp., Austin, TX, USA) are used to control flow speed (U_∞), foil heave (h), and frequency of motion (f).

$$C_T = \frac{F_x}{\frac{1}{2}\rho U_\infty^2 sc}$$

Equation 4-1

$$C_P = \frac{F_y \dot{h}}{\frac{1}{2}\rho U_\infty^3 sc}$$

Equation 4-2

$$\eta = \frac{C_T}{C_P}$$

Equation 4-3

As shown in figure 4.8, while the foil is flapping at fixed streamwise location, flow around the foil is filmed from a ventral view via a mirror set at 45° to horizontal plane, with a high-speed camera (Photron UX100 high-speed camera; 1280x1024 pixel resolution, Photron, Inc.) shooting at a frame rate of 1000 Hz. The water was seeded with nearly neutral particles and a 10-Watt green laser positioned mid-span was used to illuminate them. and the flow field around the foil was calculated then average free-stream flow was subtracted across the whole field (Davis v. 8.3.1 LaVision gmbH, Goettingen, GER). The start of each kinematics cycle was defined as when the leading edge of the foil reaches maximal lateral excursion to the right. Because the foils are opaque, the shadow of the foil blocks visualization of flow on the right side. We excluded these shadowed areas from the velocity field to ensure standard results across each frame.

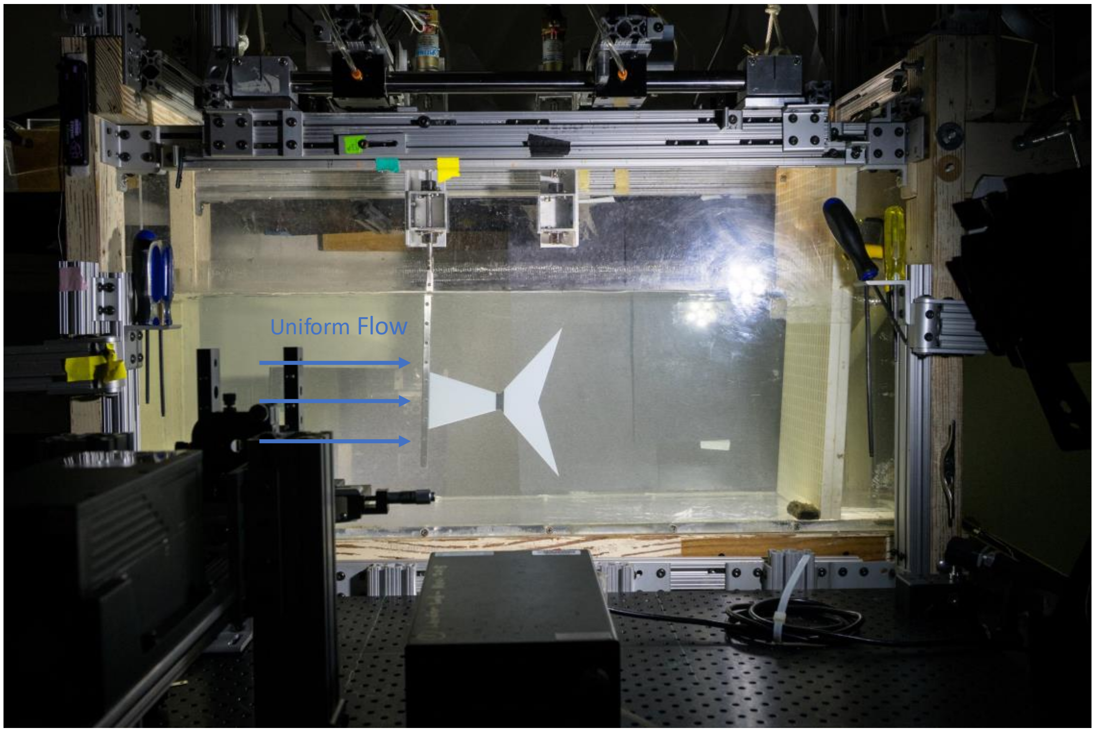

Figure 4.9 Flow Channel Setup

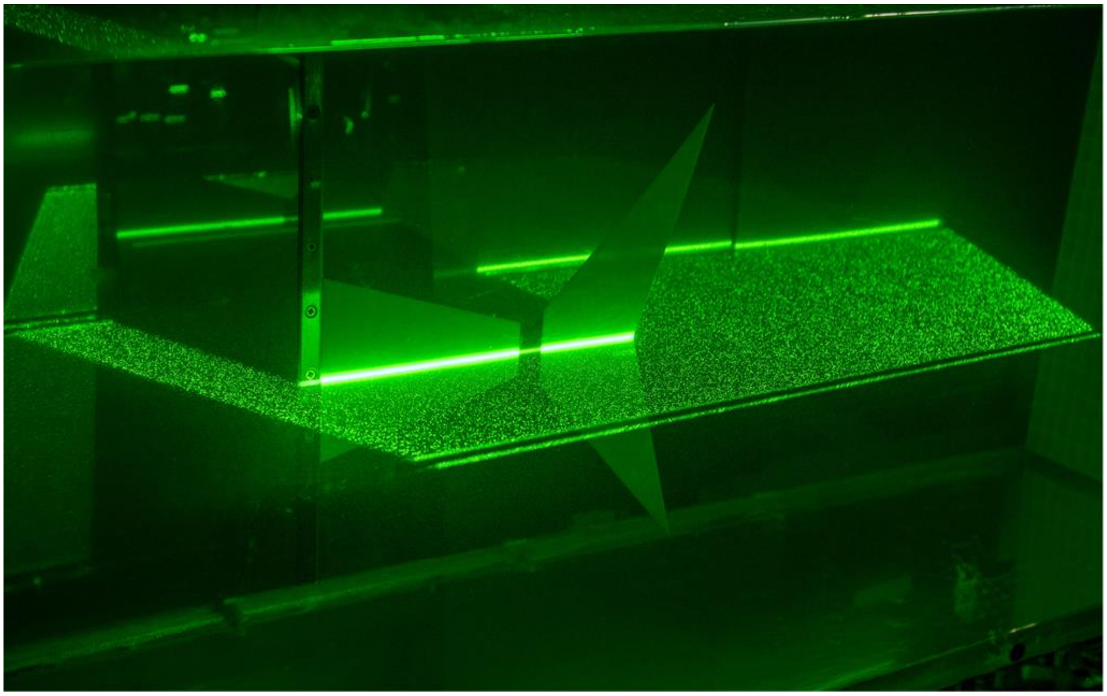

Figure 4.10 PIV Setup

4.2 Simulation Study of Phase Offset

Figure 4.6 illustrated the motion of the foil for phase differences of ϕ = 0°, 90°, 180° and 270°. When heave and pitch were in phase (ϕ = 0°), it appeared as though the caudal fin was pitching about some point in front of the leading edge. At a phase angle of ϕ = 90°, the trailing edge of the foil led the leading edge. When ϕ = 180°, the foil appeared to pitch about a point behind the leading edge. However, ϕ = 270° appeared most biomimetic, moving through the water with the lowest effective angle of attack, the angle between the foil and its instantaneous direction of velocity.

When the heave of the whole foil and bend of peduncle were in phase (ϕ = 0°), the accelerations were in phase. Thus, when the caudal fin started to accelerate laterally, it also accelerated rotationally, working against the resistance of the fluid from lateral motion, yielding a high moment that increased power consumption (Figure 4.11b). However, when heave and pitch were offset by ϕ = 270°, the lateral acceleration of the caudal fin produced a force that assisted the pitching motion, thus lowering the moment required. This is the same motion that would be achieved in a passive system where the pitch will follow the path of lowest hydrodynamic resistance. This reduction of the moment components of the caudal fin is a critical aspect of achieving high efficiency at ϕ = 270° (Figure 4.11c). In addition, the highest thrust (Figure 4.11a) happened between ϕ = 270° and 360°, which was due to a combination of high power input (Figure 4.11b) and efficiency (Figure 4.11c).

a) Thrust

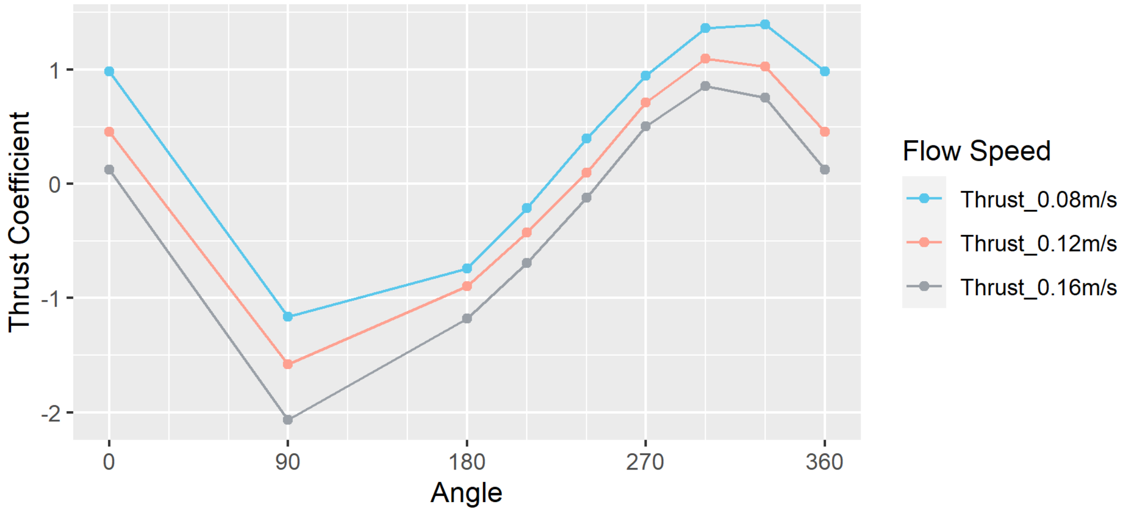

b) Power

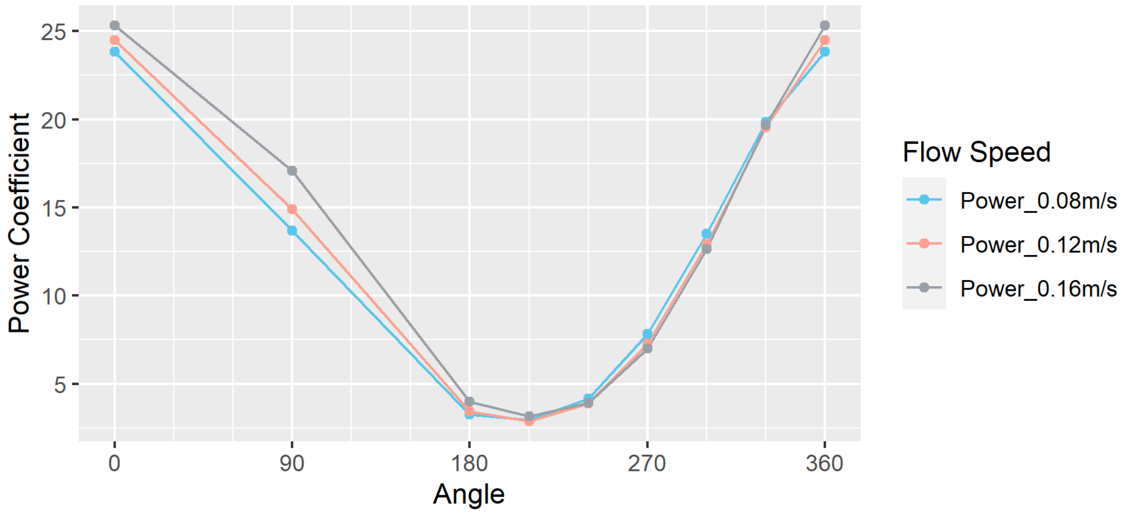

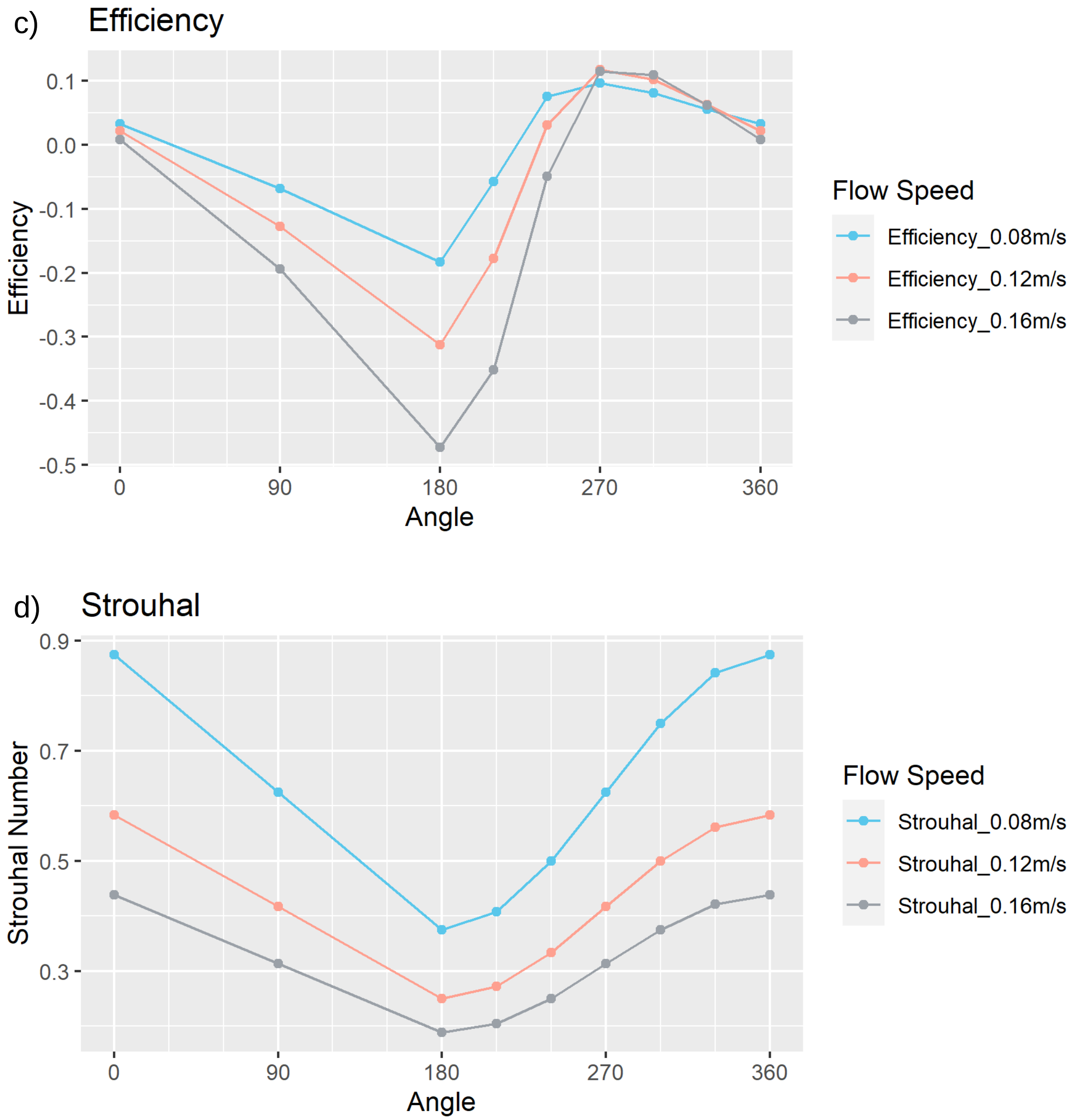

Figure 4.11 (a) Thrust coefficient, (b) Power coefficient, (c) Efficiency, and (d) Strouhal number for each simulation case. Values are plotted against phase offset angle (°), and each series represents all cases with the same incoming flow speed.

To relate the performance with Strouhal number (explained in detail in Chapter 2.1), we plot efficiency versus Strouhal number in figure 4.12a. In contrast to the common belief (Eloy, 2012) that the optimal efficiency occurs at Strouhal number range of 0.2 – 0.4, there is no significant advantage for those strouhal numbers in this case. This is mostly because when two cases such as ϕ = 90° and 270° share the same Strouhal number (Figure 4.11d), their kinematics at instant time is, however, the opposite (Figure 4.6). The 270° case has higher efficiency since the foil is able to maintain its maximum angle of attack below the critial angle of attack (where stalling happens) through the oscillation cycle (Figure 4.12b). Efficiency trends compared with maximum angle of attack trends (Figure 4.12c) show that when the maximum angle of attack gets closer to 10° as the phase offset angle is around 270°, the foil is able to achieve higher propulsive efficiency. The critial angle of attack for the flat foil used in simulation is around 10°, as shown in Figure 4.12d, where propuslive efficiency starts to drop beyond max angle attack of 10°.

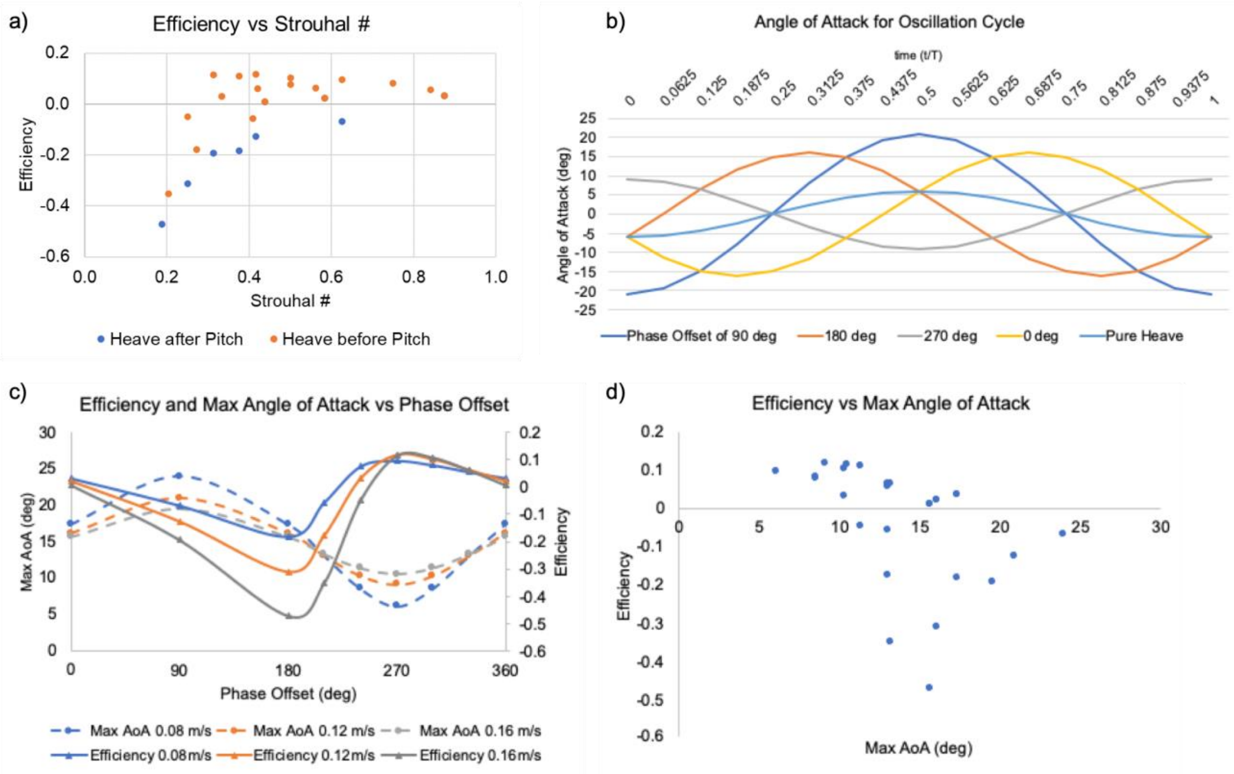

Figure 4.12 (a) Efficiency versus Strouhal number for all simulation cases. Heave after pitch indicates $\phi \leq 180°$, while heave before pitch indicates $\phi > 180°$; (b) Time series data of angle of attack for representative phase offset angles at 0.12 m/s (calculating method depicted in Figure 4.14), maximum angle of attack defined as amplitude of sinusoidal curve; (c) Efficiency trends compared with maximum angle of attack trends for all phase offset angles and incoming flow speeds; (d) Time-averaged efficiency versus maximum angle of attack for all kinematic configurations.

4.3 Experiments of Foils with Passive Peduncle Stiffness

4.3.1 Performance

Since the tail section of our foils was activated passively, their motion was similar to the computational model with ϕ = 270°. In general, thrust production increased and became positive with both increasing heave amplitude and flapping frequency (Figure 4.13). When the heave amplitude was small (2.5 cm), the effect of stiffness was minimal on the thrust (Figure 4.13a). At heave ampltitude of 3.75 cm, the foil with the most flexible peduncle joint (S1) generated less thrust than the other foils at lower frequencies, but more thrust at higher frequencies (Figure 4.13b). At the largest heave amplitude of 5 cm, S1 consistently produced less thrust than the other foils, while the foil with the second highest stiffness (S3) was able to achieve the highest thrust at highest frequencies (Figure 4.13c).

First resonant frequency is not as easy to observe in the cases of bio-inspired foil as canoncial cases in previous study (Dewey et al., 2013; Quinn et al., 2014). The most obvious example is S3 (purple line) in Figure 4.13a, where the thrust achieves a local maxium around frequency of 1 Hz, which is the first resonant frequeuncy for S3 with heave amplitude of 2.5 cm. When looking at S3 at 1 Hz in Figure 4.13d, it also shows a maxium of efficiency, which paritially validates the findings from previous work that underwater propulsors achieve (local) maxiums at first resonant frequency. However, the complex planform shape interacts with the non-uniform stiffness of the foil, which previous literature (Feilich & Lauder, 2015) has pointed out to make studying the role of resonance much harder.

The relationships between peduncle stiffness and efficiency were more complicated. At small amplitude (2.5 cm) and low frequeny (<1.2 Hz), S1 and S3 outperformed the other models, with S3 being the more efficient of the two (Figure 4.13d). At higher frequencies all foils maintained positive efficiencies and S3 continued to be the most efficient. At heave amplitude of 3.75 cm, all foils reached peak efficiency around 1 Hz. From frequency of 0.8 to 1.2 Hz, the foils ranked from most to least efficient were S2, S3, S4, and S1 (Figure 4.13e). The foils with intermediate joint stiffness outperformed the others. At large heave amplitude (5 cm) most foils performed similarly with the exception of S1, which was far less efficient than any other foil (Figure 4.13f).

a)

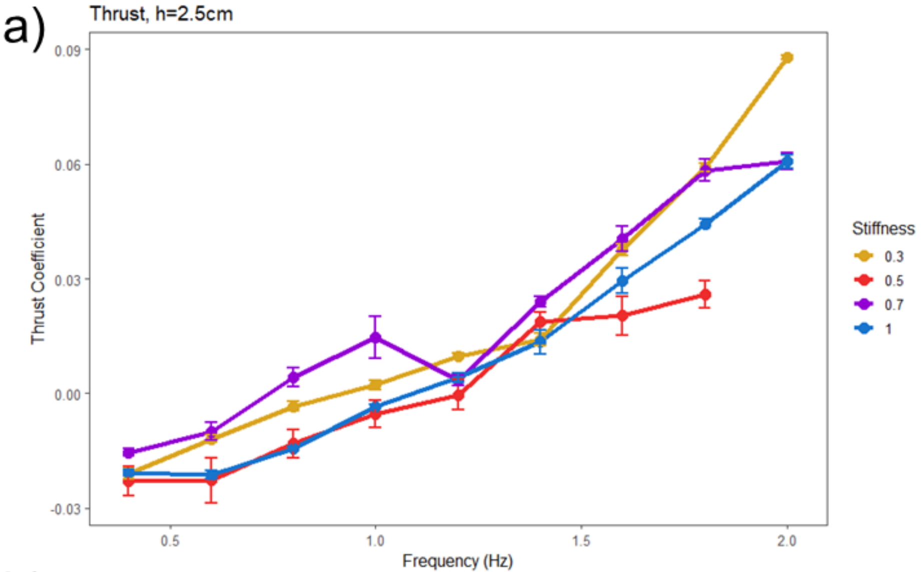
Thrust, h=2.5cm
Thrust Coefficient
0.09
0.06
0.03
0.00
-0.03
0.5
1.0
1.5
2.0
Frequency (Hz)
Stiffness
0.3
0.5
0.7
1

b)

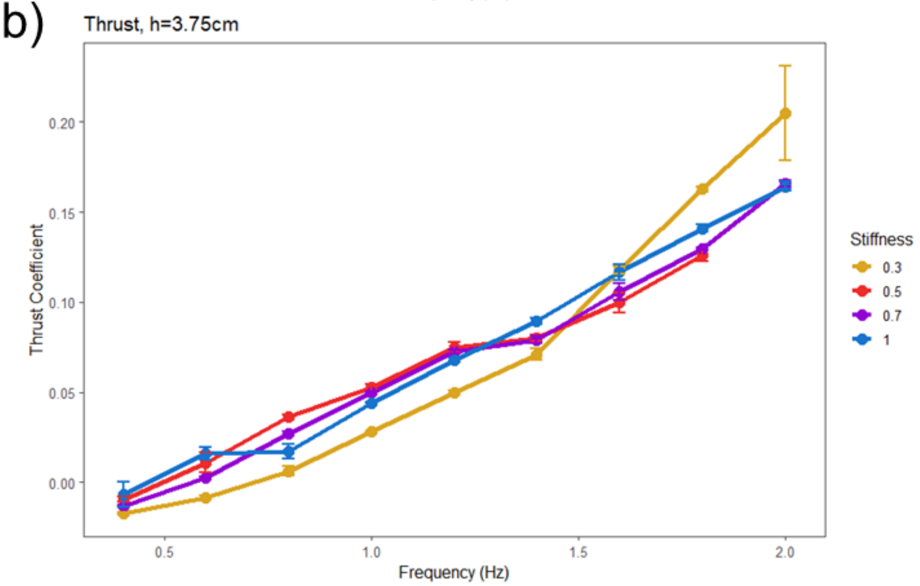
Thrust, h=3.75cm
Thrust Coefficient
0.20
0.15
0.10
0.05
0.00
0.5
1.0
1.5
2.0
Frequency (Hz)
Stiffness
0.3
0.5
0.7
1

c)

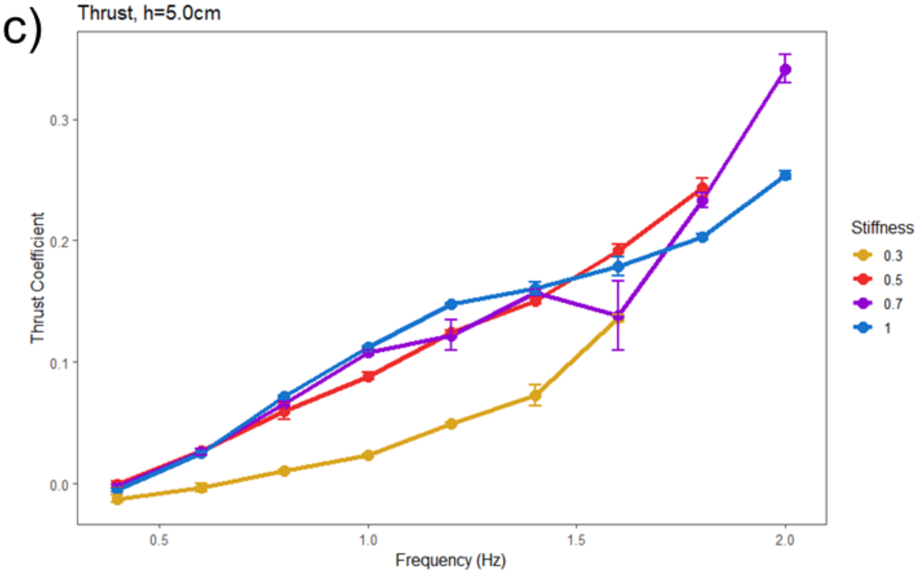
Thrust, h=5.0cm
Thrust Coefficient
0.3
0.2
0.1
0.0
0.5
1.0
1.5
2.0
Frequency (Hz)
Stiffness
0.3
0.5
0.7
1

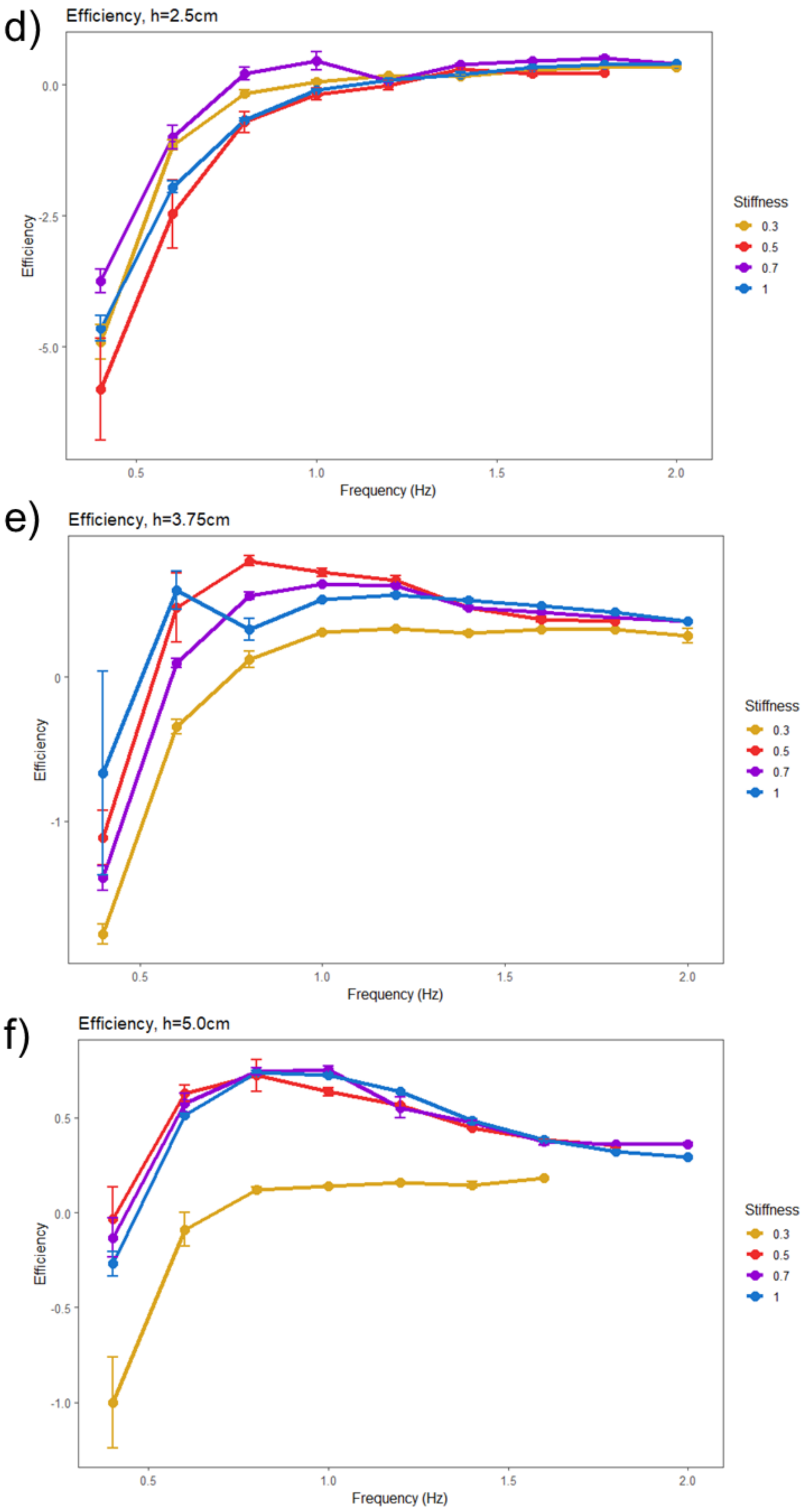
d)
Efficiency, h=2.5cm
Efficiency
0.0
-2.5
-5.0
0.5
1.0
1.5
2.0
Frequency (Hz)
Stiffness
0.3
0.5
0.7
1
e)
Efficiency, h=3.75cm
Efficiency
0
-1
0.5
1.0
1.5
2.0
Frequency (Hz)
Stiffness
0.3
0.5
0.7
1
f)
Efficiency, h=5.0cm
Efficiency
0.5
0.0
-0.5
-1.0
0.5
1.0
1.5
2.0
Frequency (Hz)
Stiffness
0.3
0.5
0.7
1

Figure 4.13 Thrust coefficient and efficiency for each peduncle stiffness at 3 different leading edge heave amplitudes. Thrust increased with heave frequency for all peduncle stiffnesses, but the effect of stiffness on thrust was non-linear. Efficiency increased at first with frequency but changed differently dependent on peduncle stiffness and heave amplitude. Errors are based on 5 repeated trials.

4.3.2 Flow Visualization

To understand the importance of the pitch angle in thrust production, we first consider how thrust is generated by heave-only motions (Figure 4.14a). Thrust production in heave is lift based, meaning that the lateral velocity of the foil combines with the freestream velocity U_{free} into an effective foil velocity U_{foil} that produces lift L. Because the lift vector is perpendicular to U_{foil}, L has components in the lateral and streamwise directions (Fy and Fx, respectively), with the latter being the thrust. To produce thrust efficiently, we need to avoid dynamic stall; thus we need to limit the maximum angle of attack α (Figure 4.15). To produce higher thrust, however, we need to increase the heave velocity, which will then increase the angle of attack.

This conflict can be mitigated by adding pitch to the heave motion such that the angle of attack is reduced. Consider a heaving foil with fishlike pitching motion added to the tail ($\phi = 270$ deg) (Figure 4.14b). Compared to heave-only motions, the heave velocity is greater but the angle of attack is the same due to the addition of appropriate pitch. The increased heave velocity increases the lift and rotates more of it in the thrust direction, increasing the efficiency. Thus, the phase difference between the heave and pitch motions is a crucial factor in determining the propulsive performance of the fish-shaped foil.

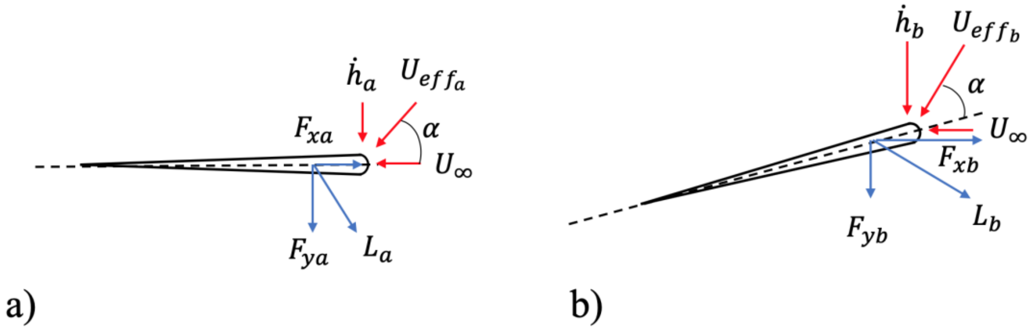

Figure 4.14 Heaving foil (a) without and (b) with added pitch motion. Streamwise, heave, and effective velocities are shown in red; and resulting lift-based forces are shown in blue.

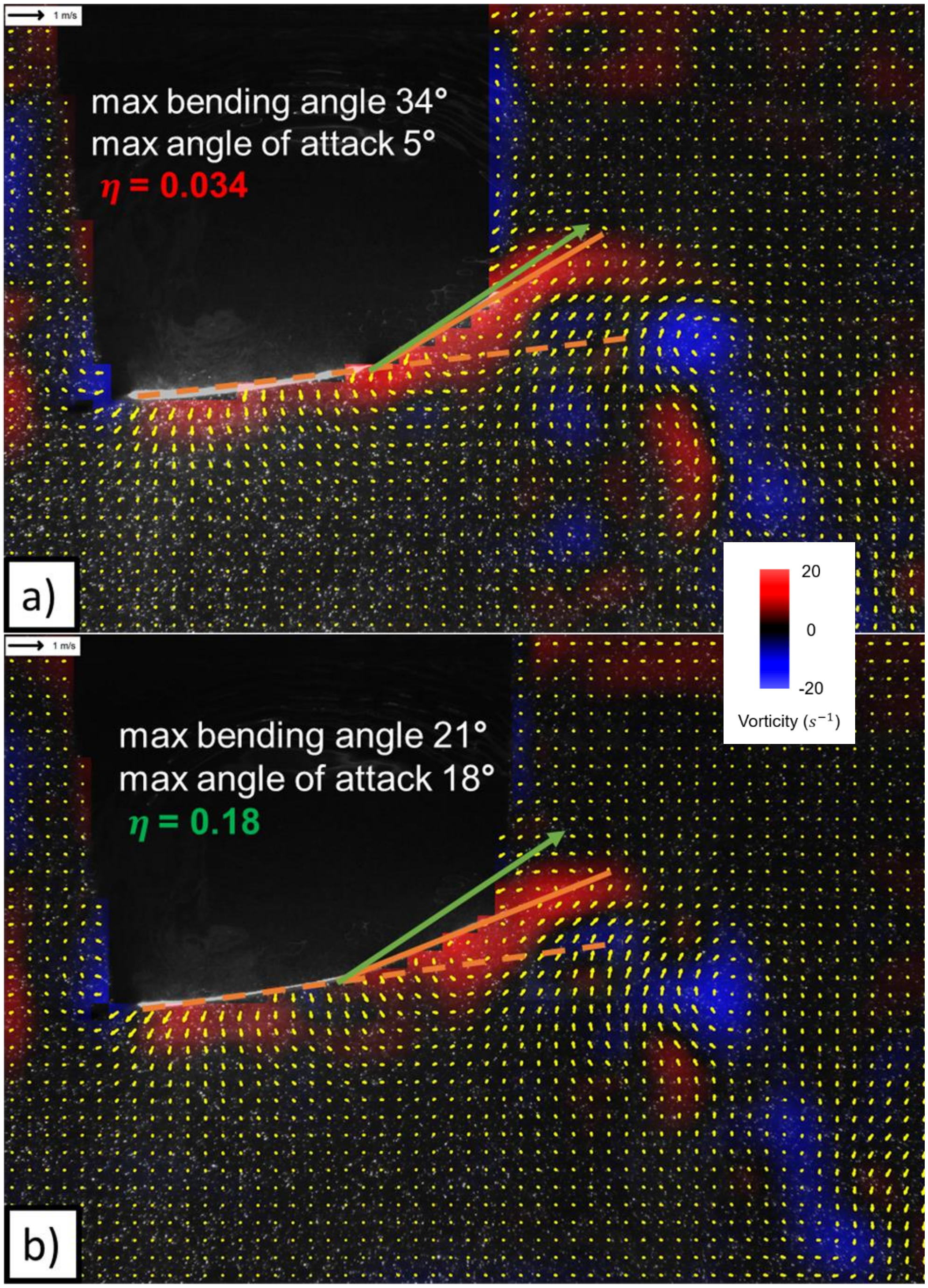

Figure 4.15 Kinematics and PIV of chordwise vorticity for (a) foil S2 (b) S3 at h = 5cm and f = 1 Hz when the foil heave downwards at maximum speed. Maximum bending angle is measured between the solid orange line tracing the caudal fin and the dashed orange line tracing the body.

Maximum angle of attack is measured between the green arrow tracing the effective flow velocity and the caudal fin.

From the flow visualization of chordwise vorticity in Figure 4.15, we observed that S3 has a smaller maxium bending angle compared to S2, which results in higher efficiency due to a larger angle of attack (still under critical value). In terms of wake strucutre behind the trailing edge, S3 also shows a more concentrated wake, which means the energy input from leading edge is less dissipated through the motion, thus also contributing to higher efficiency.

To relate the simulation with experiments, a qualatative comparison of kinematics and flow structure is shown in Figure 4.16. Here we can see that the passive bending of foil at different time steps is very close to the kinematics prescribed in simulation. Vortex structure are also similar, providing new validation in addition to previous baseline validation cases (Wang et al., 2019).

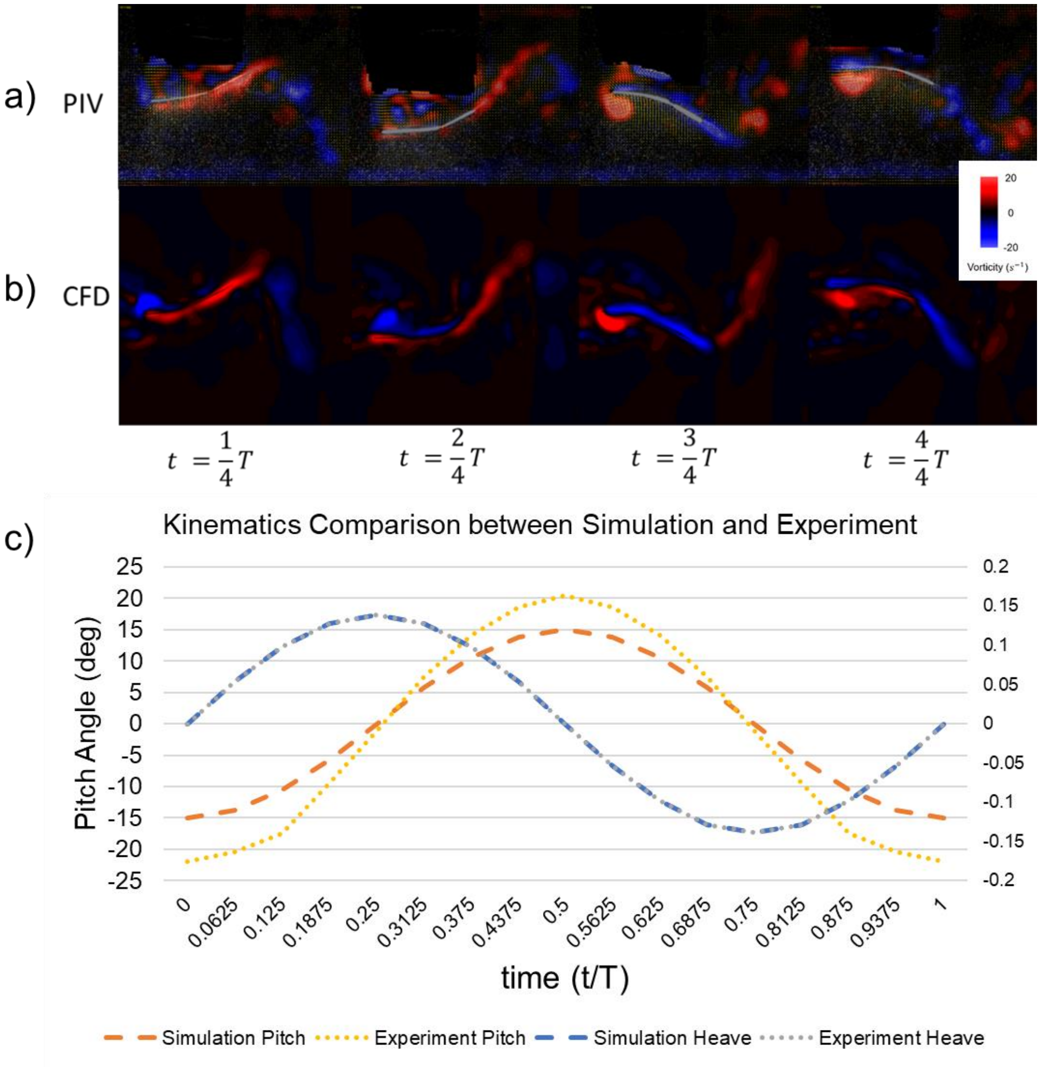

Figure 4.16 (a) PIV of chordwise vorticity for S3 at h = 5 cm, f =1 Hz and CFD of the phase offset of 270° at quarter of motion period; (b) Heave and pitch motion measured in PIV and prescribed in CFD (c) Kinematics comparison between PIV experiment and CFD simulation.

4.4 Summary of Chapter

From the results of computational study of phase offset, we have concluded that a passively flexing foil (with kinematics similar to that of prescribed phase offset of 270° as shown in Figure 4.16) is as efficient or more efficient than any model where the caudal peduncle is actively controlled (however not in a bio-inspired fashion, for example when the heave and pitch are completely out of phase). From the experimental results of the four foils with different peduncle joint stiffness, it is evident that the effects of stiffness on lateral displacement, efficiency, and thrust are complex and not easily predicted across a wide parameter space. However, it seems like there are interesting results within slightly constrained parameter spaces. For instance, S3 is really efficient at low frequencies and low amplitude. We conclude that although there is no one optimal stiffness across all parameter spaces, there are clear differences in performance due to peduncle stiffness. Figure 4.13 shows that the most flexible peduncle S1 starts to lose thrust and efficiency at higher efficiency. Therefore, we should focus design on the ability to actively modulate stiffness such that we can achieve optimal performance at any set of swimming parameters.

Here we study the role of stiffness in the peduncle joint of tuna-like swimmers by using a more complex bio-inspired model than have been used before. We are able to partially recreate the complex kinematics and hydrodynamic pattern introduced by interaction between lateral body and caudal fin. Our findings add to a growing body of work indicating that future studies will require adding a full body and a more bio-mimetic caudal fin with air-foil cross section to fully explore the mechanics and kinematics of fish swimming. Researchers in the field of biology, biomechanics, fluid dynamics and robotics must continue to work together to develop more systematic ways of investigating the interactions between motion and morphology to deepen our understanding of the physics behind fish swimming.

5. PROPULSORS WITH SINGLE DIRECTIONAL STIFFNESS

Simplified physical models and more bio-inspired models have been developed to study the effects of shape and flexibility on swimming performance(Affleck, 1950; Chopra, 1974; Karpouzian et al., 1990; Lighthill, 1970; Wu, 1971). It is a challenge to uncouple these two parameters in order to quantify their respective roles in the propulsive performance. Attempts have been made to decompose underwater animal locomotion orthogonally(F. Fish et al., 2016; G. Liu et al., 2015). For more simplified models, experimental flow tunnel tests of homogenous flexible foils(Dewey et al., 2013; Kancharala & Philen, 2014; Quinn et al., 2014; Shelton et al., 2014) exhibit a combination of chordwise and spanwise deformations but the relative contributions cannot be determined. Additionally, the amount of flexion exhibited in either orientation is greatly influenced by the method of attachment at the leading edge. In almost all the flow tunnel tests, the homogeneous flexible foils exhibit dominantly chordwise flexibility, due to the common leading-edge fixture method, where the leading edge is fully mounted to the pitching/heaving rod. The previous numerical study has explored the effects of spanwise versus chordwise flexibility of airfoil panels under low versus high Reynolds number condition(Q. Zhu, 2007). The simulation prescribed pitching motion with pure chordwise or spanwise flexibility by changing the fixed boundary from leading edge to mid-span, which is challenging for real physical propulsor.

To address the challenges of these previous studies, in first part of the chapter, two structurally anisotropic flexible panels have been designed and tested. One panel achieves chordwise flexibility, and one achieves spanwise flexibility. We focused on the steady swimming performance of the two panels and one rigid panel (as baseline case), by measuring their self-propelled speed, power consumption and kinematics over a frequency sweep inside a water tunnel.

Using high-resolution videography, the experimental kinematics were reconstructed and used in immersed boundary method simulations (Mittal et al., 2008), to investigate the flow structure.

We hypothesize that our anisotropic structure design can produce passive directional flexibility, without changing kinematic boundary conditions as in the previous numerical study. Also, the resulting change in propulsive performance will follow similar trends as in other studies of chordwise and spanwise flexibility in the water.

In second part of the chapter, simulation of a limited parameter space of heaving foils with non-uniform stiffness is performed to get preliminary understanding of effects of stiffness distribution and aspect ratio on propulsive performance.

Chapter 5 demonstrates the study of the effects of shape and stiffness on flexible rectangular propulsors. First conclusion is that for a rectangular panel at free swimming state, adding chordwise flexibility improves its performance over fully rigid or spanwise flexible case. Second conclusion is that performance of a heaving flexible foil affected by both its frequency and aspect ratio.

Most results in Chapter 5 serve as inspiration for work in Chapter 6.

5.1 Pitching Anisotropic Panels

5.1.1 Methodology

Figure 5.1a and b shows the design of these two panels. In both cases, the main structure of panel is divided into five equally spaced sections in the flexible direction; two lightly colored sections have 1/6 thickness of the dark-colored sections, which theoretically should result in 216 times more deflection under the same load condition since the moment of area is proportional to cube of thickness. The structure with dimensions listed in Table 1 is then printed using ABS plastic material with a flexural modulus of 2.1 GPa (bending against printed layer direction). The modulus value is provided by Stratasys.

To allow flexibility in both directions, we employ a modified method to attach the panel to the driving rod. As shown in Figure 5.1c, we use an additional fixture part to fix the mid 20 percent of mid-span and leading edge, so that the rest of the panel is free to bend under load.

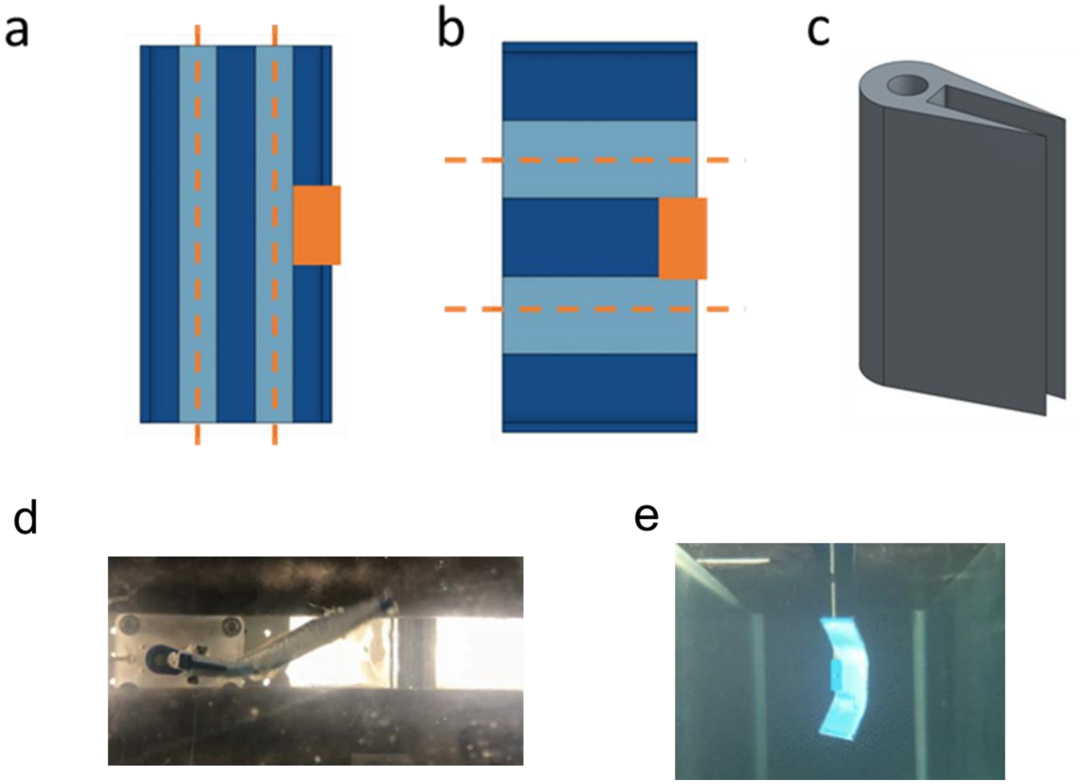

Figure 5.1 (a) Chordwise, (b) Spanwise design and (c) Panel fixture (represented as orange rectangular in sketch); (d) Chordwise and (e) Spanwise prototypes in experiments.

Table 5.1 Dimensions of structure design

Property	Measurement (mm)
Chord *c*	100
Span *s*	200
Segment in Chord Direction	20

Segment in Span Direction	40
Thickness *t* (Darker)	1.5
Thickness *t* (Lighter)	0.25

A sequence of tests is run using the input parameters shown in Table 5.2, and servo torque τ, angular speed ω, and self-propelling speed U of panels are recorded.

A similar test protocol and setup as in Lewis' master thesis (2017) is used:

1. Ensure the propulsor is in a proper neutral position with respect to the incoming flow.
2. The test is started and the propulsor begins to swim forward.
3. Once it reaches the front of the rig, the flow speed is slowly increased until it settles with no (or very small) oscillations about the center point of the water channel. This is assumed to be steady-swimming, and torque and angular position are then recorded over 10 cycles, with final swimming speed logged.

Table 5.2 Input and Output of Tests

	Rigid	Chordwise	Spanwise
Frequency *f* (0.25 Hz increment)	0.5 to 2.5 Hz	0.5 to 2.0 Hz	1 to 2.25 Hz
Amplitude *A*	30 deg on each side		

5.1.2 Performance

Experiments using the three panels (fully rigid, chordwise and spanwise flexible) were performed with the frequency varied from 0.5 up to 2.5 Hz for the same input amplitude. The self-propelling speed was recorded when the panel was able to stay at the same streamwise location and the results are shown in Figure 5.2a. Compared to the rigid panel, there are clear disadvantages to having spanwise flexibility. The swimming speed attained at all frequencies is lower than that of the rigid foil. Chordwise flexibility does not improve swimming speed performance.

During the self-propelling tests, we measure the average power consumption by:

$$P = \overline{\tau\omega} \ ,$$

Equation 5-1

where τ is toque reading from servo motor and ω is angular speed of servo motor.

Then economy is calculated as the power consumption P divided by free swimming speed U:

$$CoT = \frac{P}{U}$$

Equation 5-2

When one now looks at the economy, it is clear that flexibility becomes important to performance. Figure 5.2b presents economy data for the three foils. It is clear that chordwise flexibility significantly increases economy of swimming—in some cases as much as 300%. Conversely, spanwise flexibility appears to be slightly detrimental to the swimming economy, coming very close to the economy of the rigid foil. By examining the Strouhal number, the chordwise flexible foil allows the artificial propulsor to operate in a range that produces efficient propulsion. As shown in Figure 5.2c, the rigid case shows increasing Strouhal number as frequency increases, while adding chordwise flexibility can keep the Strouhal number within the efficient region (0.2 < St < 0.4). Strouhal number is defined as:

$$St = \frac{fA}{U}$$

Equation 5-3

Last, the overall trend of economy versus Strouhal number, as shown in Figure 5.2d is very similar compared to others' findings (M. S. Triantafyllou & Triantafyllou, 1995). The optimal Strouhal number range (0.2 ~ 0.4) agrees with the ranges found in hydrofoil experiments (G. S. Triantafyllou et al., 1993) and biology study (Taylor et al., 2003).

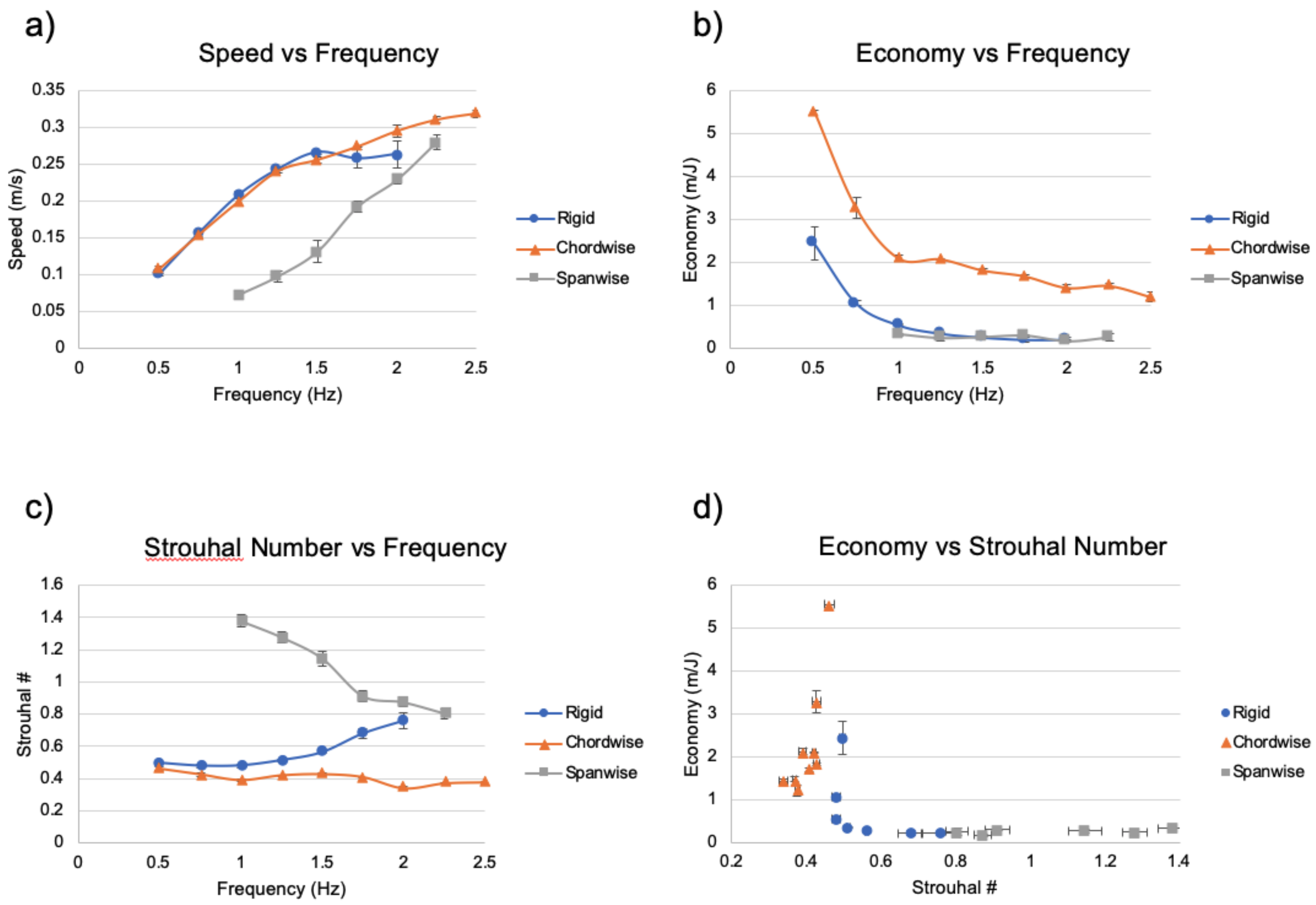

Figure 5.2 Flow tunnel test results - error bars are based on 3 repeated trials and smaller than size of symbols when not shown in plots.

5.1.3 Flow Visualization

Using reconstructions of the kinematics from the tests, preliminary computational simulations to calculate the vortex flow structures were carried out. Using the immersed boundary method, we can determine the magnitude and time history of the hydrodynamic forces generated by the pitching panels. These preliminary results highlight some interesting features in the flow field that may explain the differences in performance measured experimentally. Take one frame as shown in Figure 5.3 for example, adding chordwise flexibility reduces the amount of smaller-scale vortices, which have much less contribution to generating thrust compared to the large horseshoe vortex rings shed from the oscillating trailing edge.

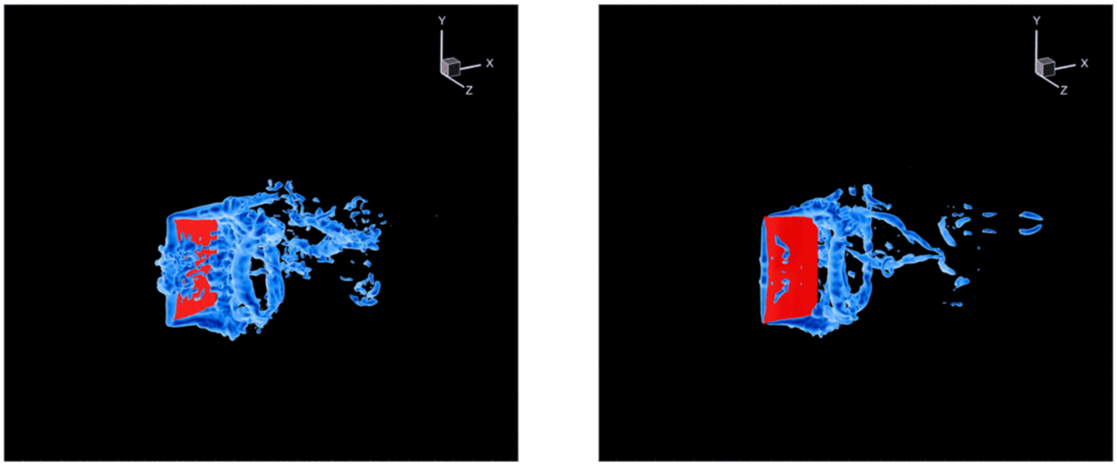

Figure 5.3 Flow structure of rigid (left) vs. chordwise (right) case

Spanwise vortices surrounding the panel at the equivalent time frames for both rigid and chordwise flexible case are also visualized, as shown in Figure 5.4. We observe that the vortices are more concentrated and closer to the panel when we add the chordwise flexibility.

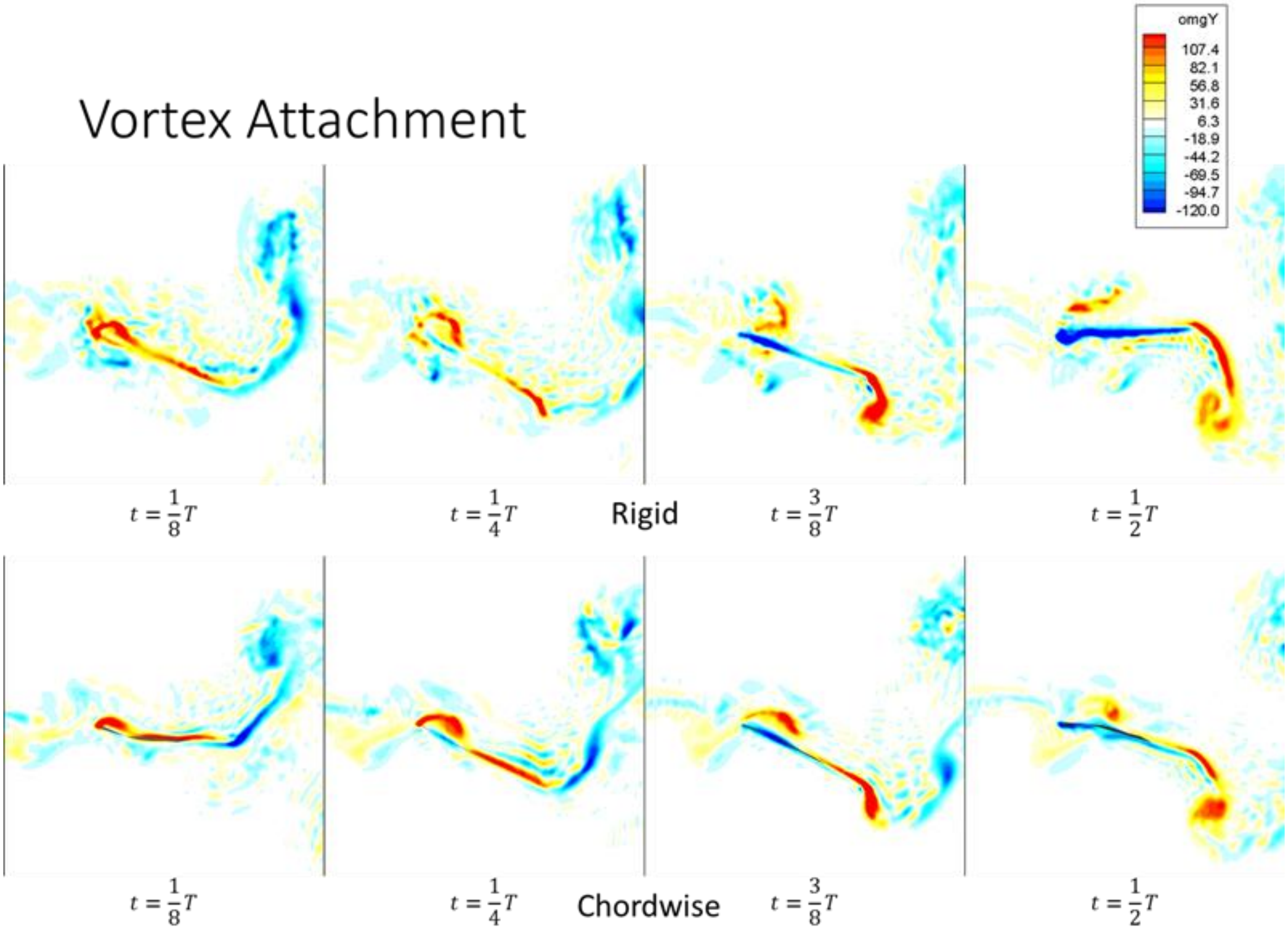

Figure 5.4 Spanwise vortices of rigid (top) vs. chordwise (bottom) case

5.1.4 Discussion

Our results agree with previous numerical work (Q. Zhu, 2007), that chordwise flexibility increases the efficiency of pitching panels, while spanwise flexibility decreases both thrust and efficiency. Our conclusion is backed not only by water tunnel measurement, but also by preliminary CFD flow visualization showing that chordwise flexibility results in cleaner flow structure and better vortex attachment.

As we observed in real tuna kinematics, there is a greater degree of chordwise bending compared to spanwise, which suggest that overall, the anisotropic flexibility should enhance the propulsive efficiency of tuna caudal fin. We are still making a lot of assumptions at the early state: we use a rectangular panel instead of a shape closer to biology; we isolate the directional flexibility instead of combining; the fin-ray inspired structure is coarser than biology; the leading edge motion is pure pitching. In future work, we plan to make modification in these aspects, and study the effects of anisotropic flexibility in a more bio-mimetic setup.

5.2 Heaving Non-Uniform Rectangular Foils

5.2.1 Methodology

Our simulation uses 3 flexible foil with aspect-ratio $AR \equiv L/H = 1$, 1.5 and 2, where L is chord length and H is span length. Here the aspect ratio is defined in the same way as in previous literature (Yeh & Alexeev, 2016) to ensure clear comparison when discussing effects of side edge vortices. The leading edge of the foil is prescribed with a sinusoidal lateral heave motion, i.e. its lateral displacement is

$$Y = \frac{h_0}{2}\sin(2\pi f t),$$

Equation 5-4

where h_0 is the peak-to-peak heaving amplitude and f is the heaving frequency. In contrast, the rest of the plate moves and deforms passively. Figure 5.5a shows the heaving motions of the flexible foil in an incoming flow of velocity U. Figure 5.5b shows how the stiffness was modulated in chordwise direction. The foils on the left are the most flexible design with uniform stiffness of EI = 1.9E-5 Nm^2. We increased stiffness by thickening chordwise quartiles of the foil. The thickened regions, illustrated with a darker orange color, had a higher stiffness of EI = 5.5E-5 m^2. The stiffness values (same in Chapter 6) are chosen to represent upper and lower bounds of bio-propulsor stiffness (Lucas et al., 2015). The approach of adding thickness is due to the limitation of the structure solver, as it only allows prescribing one value of material modulus.

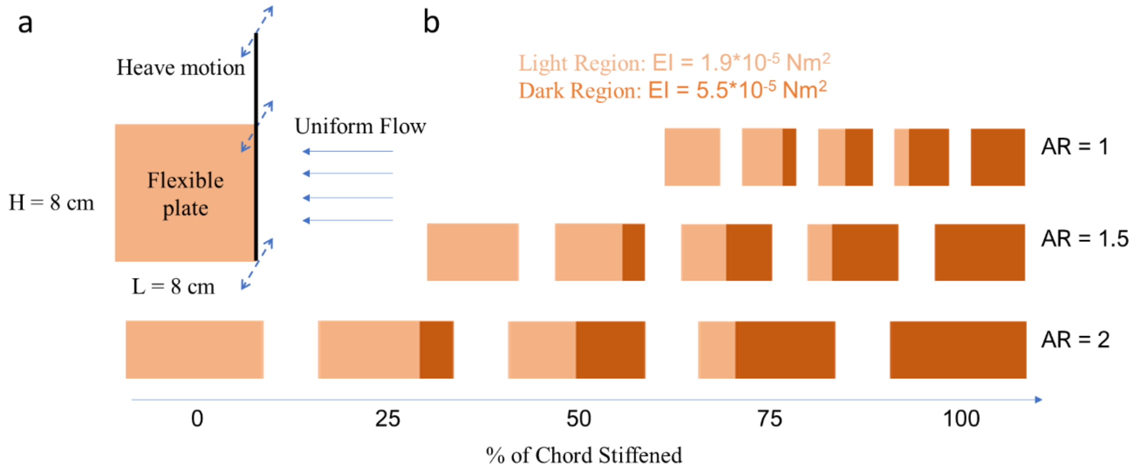

Figure 5.5 (a) Schematics of a flexible square heaving foil with incoming flow (b) Configurations of non-uniform rectangular foils (leading edge on the right side)

In this study, the non-dimensional parameters of Reynolds number Re and Strouhal numbers St are defined as follows:

$$Re = \frac{UL}{\nu}$$

Equation 5-5

$$St = \frac{fh_0}{U}$$

Equation 5-6

where ν is the kinematic viscosity of the fluid. The thrust coefficient C_T, power coefficient C_PW , and propulsive efficiency η are defined to quantify the performance of the flexible plate as follows:

$$C_\mathrm{T} = \frac{F_x}{\frac{1}{2}\rho U^2 LH}$$

Equation 5-7

$$C_\mathrm{P} = \frac{F_y \dot{h}}{\frac{1}{2}\rho U^3 LH}$$

Equation 5-8

$$\eta = \frac{C_\mathrm{T}}{C_\mathrm{P}}$$

Equation 5-9

where F_x is the thrust force (force produced by heaving foil in the opposite direction as the incoming flow) and P_out is the power output (power consumed by the foil during propulsion). The thrust coefficient normalizes thrust by a typical dynamic pressure times foil area. The power coefficient normalizes power output by a typical dynamic pressure times foil area times a typical foil lateral speed. Froude or propulsive efficiency η is the ratio between thrust and power coefficient. Table 5.3 provides a summary of all the parameters involved in this study.

Table 5.3 Case setup parameter space

Parameter	Range
Free Stream Velocity	U = 0.1 m/s
Chord	L = 0.08, 0.12 and 0.16 m
Span	H = 0.08 m
Aspect Ratio	$AR = L/H$ = 1, 1.5 and 2
Heave Frequency	f = 1, 2 Hz
Heave Amplitude	h_0 = 0.015 m
Reynolds Number	$Re = \frac{UL}{\nu} = 8000$
Strouhal number	$St = \frac{2fh_0}{U} = 0.3$ and 0.6
Mass per Chord Length	$\mu = 0.16$ kg/m
Density of Foils/Fluid	$\rho_s = \rho_f = 1000$ kg/m^3
Stiffness Distribution	0, 1, 2, 3, 4 fourths of anterior portion thickened

5.2.2 Results and Discussion

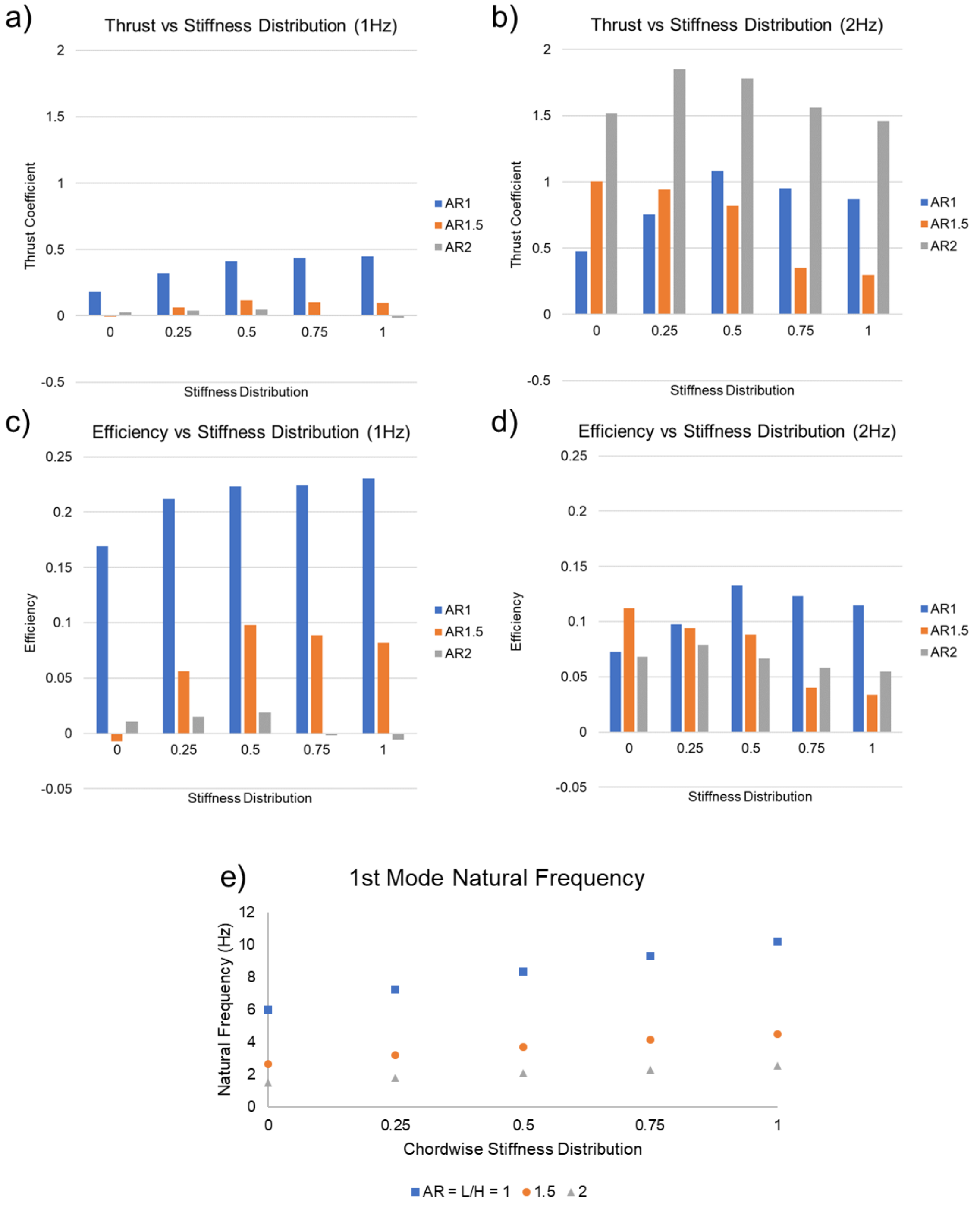

Figure 5.6 Thrust and efficiency for all cases at (a, c) 1 Hz and (b, d) 2 Hz; (e) first mode resonant frequencies for all foils

The data set here is limited in terms of frequency due to the time cost of simulation. A larger data set with more frequency and stiffness distribution is presented and discussed in Chapter 6. Here the focus of discussion will be on qualitative effects of aspect ratio and resonance on propulsive performance (thrust and efficiency).

Since only 2 frequencies are simulated within the parameter space, we cannot determine the exact resonant frequency values of the foils from simulation results. Using the scaling laws (Equation 5-10~14) developed in previous literature (Dewey et al., 2013, Weaver, Timoshenko and Young, 1990), we know that when the flexible foils demonstrating first mode bending get longer (chord increases when span stays the same) and more flexible (lower stiffness distribution), the peak of efficiency should move towards lower frequency.

$$\Pi_k = \left(\frac{E}{\rho_f f^2 L^2}\right)\left(\frac{1}{AR}\right)\left(\frac{h^3}{L^3}\right)$$

Equation 5-10

$$\Pi_m = \left(\frac{\rho_s}{\rho_f}\right)\left(\frac{1}{AR}\right)\left(\frac{h}{L}\right)$$

Equation 5-11

$$\frac{f_1^2}{f^2} \propto \omega_1^2 = \beta_1^4 \frac{\Pi_k}{\Pi_m} = \beta_1^4 \left(\frac{E}{\rho_s f^2}\right)\left(\frac{h^2}{L^4}\right)$$

Equation 5-12

$$f_1 \propto f\omega_1 = \beta_1^2 \left(\frac{E}{\rho_s}\right)^{\frac{1}{2}} \left(\frac{h}{L^2}\right), \text{ where } \frac{\beta_1 L}{\pi} = 0.59686$$

Equation 5-13

$$f_1 = \beta_1^2 \sqrt{\frac{EI}{\mu}} = \frac{3.5161}{L^2} \sqrt{\frac{EI}{\mu}}$$

Equation 5-14

Lower resonant frequency for foils with longer chords (Figure 5.6e) helps explaining that the thrust and efficiency of AR = 2 foils show larger extent of increase compared to AR = 1 foils (Figure 5.6 b, d compared to a, c), since those high AR foils approach first resonance peak when frequency increases from 1 to 2 Hz. The scaling laws developed for uniform foils are approximated for non-uniform foils in this study. Scaling laws for non-uniform foils still need to be developed using larger experimental parameter space in the future.

At frequency of 1 Hz, for AR = 1, highest efficiency occurs at stiffness distribution of 1, while for AR = 1.5 and 2, highest efficiency occurs at 0.5. At frequency of 2 Hz, for AR = 1, highest efficiency occurs at 0.5, and 0 for AR = 1.5 and 0.25 for AR =0.5.

For majority of the parameter space, as aspect ratio increases, efficiency decreases. Previous research (Yeh & Alexeev, 2016) shows that this is partially caused by increased effects of side edge vortices (SEV). For lower aspect ratio (wider) propulsors, the SEV size to span ratio is smaller, thus reducing the overall drag. Additionally, Dewey (2013) shows that when a foil has shorter span length, the performance peaks move towards higher frequency due to increased 3D effects from the foil shape.

The results may also help evaluate whether the bending pattern observed in biological propulsors is optimizing performance or not. Previous study (Lucas et al., 2014) found that many flexible biological propulsors tend to have the most bending at 0.6 or larger of the way down their length. If the rectangular foils are compared with biological propulsors analyzed by Lucas et al., we can conclude that the nature has not necessarily chosen the pattern that generates highest efficiency or thrust for all species, since there are cases in my study where a stiffness distribution of 0.25 yielding highest efficiency. Another limitation to the previous study is that all bending observations were made without considering the role of frequency of oscillation or moving speed of animals. These parameters, especially the frequency as shown in calculation of resonant frequency, have effects on performance of underwater propulsion.

5.3 Summary of Chapter

A preliminary method to add anisotropic stiffness distribution to propulsors is developed and verified through experiments and simulation. Results show that pure chordwise flexibility increases the efficiency of pitching foils with aspect ratio of 0.5, while pure spanwise flexibility decreases both thrust and efficiency.

For heaving rectangular foils with different aspect ratios at 1 Hz, chordwise stiffness distribution greater or equal to 0.5 provides highest efficiency. For heaving rectangular foils with different aspect ratios at 2 Hz, chordwise stiffness distribution less or equal to 0.5 provides highest efficiency. There is no clear best pattern as predicted in previous statistical study of observation in nature.

These conclusions from preliminary experiments and simulation lay the foundation for simulation design in Chapter 6.

6. SQUARE FOILS WITH COMBINED STIFFNESS

We present the effects of stiffness distribution on the propulsive performance of square hydrofoils undergoing heave oscillations in a uniform flow. To identify the role of non-uniform flexural stiffness, we simulated thirteen foils with varying degrees of chordwise and spanwise non-uniform stiffness. Stiffness was controlled by increasing/decreasing the thickness of discrete regions of the foil. In our simulation, we measured the thrust, power and propulsive efficiency of the foils at five different frequencies. We found that non-uniform chordwise stiffness distributions produce higher thrusts and efficiencies than non-uniform spanwise stiffness distributions. The propulsive benefits of hybrid cases (combined chordwise and spanwise flexibility) can be predicted to within 15% by decomposing the stiffness distribution into chordwise and spanwise components. Such decomposition strategy may offer a way to predict performance of foils with complex two-dimensional stiffness profiles, such as real fish caudal fins.

6.1 Introduction

Fluid-structure interaction (FSI) plays an important role in underwater biological propulsion, such as in cases of flexible fish caudal fins (Esposito et al., 2012; Lauder et al., 2011). In general, uniform flexibility can improve the thrust and efficiency of fins (Dewey et al., 2013; Quinn et al., 2015). Simplified and biomimetic models mimicking caudal fins have been used to study individual forms of flexibility, such as chordwise flexibility (J. Katz & Weihs, 1978; Lucas, Thornycroft, Gemmell, Colin, & Costello, n.d.; Prempraneerach et al., 2003), spanwise flexibility (P. Liu & Bose, 1997; Q. Zhu, 2007), and fin ray rigidity (Flammang et al., 2013; Tangorra et al., 2010). However, the stiffness distributions designed in the previous studies are either purely chordwise, purely spanwise, or a complex replica of a biological fin. There has not been a parametric study of how two-dimensional (2D) distributions of chordwise and spanwise stiffness collectively affect the propulsive performance of a canonical propulsor like a heaving foil.

We therefore conducted a computational study of square foils with varying stepwise distributions of chordwise and spanwise stiffness. In doing so, we isolated the individual and combined effects of chordwise and spanwise flexibility on propulsive performance. To simulate the flow around the foil, we used an in-house immersed boundary method (IBM) that has been extensively validated (Wang et al., 2019). Simulation results show that 1) chordwise stiffness distribution produces higher thrusts and efficiency than spanwise stiffness distribution, 2) the optimal chordwise stiffness stays relatively constant compared to spanwise stiffness when heaving frequency changes, and 3) the effect of hybrid stiffness cases can be predicted by decomposing in chordwise and spanwise direction. Our simulation results offer design insights for bio-inspired propulsors. For example, predicting the combined effects of chordwise and spanwise stiffness is critical when optimizing a propulsor's geometry for thrust and/or efficiency.

6.2 Methodology

Our simulations use a flexible foil with aspect-ratio $AR \equiv L/H = 1$, where L is chord length and H is span length. The leading edge of the foil is prescribed with a sinusoidal lateral heave motion, i.e. its lateral displacement is

$$Y = \frac{h_0}{2}\sin(2\pi f t),$$

Equation 6-1

where h_0 is the peak-to-peak heaving amplitude and f is the heaving frequency. In contrast, the rest of the plate moves and deforms passively. Figure 5.1a shows the heaving motions of the flexible foil in an incoming flow of velocity U. Figure 5.1b shows how the stiffness was modulated in chordwise and spanwise direction. The foil at bottom left corner is the most flexible design with uniform stiffness of EI = $1.9*10^{-5}$ Nm^2. We increased stiffness by thickening chordwise quartiles and spanwise thirds of the foil. The thickened regions, illustrated with a darker orange color, had a higher stiffness of EI = $5.5*10^{-5}$ Nm^2. The stiffness values (same in Chapter 5.2) are chosen to represent upper and lower bounds of bio-propulsor stiffness (Lucas et al., 2015). The approach of adding thickness is due to the limitation of the structure solver, as it only allows prescribing one value of material modulus.

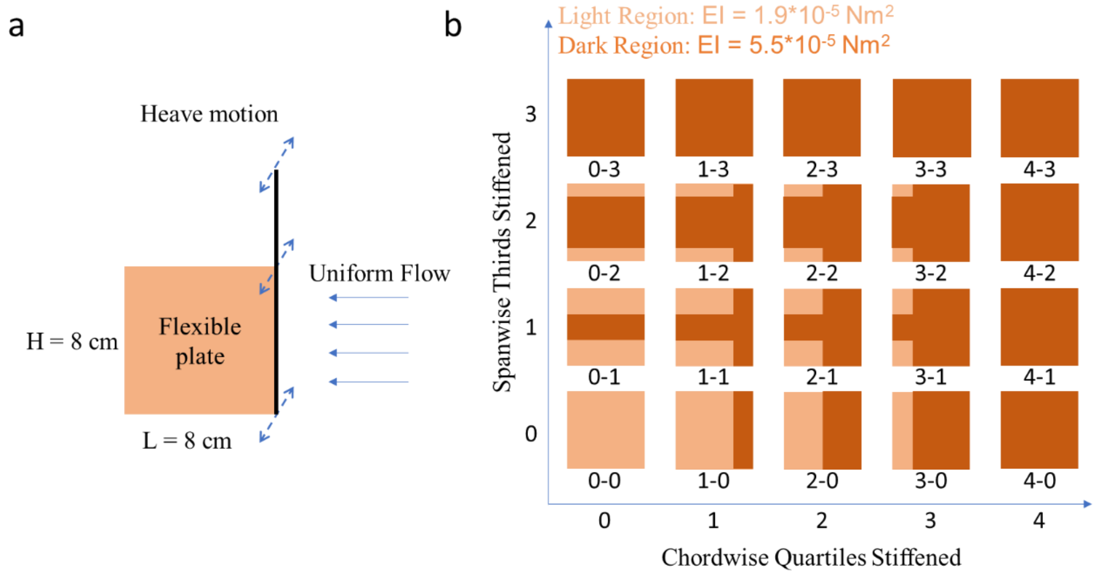

Figure 6.1 Foil geometry and stiffness distribution. (a) Schematics of a flexible heaving foil with incoming flow (b) Configurations of non-uniform foils with labels (first number represents number of chordwise quartiles stiffened; second number represents number of spanwise thirds stiffened).

In this study, the non-dimensional parameters of Reynolds number Re and Strouhal numbers St are defined as follows:

$$Re = \frac{UL}{\nu}$$

Equation 6-2

$$St = \frac{f h_0}{U}$$

Equation 6-3

where ν is the kinematic viscosity of the fluid. The thrust coefficient C_{T}, power coefficient C_{PW} , and propulsive efficiency η are defined to quantify the performance of the flexible plate as follows:

$$C_{\mathrm{T}} = \frac{F_x}{\frac{1}{2}\rho U^2 LH}$$

Equation 6-4

$$C_{\mathrm{P}} = \frac{F_y \dot{h}}{\frac{1}{2}\rho U^3 LH}$$

Equation 6-5

$$\eta = \frac{C_{\mathrm{T}}}{C_{\mathrm{P}}}$$

Equation 6-6

where F_x is the thrust force (force produced by heaving foil in the opposite direction as the incoming flow) and P_{out} is the power output (power consumed by the foil during propulsion). The thrust coefficient normalizes thrust by a typical dynamic pressure times foil area. The power coefficient normalizes power output by a typical dynamic pressure times foil area times a typical foil lateral speed. Froude or propulsive efficiency η is the ratio between thrust and power coefficient. Table 6.1 provides a summary of all the parameters involved in this study.

Table 6.1 Case setup parameter space

Parameter	Range
Free Stream Velocity	U = 0.1 m/s
Chord	H = 0.08 m
Span	L = 0.08 m
Heave Frequency	f = 0.5, 1, 1.5, 2 and 2.5 Hz
Heave Amplitude	h_0 = 0.015 m
Reynolds Number	$Re = \frac{UL}{\nu} = 8000$
Strouhal number	$St = \frac{fh_0}{U} =$ 0.15, 0.3, 0.45, 0.6 and 0.75
Flexibility Distribution	0, 1, 2, 3, 4 fourths of anterior portion thickened
	0, 1, 2, 3 thirds of mid-span thickened

6.3 Chordwise vs Spanwise

First, we compare the propulsive performance of pure chordwise versus pure spanwise stiffness distributions. Figure 6.2 shows the thrust coefficient of panels with chordwise stiffness (6.2a) and spanwise stiffness (6.2b). In both cases, thrust increases monotonically with frequency but has a more complex dependence on stiffness. Chordwise stiffness has almost no effect on thrust at low frequencies ($f <\approx 1.5$ Hz) but can increase thrust by ≈ 25% at higher frequencies. To create this increase, chordwise stiffness should be between 0.5 and 0.75, not at its maximum value. This intermediate optimal stiffness is consistent with previous studies that have demonstrated the importance of resonance in optimal propulsion (Heathcote & Gursul, 2007; Masoud & Alexeev, 2010). As with the effects of chordwise stiffness, the effects of spanwise stiffness are more pronounced at higher frequencies. However, the highest thrust occurred at the maximum stiffness distribution of 1, not at an intermediate value. Overall, thrust was increased more by chordwise stiffness than by spanwise stiffness, despite the cross-sectional area of the foils being the same.

In terms of power, chordwise and spanwise stiffness produce similar trends (Figure 6.2c,d). The power consumption of foils is almost exclusively a function of heaving frequency. Compared to their effects on thrust, chordwise and spanwise stiffness have relatively little effect on power consumption.

The ratio of the thrust and power coefficients gives the propulsive efficiency, which exhibits more complex trends than thrust and power individually. As frequency increases, efficiency first increases then decreases, peaking between $f =1$ and 1.5 Hz. This rise and fall of efficiency with frequency has been observed in previous experiments and has been linked to a narrow range of optimally efficient Strouhal numbers (Taylor et al., 2003; M. S. Triantafyllou & Triantafyllou, 1995). Efficiency also increases with added stiffness, consistent with previous work showing the effects of stiffness on efficiency (Dewey et al., 2013). Comparing the area of highest efficiency in

Figure 6.2e and 6.2f, we conclude that chordwise stiffness helps the foil reach slightly higher efficiencies than does spanwise stiffness, as on average chordwise stiffness is 5.9% higher than spanwise stiffness in terms of efficiency.

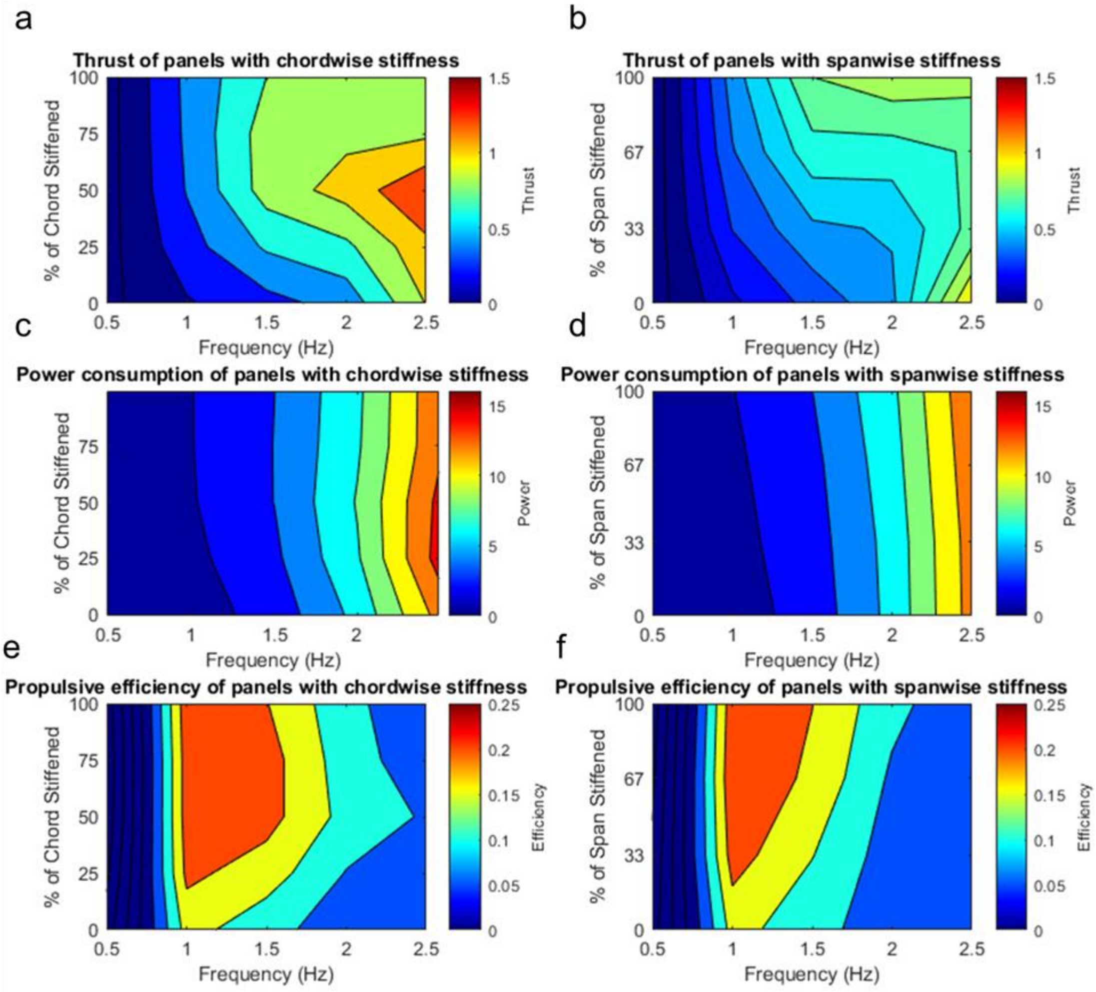

Figure 6.2 Propulsive performance of foils with purely chordwise or spanwise stiffness. (a,b) Thrust, (c,d) power consumption, and (e,f) propulsive efficiency of foils with chordwise stiffness versus foils with spanwise stiffness.

Previous studies show that efficiency can peak below (Ramananarivo et al., 2010), at (Michelin & Llewellyn Smith, 2009), or above (Masoud & Alexeev, 2010) the resonant frequency. And Dewey (2013) further demonstrated that the resonant frequency is not a sufficient condition for achieving optimal efficiency for flexible propulsors. Instead a Strouhal number within 0.25 ~ 0.35 plays a more significant role in determining the optimal efficiency of flexible propulsors. Given the limited number of frequency tested, we find that 1 Hz is the only frequency that yields a Strouhal number that falls within the optimal range of 0.25 ~ 0.35, thus explaining that for almost all foil design the optimal efficiency is achieved at 1 Hz.

6.4 Combined Stiffness

Figure 6.3 shows efficiency for the hybrid foil cases (both spanwise and chordwise stiffness). As in the pure spanwise and chordwise stiffness cases, efficiency first increases, then decreases, with frequency. To better under the optimal design for each frequency, we plotted frequency over chordwise and spanwise stiffness distribution as shown in Figure 5.3b-f. For the lowest frequency, choosing the most flexible design is optimal for efficiency (Figure 5.3b). If the incoming flow velocity is reduced, the foil should be able to self-propel at a lower velocity. As frequency increases (excluding the lowest frequency), the location of optimal efficiency shifts downwards, which means the foil needs to be more flexible in the spanwise direction to maintain high efficiency. However, the horizontal location of optimal efficiency stays around the same location, which shows that a 0.5 ~ 0.75 chordwise stiffness stays as the optimal design for square foils.

Two-way ANOVA (Analysis of Variance) with a similar setup (confidence interval of 0.05) as in previous study (Lucas et al., 2015) is also conducted to evaluate the effects of frequency or stiffness distribution on propulsive efficiency (Table 6.2). Two-way ANOVA are conducted for the whole parameter space, using frequency and stiffness distribution as categorical factors. Based on the p values, we can see that frequency ($p < 0.001$) has significant effects on propulsive efficiency of heaving flexible foils, while the effects of stiffness distribution ($p = 0.516$) on the average propulsive efficiency for the whole range of frequency cannot be determined in a purely statistical way. However, when the range of frequency is limited to the intermediate range of 1~2 Hz, the effects of stiffness distribution is significant ($p < 0.001$). This is because adding stiffness in general increases efficiency at intermediate frequencies, while decreasing efficiency at the lowest (0.5 Hz) and highest (2.5 Hz) frequency. The opposing effects (Figure 6.5) cancel out each other when comparing the mean efficiency values of the whole frequency range, thus yielding high P-value.

Table 6.2 ANOVA of parameter space

	MS	*F*	*P-value*	*F crit*
Frequency (0.5~2.5 Hz)	0.342661	786.4234	8.22E-46	4.21025
Stiffness (0.5~2.5 Hz)	0.000411	0.944251	0.516194	2.740578
Frequency (1~2 Hz)	0.050274	256.0409	7.83E-18	3.369016
Stiffness (1~2 Hz)	0.001281	6.523689	2.63E-05	2.119166

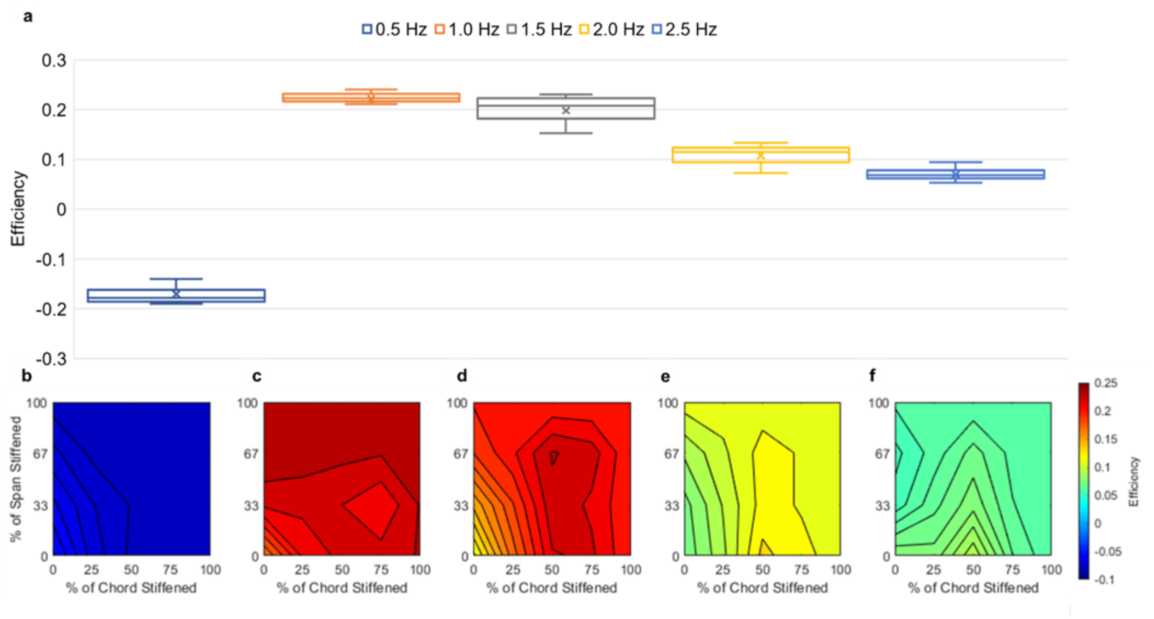

Figure 6.3 Propulsive performance of foils with hybrid stiffness (chordwise and spanwise). (a) Average efficiency across all fin types at each frequency. (b-f) Efficiency as a function of chordwise and spanwise stiffness distributions at frequencies of 0.5, 1.0, 1.5, 2.0, and 2.5 Hz

6.5 Predicting Combined Effects of Chordwise and Spanwise Stiffness

Using the efficiency data presented, we explored the possibility of predicting efficiency performance of hybrid cases by decomposing the stiffness distribution into chordwise and spanwise components (Figure 5). Efficiency gain of a certain foil (efficiency η) over the most flexible 0-0 design is defined as:

$$\text{gain} = \frac{\eta - \eta_{0-0}}{\eta_{0-0}}$$

Efficiency gains are presented in fractions, so an efficiency gain value of 1 means 100% efficiency enhancement. Consider Figure 5e as example. For foil 3-1, we first calculate its actual efficiency gain over the most flexible foil (0-0). Then we consider the foil with the same spanwise stiffness but no chordwise stiffness (foil 0-1) and the foil with the same chordwise stiffness but no spanwise stiffness (foil 3-0). The grey ‘prediction’ bar represents the sum of the efficiency gains from the pure chordwise and spanwise cases, with efficiency gains from the overlapping area subtracted to avoid them being double counted. The potential benefits of such a decomposition (Figure 6.4) is that we can reduce the size of the parameter space from m*n to m+n, where m and n are the number of chordwise and spanwise divisions. In our study, m is 4 and n is 3.

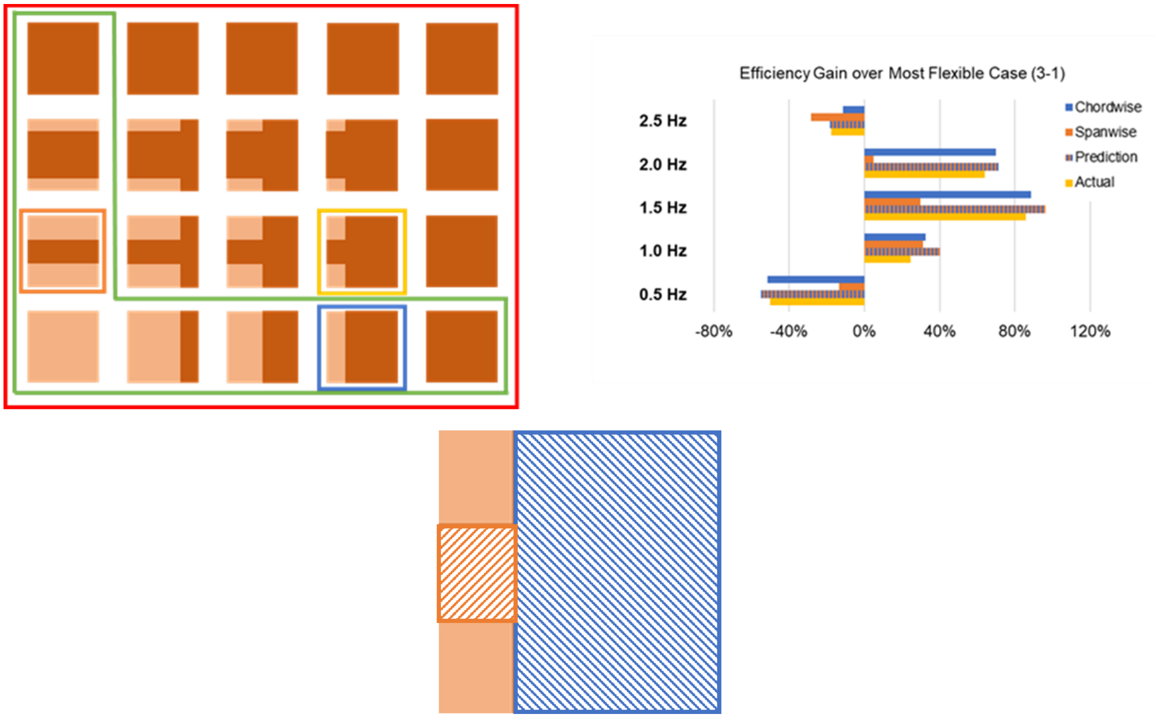

Figure 6.4 Decomposition strategy, using foil 3-1 as an example: when calculating the combined prediction of efficiency gain, chordwise stiffness is chosen first, then spanwise stiffness is added without the portion overlapped with chordwise stiffness. Efficiency gain in spanwise direction is reduced proportionally based on reduced area.

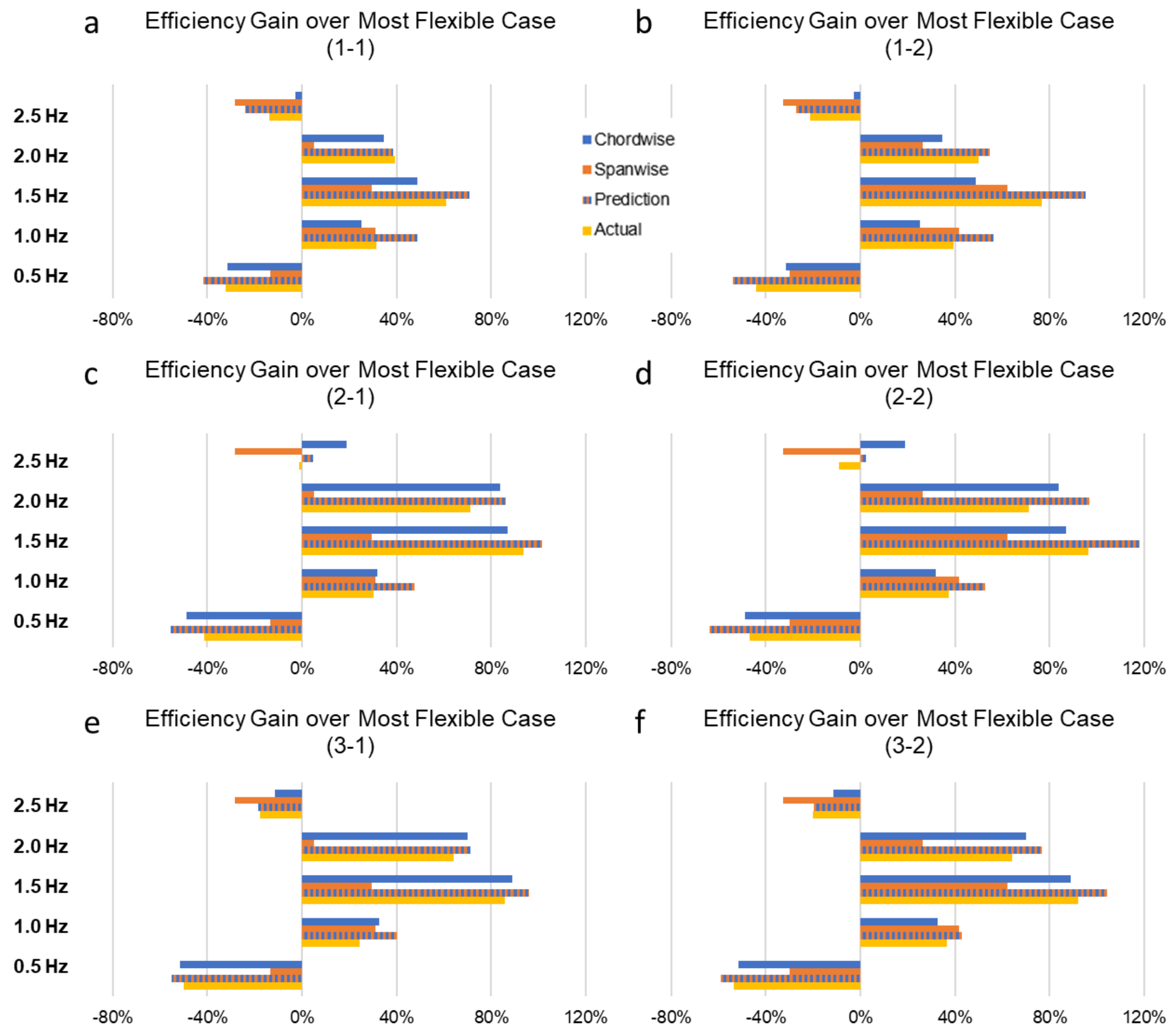

Figure 6.5 Comparing predicted with actual efficiency boost in the hybrid stiffness cases. Efficiency gains over the most flexible design are compared for each foil: (a) 1-1 (b) 2-1 (c) 3-1 (d) 1-2 (e) 2-2 and (f) 3-2.

From the comparison of actual and predicted efficiency gains shown in Figure 6.4, we see that the actual and predicted gains have the same sign except for two high frequency cases (foil 2-1 and 2-2 at 2.5Hz), where the actual gain is slightly negative and the predicted gain is slightly positive. In cases where the signs agree, the magnitude of the actual gain is generally smaller than the predicted gain, the two exceptions being foil 1-1 at 2.0 Hz and foil 3-2 at 2.5Hz.

The difference between actual and predicted gains suggests some nonlinear interactions between spanwise and chordwise stiffness. Presumably at higher frequencies, the foil deforms more due to larger fluid forces on its surface, thus breaking the linearity of its structure behavior (Ladevèze & Simmonds, 1998). We used bio-inspired stiffnesses (McHenry, Pell, & Long, 1995; Tytell, Hsu, Williams, Cohen, & Fauci, 2010), but higher stiffnesses may be able to preserve the linearity of the system at higher flapping frequencies. These types of nonlinear effects have been previously studied in the case of elastic airfoils (Conner, Tang, Dowell, & Virgin, 1997). The fact that the predicted gains are consistently overestimates (Figure 6.5) implies some destructive interaction between chordwise and spanwise stiffness in terms of efficiency. Nevertheless, the disagreement between actual and predicted gains is mostly around 20 ~30 % and never more than 65%, suggesting that spanwise and chordwise stiffness have a strong linear component over the range we considered.

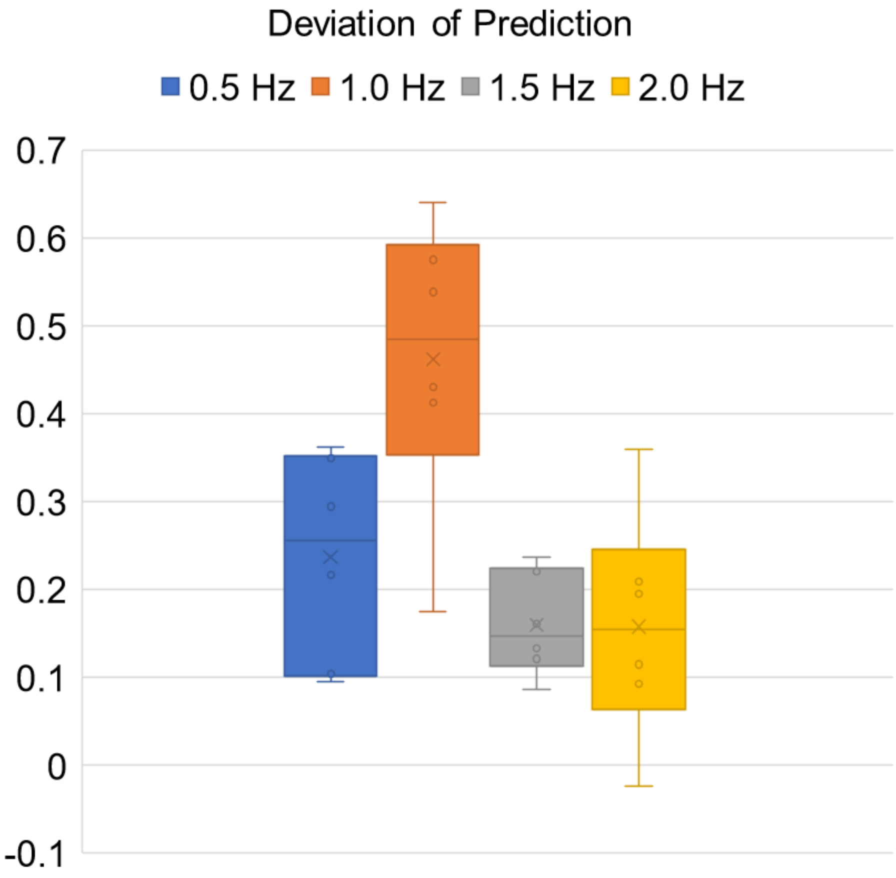

Figure 6.6 Deviation of prediction at each frequency

6.6 Summary of Chapter

By conducting a parameter sweep of chordwise and spanwise stiffness, we determined how chordwise and spanwise stiffness relate and interact for square foils. Foils with pure chordwise stiffness distribution exhibit higher thrust and efficiency overall compared to foils with pure spanwise stiffness distribution. Regardless of the stiffness distribution, efficiency increased then decreased with frequency, peaking at an intermediate Strouhal number. Adding stiffness generally helps to enhance efficiency at intermediate frequencies. When heaving at the lowest frequency, the most flexible foil is most efficient (if the incoming flow velocity is reduced, the foil should be able to self-propel at a lower velocity). As frequency increases, it becomes advantageous to add chordwise stiffness to the first half (or slightly more) of the chord and decrease the spanwise stiffness at the midspan. Based on the deviation between predicted and actual efficiency boosts (Figure 6.4 and 6.5), engineers could potentially test pure chordwise and spanwise stiffness cases, then use the results to predict efficiency gain in hybrid cases. The prediction would likely be an overestimate but could offer preliminary guidance when designing 2D stiffness distributions for foils operating at in the range of 0~2 Hz.

The recommended design of an efficient heaving foil seems to agree with observation made on fish caudal fins, where the leading edge is stiffer. The stiffer mid span of a tuna caudal fin could be due to limitation of biology as it does not provide performance enhancement at higher frequency. In future study, varying the spanwise stiffness of a bio-inspired foil is worth investigating.

Last but not least, the stiffness values are chosen based on biology observation (Lucas et al., 2015) and may not work well for higher frequencies. For future study with higher frequency values, researchers should carefully choose higher stiffness values or use effective stiffness scaled by frequency for cross-study comparison.

7. CONCLUSION

- **What is the range of structural and material flexibility observed in biology (tuna)?**

Mechanical testing is employed to determine the range of biological stiffness observed in biology, especially the fin rays and tendons of tuna. The modulus properties of these tissues are comparable with ABS plastics (Suarez, Barlow, & Paul, 1984). Thus it is feasible to use rapid prototyping techniques to design propulsors inspired by tuna.

Video tracking is employed to quantify direction and extent of bending in thunniform swimming. The bending in both chordwise and spanwise directions is dominantly passive.

- **How does peduncle joint (stiffness) affect propulsive performance of a bio-inspired foil?**

From the results of computational study of phase offset, we have concluded that a passively flexing foil is as efficient or more efficient than any model where the caudal peduncle is actively controlled. From the experimental results of the four foils with different peduncle joint stiffness, it is evident that the effects of stiffness on lateral displacement, efficiency, and thrust are complex and not easily predicted across a wide parameter space. So we conclude that although there is no one optimal stiffness across all parameter spaces, there are clear differences in performance due to peduncle stiffness. Therefore, we should focus future design on the ability to actively modulate stiffness such that we can achieve optimal performance at any set of swimming parameters.

- **How does shape and directional stiffness affect performance of rectangular foils?**

Results show that pure chordwise flexibility increases the efficiency of pitching foils with aspect ratio of 0.5, while pure spanwise flexibility decreases both thrust and efficiency.

For heaving rectangular foils with different aspect ratios at 1 Hz, chordwise stiffness distribution greater or equal to 0.5 provides highest efficiency. When aspect ratio increases, efficiency decreases due to increased drag from side edge vortices.

- **Using a square foil as baseline, how should engineers design a bio-inspired propulsor, from the perspective of stiffness distribution?**

Square foils with pure chordwise stiffness distribution have overall higher thrust and efficiency than foils with pure spanwise stiffness distribution Adding stiffness to a fully flexible (near the lower bound of fish stiffness) foil generally helps enhancing efficiency at intermediate efficiency. When heaving at lowest frequency, the most flexible foil performs most efficiently. Once frequency increases, it is optimal to add a chordwise stiffness distribution to the first half of the chord (or slightly more) and gradually decreases the spanwise stiffness from most to least. Lastly, when designing 2D stiffness distribution for a foil operating at in the range of 0~2 Hz, engineers can potentially test the pure chordwise and spanwise cases only, and use the results to predict efficiency gain with a slight overestimate for cases with hybrid distribution design.

8. FUTURE WORK

8.1 Maneuverability and Control

Animals and bio-inspired underwater vehicles need to be able to efficiently generate not only streamwise net thrust, but also forces that are transverse to the direction of motion to maneuver quickly. A clear understanding of the generation of these forces is required to properly characterize the maneuverability of bio-inspired propulsion and inform future design of bio-inspired propulsors.

8.2 Complex Geometry

Chapter 5 and 6 focus on flexible propulsors with canonical shapes. The simplified shapes make deriving design guidelines possible, however the effects of more complex geometry are missing. Apply the guidelines to design of propulsors with more complex and biomimetic shapes will be helpful in evaluating the robustness of these design guidelines.

8.3 Biological Considerations

One of the central topics of this thesis is that passive flexibility can be exploited to enhance propulsive efficiency. Results show that for different kinematics configurations (frequency, amplitude etc.), the optimal stiffness changes. Animals including tuna may actively tunes its stiffness to remain in an efficiency regime while swimming under different conditions. Further analysis in this area could be helpful in determining the actual mechanisms employed by animals.

BIBLIOGRAPHY

Affleck, R. J. (1950). Some points in the function, development and evolution of the tail in fishes. *Proceedings of the Zoological Society of London*, *120*(2), 349–368. https://doi.org/10.1111/j.1096-3642.1950.tb00954.x

Borazjani, I., & Sotiropoulos, F. (2010). On the role of form and kinematics on the hydrodynamics of self-propelled body/caudal fin swimming. *Journal of Experimental Biology*, *213*(1), 89–107. https://doi.org/10.1242/jeb.030932

Borazjani, Iman, & Daghooghi, M. (2013). The fish tail motion forms an attached leading edge vortex. *Proceedings. Biological Sciences / The Royal Society*, *280*(1756), 20122071. https://doi.org/10.1098/rspb.2012.2071

Breder, C. (1926). The locomotion of fishes. *Zoologica : Scientific Contributions of the New York Zoological Society.*, *4*(5), 159–297. Retrieved from http://ci.nii.ac.jp/naid/10028166269/en/

Chopra, M. G. (1974). Hydromechanics of lunate-tail swimming propulsion. *Journal of Fluid Mechanics*, *64*(02), 375–391. https://doi.org/10.1017/S0022112077000032

Chopra, M. G., & Kambe, T. (1977). Hydromechanics of lunate-tail swimming propulsion. Part 2. *Journal of Fluid Mechanics*, *79*(1), 49–69. https://doi.org/10.1017/S0022112077000032

Conner, M. D., Tang, D. M., Dowell, E. H., & Virgin, L. N. (1997). Nonlinear behavior of a typical airfoil section with control surface freeplay: A numerical and experimental study. *Journal of Fluids and Structures*, *11*(1), 89–109. https://doi.org/10.1006/jfls.1996.0068

Cort, J. L. (1991). Age and growth of the bluefin tuna, Thunnus thynnus (L.) of the Northeastern Atlantic. *ICCAT Collective Volume of Scientific Papers*, *35: 213-2*(Tuna-fisheries), Thunnus\rbluefin tuna\rfisheries\rage. Retrieved from https://agris.fao.org/agris-search/search.do?recordID=QC2003600089

Dewar, H., & Graham, J. (1994). Studies of Tropical Tuna Swimming Performance in a Large Water Tunnel - Kinematics. *The Journal of Experimental Biology*, *192*, 45–59. Retrieved from http://jeb.biologists.org/content/jexbio/192/1/13.full.pdf

Dewey, P. A., Boschitsch, B. M., Moored, K. W., Stone, H. A., & Smits, A. J. (2013). Scaling laws for the thrust production of flexible pitching panels. *Journal of Fluid Mechanics*, *732*, 29–46. https://doi.org/10.1017/jfm.2013.384

Dong, H., Liang, Z., & Harff, M. (2009). Optimal Settings of Aerodynamic Performance Parameters in Hovering Flight, *1*(3).

Donley, J. M., Sepulveda, C. a, Konstantinidis, P., Gemballa, S., & Shadwick, R. E. (2004). Convergent evolution in mechanical design of lamnid sharks and tunas. *Nature*, *429*(May), 61–65. https://doi.org/10.1038/nature02435

Dowell, E. H., & Hall, K. C. (2001). Modeling of fluid-structure interaction. *Annual Review of Fluid Mechanics*, *33*(1), 445–490. https://doi.org/10.1146/annurev.fluid.33.1.445

Eloy, C. (2012). Optimal Strouhal number for swimming animals. *Journal of Fluids and Structures*, *30*, 205–218. https://doi.org/10.1016/j.jfluidstructs.2012.02.008

Esposito, C. J., Tangorra, J. L., Flammang, B. E., & Lauder, G. V. (2012). A robotic fish caudal fin: effects of stiffness and motor program on locomotor performance. *Journal of Experimental Biology*, *215*(1), 56–67. https://doi.org/10.1242/jeb.062711

Feilich, K. L., & Lauder, G. V. (2015). Passive mechanical models of fish caudal fins: Effects of shape and stiffness on self-propulsion. *Bioinspiration and Biomimetics*, *10*(3), 036002. https://doi.org/10.1088/1748-3190/10/3/036002

Fish, F. E. (1996). Transitions from drag-based to lift-based propulsion in mammalian swimming. *American Zoologist*, *36*(6), 628–641. https://doi.org/10.1093/icb/36.6.628

Fish, F., Schreiber, C., Moored, K., Liu, G., Dong, H., & Bart-Smith, H. (2016). Hydrodynamic Performance of Aquatic Flapping: Efficiency of Underwater Flight in the Manta. *Aerospace*, *3*(3), 20. https://doi.org/10.3390/aerospace3030020

Flammang, B. E., Alben, S., Madden, P. G. A., & Lauder, G. V. (2013). Functional morphology of the fin rays of teleost fishes. *Journal of Morphology*, *274*(9), 1044–1059. https://doi.org/10.1002/jmor.20161

Ghias, R., Mittal, R., Dong, H., & Lund, T. S. (2005). Study of tip-vortex formation using large-eddy simulation. *43rd AIAA Aerospace Sciences Meeting and Exhibit - Meeting Papers*, (January), 10853–10865. https://doi.org/10.2514/6.2005-1280

Gibb, A., Dickson, K., & Lauder, G. (1999). Tail kinematics of the chub mackerel Scomber japonicus: testing the homocercal tail model of fish propulsion. *The Journal of Experimental Biology*, *202*(Pt 18), 2433–2447. Retrieved from http://www.ncbi.nlm.nih.gov/pubmed/10460731

Han, P., Dong, H., di Santo, V., Lauder, G., Han, P., Dong, H., … Lauder, G. (2017). Kinematics and Hydrodynamics of Burst-and-Coast Strategy in Carangiform Swimming. *APS*, L9.003. Retrieved from https://ui.adsabs.harvard.edu/abs/2017APS..DFD.L9003H/abstract

Han, P., Lauder, G. V., & Dong, H. (2020). Hydrodynamics of median-fin interactions in fish-like locomotion: Effects of fin shape and movement. *Physics of Fluids*, *32*(1), 011902. https://doi.org/10.1063/1.5129274

Heathcote, S., & Gursul, I. (2007). Flexible flapping airfoil propulsion at low reynolds numbers. *AIAA Journal*, *45*(5), 1066–1079. https://doi.org/10.2514/1.25431

Kancharala, a K., & Philen, M. K. (2014). Study of flexible fin and compliant joint stiffness on propulsive performance: theory and experiments. *Bioinspiration & Biomimetics*, *9*(3), 036011. https://doi.org/10.1088/1748-3182/9/3/036011

Kang, C. K., Aono, H., Cesnik, C. E. S., & Wei, S. (2011). Effects of flexibility on the aerodynamic performance of flapping wings. In *6th AIAA Theoretical Fluid Mechanics Conference*. https://doi.org/10.2514/6.2011-3121

Karpouzian, G., Spedding, G., & Cheng, H. K. (1990). Lunate-tail swimming propulsion. Part 2. Performance analysis. *Journal of Fluid Mechanics*, *210*(1), 329. https://doi.org/10.1017/S0022112090001318

Kato, N. (2000). Control performance in the horizontal plane of a fish robot with mechanical pectoral fins. *IEEE Journal of Oceanic Engineering*, *25*(1), 121–129. https://doi.org/10.1109/48.820744

Katz, J., & Weihs, D. (1978). Hydrodynamic propulsion by large amplitude oscillation of an airfoil with chordwise flexibility. *Journal of Fluid Mechanics*, *88*(3), 485–497. https://doi.org/10.1017/S0022112078002220

Katz, S. L., Syme, D. a, & Shadwick, R. E. (2001). High-speed swimming. Enhanced power in yellowfin tuna. *Nature*, *410*(6830), 770–771. https://doi.org/10.1038/35071170

Khalid, M. S. U., Akhtar, I., & Dong, H. (2016). Hydrodynamics of a tandem fish school with asynchronous undulation of individuals. *Journal of Fluids and Structures*, *66*, 19–35. https://doi.org/10.1016/j.jfluidstructs.2016.07.008

Ladevèze, P., & Simmonds, J. (1998). New concepts for linear beam theory with arbitrary geometry and loading. *European Journal of Mechanics, A/Solids*, *17*(3), 377–402. https://doi.org/10.1016/S0997-7538(98)80051-X

Lauder, G. V., Anderson, E. J., Tangorra, J., & Madden, P. G. A. (2007). Fish biorobotics: Kinematics and hydrodynamics of self-propulsion. *Journal of Experimental Biology*, *210*(16), 2767–2780. https://doi.org/10.1242/jeb.000265

Lauder, G. V., Flammang, B., & Alben, S. (2012). Passive robotic models of propulsion by the bodies and caudal fins of fish. *Integrative and Comparative Biology*, *52*(5), 576–587. https://doi.org/10.1093/icb/ics096

Lauder, G. V., Madden, P. G. a, Tangorra, J. L., Anderson, E., & Baker, T. V. (2011). Bioinspiration from fish for smart material design and function. *Smart Materials and Structures, 20,* 094014. https://doi.org/10.1088/0964-1726/20/9/094014

Leftwich, M. C., Tytell, E. D., Cohen, a. H., & Smits, a. J. (2012). Wake structures behind a swimming robotic lamprey with a passively flexible tail. *Journal of Experimental Biology*, *215*(3), 416–425. https://doi.org/10.1242/jeb.061440

Lighthill, M. J. (1970). Aquatic animal propulsion of high hydromechanical efficiency. *Journal of Fluid Mechanics*, *44*(02), 265. https://doi.org/10.1017/S0022112070001830

Lindsey, C. C. (1978). Form, function, and locomotory habits in fish. In *Fish Physiology* (Vol. 7, pp. 1–100). Academic Press. https://doi.org/10.1016/S1546-5098(08)60163-6

Liu, G., Ren, Y., Zhu, J., Bart-Smith, H., & Dong, H. (2015). Thrust producing mechanisms in ray-inspired underwater vehicle propulsion. *Theoretical and Applied Mechanics Letters*. https://doi.org/10.1016/j.taml.2014.12.004

Liu, P., & Bose, N. (1997). Propulsive performance from oscillating propulsors with spanwise flexibility. *Proceedings of the Royal Society A*, *453*(1963), 1763–1770. https://doi.org/10.1098/rspa.1997.0095

Lucas, K. N., Johnson, N., Beaulieu, W. T., Cathcart, E., Tirrell, G., Colin, S. P., … Costello, J. H. (2014). Bending rules for animal propulsion. *Nature Communications*, *5*. https://doi.org/10.1038/ncomms4293

Lucas, K. N., Thornycroft, P. J. M., Gemmell, B. J., Colin, S. P., & Costello, J. H. (n.d.). Effects of non-uniform stiffness on the swimming performance of a passively- fl exing , fi sh-like foil model. *Bioinspiration & Biomimetics*, *10*(5), 56019. https://doi.org/10.1088/1748-3190/10/5/056019

Lucas, K. N., Thornycroft, P. J. M., Gemmell, B. J., Colin, S. P., Costello, J. H., & Lauder, G. V. (2015). Effects of non-uniform stiffness on the swimming performance of a passively-flexing, fish-like foil model. *Bioinspiration and Biomimetics*, *10*(5). https://doi.org/10.1088/1748-3190/10/5/056019

Masoud, H., & Alexeev, A. (2010). Resonance of flexible flapping wings at low Reynolds number. *Physical Review E - Statistical, Nonlinear, and Soft Matter Physics*, *81*(5), 056304. https://doi.org/10.1103/PhysRevE.81.056304

McHenry, M. J., Pell, C. A., & Long, J. H. (1995). Mechanical control of swimming speed: stiffness and axial wave form in undulating fish models. *The Journal of Experimental Biology*, *198*(Pt 11), 2293–2305. Retrieved from https://jeb.biologists.org/content/jexbio/198/11/2293.full.pdf

Michelin, S., & Llewellyn Smith, S. G. (2009). Resonance and propulsion performance of a heaving flexible wing. *Physics of Fluids*, *21*(7), 071902. https://doi.org/10.1063/1.3177356

Mittal, R., Dong, H., Bozkurttas, M., Najjar, F. M., Vargas, A., & von Loebbecke, A. (2008). A versatile sharp interface immersed boundary method for incompressible flows with complex boundaries. *Journal of Computational Physics*, *227*(10), 4825–4852. https://doi.org/10.1016/j.jcp.2008.01.028

Potthoff, T. (1975). Complex , the Vertebral Column , and the Pterygiophores in the Blackfin Tuna (Thunnus, *25*(2), 205–231.

Prempraneerach, P., Hover, F. S., & Triantafyllou, M. S. (2003). The effect of chordwise flexibility on the thrust and efficiency of a flapping foil. In *International Symposium on Unmanned Untethered Submersible Technology*. Retrieved from http://web.mit.edu/arg/www/towtank/papers/FlexibleFoil_Paper.pdf%5Cnpapers3://publication/uuid/2586F91D-B411-406F-9BE7-F472F3577380

Quinn, D. B., Lauder, G. V., & Smits, A. J. (2015). Maximizing the efficiency of a flexible propulsor using experimental optimization. *Journal of Fluid Mechanics*, *767*(September), 430–448. https://doi.org/10.1017/jfm.2015.35

Quinn, D. B., Lauder, G. V, & Smits, A. J. (2014). Scaling the propulsive performance of heaving flexible panels. *Journal of Fluid Mechanics*, *738*, 250–267. https://doi.org/10.1017/jfm.2013.597

Ramananarivo, S., Godoy-Diana, R., & Thiria, B. (2010). Rather than resonance, flapping wing flyers may play on aerodynamics to improve performance. https://doi.org/10.1073/pnas.1017910108

Ren, Y., Dong, H., Deng, X., & Tobalske, B. (2016). Turning on a dime: Asymmetric vortex formation in hummingbird maneuvering flight. *Physical Review Fluids*, *1*(5), 050511. https://doi.org/10.1103/physrevfluids.1.050511

Rosic, M. L. N., Thornycroft, P. J. M., Feilich, K. L., Lucas, K. N., & Lauder, G. V. (2017). Performance variation due to stiffness in a tuna-inspired flexible foil model. *Bioinspiration and Biomimetics*, *12*(1). https://doi.org/10.1088/1748-3190/aa5113

Rosic, M. N., Thornycroft, P. J. M., Feilich, K. L., Lucas, K. N., & Lauder, G. V. (2017). Performance variation due to stiffness in a tuna-inspired flexible foil model. *Bioinspiration & Biomimetics*, *12*(1), 016011. https://doi.org/10.1088/1748-3190/aa5113

Shadwick, R. E. (1990). Elastic energy storage in tendons: Mechanical differences related to function and age. *Journal of Applied Physiology*, *68*(3), 1033–1040. https://doi.org/10.1152/jappl.1990.68.3.1033

Shadwick, Robert E., Rapoport, H. S., & Fenger, J. M. (2002). Structure and function of tuna tail tendons. *Comparative Biochemistry and Physiology - A Molecular and Integrative Physiology*, *133*, 1109–1125. https://doi.org/10.1016/S1095-6433(02)00215-5

Shelton, R. M., Thornycroft, P. J. M., & Lauder, G. V. (2014). Undulatory locomotion of flexible foils as biomimetic models for understanding fish propulsion. *The Journal of Experimental Biology*, *217*, 2110–2120. https://doi.org/10.1242/jeb.098046

Suarez, H., Barlow, J. W., & Paul, D. R. (1984). Mechanical properties of ABS/polycarbonate blends. *Journal of Applied Polymer Science*, *29*(11), 3253–3259. https://doi.org/10.1002/app.1984.070291104

Tangorra, J. L., Lauder, G. V, Hunter, I. W., Mittal, R., Madden, P. G. a, & Bozkurttas, M. (2010). The effect of fin ray flexural rigidity on the propulsive forces generated by a biorobotic fish pectoral fin. *Journal of Experimental Biology*, *213*(23), 4043–4054. https://doi.org/10.1242/jeb.048017

Taylor, G. K., Nudds, R. L., & Thomas, A. L. R. (2003). Flying and swimming animals cruise at a Strouhal number tuned for high power efficiency. *Nature*, *425*(6959), 707–711. https://doi.org/10.1038/nature02000

Triantafyllou, G. S., Triantafyllou, M. S., & Grosenbaugh, M. A. (1993). Optimal Thrust Development in Oscillating Foils with Application to Fish Propulsion. *Journal of Fluids and Structures*, *7*(2), 205–224. https://doi.org/10.1006/jfls.1993.1012

Triantafyllou, M. S., & Triantafyllou, G. S. (1995). An efficient swimming machine. *Scientific*

American, *272*(3), 40–48. https://doi.org/10.1038/scientificamerican0395-64

Triantafyllou, Michael S, & Triantafyllou, G. S. (1995). An Efficient Swimming Machine. *Scientific American*, *272*(3), 64–70. https://doi.org/10.1038/scientificamerican0395-64

Tytell, E. D., Hsu, C. Y., Williams, T. L., Cohen, A. H., & Fauci, L. J. (2010). Interactions between internal forces, body stiffness, and fluid environment in a neuromechanical model of lamprey swimming. *Proceedings of the National Academy of Sciences of the United States of America*, *107*(46), 19832–19837. https://doi.org/10.1073/pnas.1011564107

Van Buren, T., Floryan, D., & Smits, A. J. (2019). Scaling and performance of simultaneously heaving and pitching foils. *AIAA Journal*, *57*(9), 3666–3677. https://doi.org/10.2514/1.J056635

Vanella, M., Fitzgerald, T., Preidikman, S., Balaras, E., & Balachandran, B. (2009). Influence of flexibility on the aerodynamic performance of a hovering wing. *Journal of Experimental Biology*, *212*(1), 95–105. https://doi.org/10.1242/jeb.016428

Wainwright, D. K., & Lauder, G. V. (2020). Tunas as a high-performance fish platform for inspiring the next generation of autonomous underwater vehicles, 1–46.

Wang, J., Deng, X., Lauder, G. V., & Dong, H. (2019). Numerical Investigation on Hydrodynamic Performance of Flapping Plates with Non-Uniform Spanwise Flexibility Using Fluid Structure Interaction, (June), 1–10. https://doi.org/10.2514/6.2019-3434

Wang, J., Han, P., Zhu, R., Liu, G., Deng, X., & Dong, H. (2018). Wake capture and aerodynamics of passively pitching tandem flapping plates. https://doi.org/10.2514/6.2018-3236

Wang, J., Wainwright, D. K., Lindengren, R. E., Lauder, G. V., & Dong, H. (2020). Tuna locomotion: A computational hydrodynamic analysis of finlet function. *Journal of the Royal Society Interface*, *17*(165). https://doi.org/10.1098/rsif.2019.0590

Weaver Jr, W., Timoshenko, S. P., & Young, D. H. (1990). Vibration problems in engineering. John Wiley & Sons.

Westneat, M. W., Hoese, W., Pell, C. a, & Wainwright, S. a. (1993). The horizontal septum: Mechanisms of force transfer in locomotion of Scombrid fishes (Scombridae, Perciformes). *Journal of Morphology*, *217*, 183–204. https://doi.org/10.1002/jmor.1052170207

Westneat, M. W., & Wainwright, S. A. (2001). 7. Mechanical design for swimming: muscle, tendon, and bone. *Fish Physiology*, *19*(C), 271–311. https://doi.org/10.1016/S1546-5098(01)19008-4

Wu, T. Y.-T. (1971). Hydromechanics of swimming propulsion. Part 1. Swimming of a two-dimensional flexible plate at variable forward speeds in an inviscid fluid. *Journal of Fluid Mechanics*, *46*(02), 337. https://doi.org/10.1017/S0022112071000570

Yeh, P. D., & Alexeev, A. (2016). Effect of aspect ratio in free-swimming plunging flexible plates. *Computers and Fluids*, *124*, 220–225. https://doi.org/10.1016/j.compfluid.2015.07.009

Zhu, J., White, C., Wainwright, D. K., Di Santo, V., Lauder, G. V, & Bart-Smith, H. (2019). Tuna robotics: A high-frequency experimental platform exploring the performance space of swimming fishes. *Science Robotics*, *4*(34), 4615. https://doi.org/10.1126/scirobotics.aax4615

Zhu, Q. (2007). Numerical Simulation of a Flapping Foil with Chordwise or Spanwise Flexibility. *AIAA Journal*, *45*(10), 2448–2457. https://doi.org/10.2514/1.28565

Zhu, R., Wang, J., Dong, H., & Bart-Smith, H. (2020). Effects of Chordwise Non-uniform Stiffness on Propulsive Performance of Passively-flexing Square Foil. https://doi.org/10.2514/6.2020-0804

Zhu, R., Wang, J., Dong, H., Quinn, D., Bart-Smith, H., Di Santo, V., … Lauder, G. (2019). Computational study of fish-shaped panel with simultaneously heaving and bending motion.

In *AIAA Scitech 2019 Forum*. Reston, Virginia: American Institute of Aeronautics and Astronautics. https://doi.org/10.2514/6.2019-1655

Zhu, R., Wang, J., Lewis, G., Zhu, J., Dong, H., Bart-Smith, H., … Lauder, G. V. (2017). Propulsive Performance of Pitching Panels with Bio-Inspired Passive Directional Flexibility. In *47th AIAA Fluid Dynamics Conference*. https://doi.org/10.2514/6.2017-3980